Behavior of Bitumen-coated Fine Solids in Organic Media from Non-aqueous Extraction of Oil Sands

by

Jing Liu

A thesis submitted in partial fulfillment of the requirements for the degree of

Doctor of Philosophy

in

Chemical Engineering

Department of Chemical and Materials Engineering
University of Alberta

Abstract

The non-aqueous extraction (NAE) technique for recovering bitumen from oil sands ore has been proposed as a potential substitute to the conventional water-based extraction method in order to reduce the environmental and carbon footprint of extracting this natural resource. In the NAE process, bitumen was dissolved and liberated from raw oil sands ore by organic solvent. Due to high bitumen recovery and good applicability for all kinds of oil sands ores, as well as the generation of dry stackable extraction tailings, NAE has gained increasing attention from both the industry and academia. However, the fact that considerable amounts of fine solids are found in the produced bitumen makes the NAE bitumen unsuitable for the downstream operations, impeding the industrial application of NAE. Therefore, understanding the behavior of the fine solids in organic media is of fundamental and practical importance to solve the challenging issue inherent to the NAE process. It has been found that the indigenous fine solids are mainly composed of quartz and clays with the surface adhering layer of bitumen coatings. The presence of bitumen coatings renders the fine solids more hydrophobic and oleophilic, increasing the difficulty in removing the fine solids in oil media.

In this work, surface properties of the fine solids collected from Athabasca oil sands have been systematically characterized, which shows that the bitumen coatings are heterogeneously distributed over the solid surface. Bitumen domains and mineral regions have been distinguished on the solid surface via analyzing nano-mechanical and hydrophobicity properties of sample surface. To unravel the stabilization mechanisms of fine solids with bitumen coatings, interfacial interactions between fine solids in organic solvent have been then quantitatively analyzed using the colloidal probe AFM technique, and behaviors of bitumen adsorption to silica surface in organic solvent have been analyzed using the quartz crystal microbalance with dissipation

monitoring (QCM-D), respectively. It was found that bitumen coatings would fully extend and swell in cyclohexane, giving rise to the steric repulsion between the fine solids. With addition of heptane, the steric repulsion could be notably weakened by causing the shrink and collapse of the bitumen layer. Meanwhile, the adsorbed mass of bitumen coatings could be enhanced by slightly decreasing volume fraction of cyclohexane (φ_c) in bulk solution but could be inversely reduced if φ_c became smaller than the asphaltene precipitation onset. Sedimentation tests showed that the effectiveness of settling bitumen-coated silica particles was strongly associated with the interfacial interactions of fine solids and behavior of bitumen adsorption in organic media. Furthermore, a two-step agglomeration strategy has been developed to facilitate settling of the bitumen-coated silica particles by modifying their surface wettability using an amphiphilic polymer poly(ethylene glycol)-block-poly(propylene glycol)-block-poly(ethylene glycol) (PEG-PPG-PEG) and introducing a small amount of water to trigger the agglomeration of the particles. The results showed that the two-step method can achieve high initial settling rate (ISR) and low content of residual solids in the supernatant simultaneously. The study of underlying interaction mechanisms revealed that PEG-PPG-PEG can favorably adsorb to the bitumen-coated silica surfaces in cyclohexane to make the surfaces more less hydrophobic, thereby altering the interactions between the particle surfaces and water drops from repulsion to attraction.

This research work has developed useful methodologies for studying the behavior of bitumen-coated fine solids suspended in organic media and has explored a feasible strategy to destabilize such fine solids. Our results have improved the fundamental understanding of the interaction mechanisms among fine solids, bitumen, water drops and polymer additives in oil media, with important implications on developing more effective and economical strategies of removing fine solids from the NAE bitumen.

Preface

Chapter 3 of this thesis has been published as J. Liu, J. Wang, J. Huang, X. Cui, X. Tan, Q. Liu, H. Zeng, "Heterogeneous Distribution of Adsorbed Bitumen on Fine Solids from Non-aqueous Extraction of Oil Sands Probed by AFM", *Energy Fuels*, vol. 31, 8833-8842. I was responsible for XPS analysis, wettability measurement, PeakForce QNM imaging, data analysis and manuscript composition. J. Wang was responsible for the AFM force mapping. J. Huang was responsible for the SEM/EDX mapping. X. Cui assisted with the PeakForce imaging. Dr. X. Tan and Dr. Q. Liu contributed to manuscript edition. Dr. H. Zeng was the supervisory author and was involved in concept formation and manuscript composition.

Chapter 4 of this thesis has been published as J. Liu, X. Cui, J, Huang, L, Xie, X. Tan, Q. Liu, H. Zeng, "Understanding the Stabilization Mechanism of Bitumen-coated Fine Solids in Organic Media from Non-Aqueous Extraction of Oil Sands", *Fuel*, vol 242, 255-264. I was responsible for experimental force measurement via colloidal probe AFM, QCM-D measurements, sedimentation tests, data analysis and manuscript composition. X. Cui was responsible for AFM imaging and manuscript edition. J. Huang and L, Xie assisted with the AFM force measurement and AFM imaging. Dr. X. Tan and Dr. Q. Liu contributed to manuscript edition. Dr. H. Zeng was the supervisory author and was involved in concept formation and manuscript composition.

Chapter 5 of this thesis has been published as J. Liu, X. Cui, C. Santander, X. Tan, Q. Liu, H. Zeng, "Destabilization of fine solids suspended in oil media through wettability modification and water-assisted agglomeration", *Fuel*, vol 254, 115623. I was responsible for the sedimentation tests, AFM force measurements, QCM-D measurements, data analysis and manuscript composition. X. Cui was responsible for the wettability characterization, interfacial tension measurements and manuscript edition. C. Santander was responsible for the size distribution

measurements and data analysis, Dr. X. Tan and Dr. Q. Liu contributed to manuscript edition. Dr. H. Zeng was the supervisory author and was involved in concept formation and manuscript composition.

Chapters 1, 2, and 6 are originally written by Jing Liu, and have never been published before.

Acknowledgment

I would like to express my sincere gratitude to Dr. Hongbo Zeng and Dr. Qi Liu for their bright supervision and insightful guidance through the period of my PhD study. I appreciate their creative ideas and suggestions that provide me a great learning experience during my research work. Special thanks to Dr. Hongbo Zeng for his inspiring encouragement when I confronted with research difficulties. His enthusiasm and dedication for scientific research always inspire me to fight for my career goal as a dedicated researcher. I also would like to appreciate Dr. Xiaoli Tan for his experienced suggestions and solid support to my research work.

I wish to thank all my group members for their generous help and assistance during my study. Special thanks to Dr. Jun Huang and Dr. Xin Cui for their valuable advice for the completion of my thesis project and revision of my manuscripts.

I would like to acknowledge Dr. Yahui Zhang, Dr. Kaipeng Wang and Mrs. Lisa Brandt in Institute for Oil Sands Innovation (IOSI) for their kindly help and assistance with the characterizations including particle size determination, FTIR analysis and fine solids determination.

I gratefully acknowledge the financial support from Institute for Oil Sands Innovation (IOSI), Imperial Oil, the Natural Sciences and Engineering Research Council of Canada (NSERC) and Alberta Innovates to the research work. I also gratefully acknowledge the financial support from the Canada Foundation for Innovation (CFI), the Future Energy Systems under the Canada First Research Excellence Fund and the Canada Research Chairs Program.

Finally, my deepest gratitude goes to family for their limitless love and support.

Table of Content

List of Tables

List of Figures

List of Acronyms and Symbols

AFM	Atomic Force Microscope
QCM-D	Quartz Crystal Microbalance with Dissipation
VDW	Van der Waals
HB	Hydrophobic
PeakForce QNM	PeakForce Quantitative Nano-Mechanical
FTIR	Fourier Transform Infrared Spectroscopy
XPS	X-ray Photoelectron Spectroscopy
SEM/EDX	Scanning Electron Microscopes coupled with Energy-dispersive X-ray Spectrometry
PEG-PPG-PEG	Poly(ethylene glycol)-block-poly(propylene glycol)-block-poly(ethylene glycol)
OTS	Octadecyltrichlorosilane
SFA	Surface Force Apparatus
ISR	Initial settling rate
A	Hamaker constant
F	Measured interaction force
D	Separation between two surfaces
L	Flexible length of polymer chains

s	Average spacing between two grafted sites
C_0	Pre-exponential factor of hydrophobic interaction
D_0	Decay length of hydrophobic interaction
κ	Inverse of Debye length
E	Young's modulus
v	Poisson's ratio
R	Radius of particle or drop probe
Ψ	Surface potential
T	Temperature
γ	Interfacial tension
Δf	Frequency shift
ΔD	Dissipation shift

Chapter 1 Introduction

1.1 Non-aqueous extraction of oil sands

Canada has the world's third-largest oil reservoir, only after Venezuela and Saudi Arabia, most of which is recovered from the oil sands. Oil sands is a nature mixture of mineral solids, a type of heavy oil called bitumen and small amount of water. The valuable component, bitumen, can range from nearly 0 up to 20 wt% with an average value being about 10 wt%. Oil sands deposits are an important source of unconventional fossil fuel which require special extraction and additional refining processes to acquire petroleum and petrochemical products. Athabasca oil sands deposits in Northern Alberta is the largest one around the world, cover an area over 30,000 km^2 and have crude oil production about 1.3 million barrels per day. Most of Alberta's oil sands are too deep to be mined and can be recoverable only by in situ methods.[1] Only about 4,800 km^2 of the oil sands are close enough to the surface to be recovered economically by surface mining.[2] The mined raw oil sands are then crushed for size reduction, mixed with hot water (50-80 ºC) to form a dense slurry and is transported to extraction plants where the bitumen is skimmed off from the mineral solids with assistance of air bubbles. The work on perfecting bitumen recovery using hot water was mainly undertaken by Karl A. Clark and the associated process is known as Clark hot water extraction (CHWE).[3-4] This extraction process has been commercially adopted by most of Canadian companies in oil sands industry. However, there are many drawbacks and challenges associated with CHWE.

In the hot water-based extraction, excess water withdrawal from river (e.g., Athabasca Rive) has raised growing public concerns about the ecological sustainability of the river. On average, about 3 barrels of fresh water are required for a typical mined oil sands to produce one barrel of

synthetic bitumen.[5] Even though a large proportion (about 80%) of the water used in the process can be now recycled from the tailing ponds, importation of additional barrels of fresh water from river (i.e., make-up water) is still required to produce each barrel of oil. Data from the Alberta Energy Regulator shows that the mined oil sands increased from 378 to 466 million cubic meters from 2012 to 2016 with total volume of recycled water increasing by 33% and make-up water from the Athabasca River increasing by 5.8%. The accumulation of large volumes of tailings as a byproduct of CHWE is another intractable challenge facing the oil industry. Tailings are the mixture of water, mineral solids and residual bitumen, which are toxic to the aquatic life and need to be stored in large dam and dyke systems called tailing ponds. Tailing ponds are costly to build and detrimental to the landscape, and mineral solids in the tailings will take centuries to settle to the bottom of the ponds. To date, there is no silver-bullet technology available to restrict the size and duration of tailing ponds and almost 1.3 trillion liters of oil sands tailings has accumulated on the northern Alberta over the past 50 years. With tailing ponds continuing to grow, the risk was posed to the environment and people's daily life in the future.

To avoid dealing with the environmental impacts freshwater consumption and tailing ponds involving in the water extraction process, the non-aqueous extraction (NAE) process using organic solvents to dissolve and liberate bitumen from the mineable oil sands ore has been regarded as a potential alternative to CHWE. Due to good applicability for all kinds of oil sands, as well as the generation of dry stackable extraction tailings, NAE has gained increasing attention from the industry and academic fields. In addition, NAE process appears to promise the high extraction efficiency at a reasonable cost. Meadus and Sparks firstly developed the non-aqueous extraction process specifically for Athabasca oil sands.[6-8] Their approach was to extract bitumen using naphtha and to trigger spherical agglomeration of extracted mineral solids by adding water.

Bitumen recovery in the process reached above 95% using a solvent mixture containing 87% naphtha and 13% water. The drawbacks of this approach are that large amounts of naphtha were required to form slurry with the oil sands, and it is difficult to recover naphtha due to the high boiling point of the solvent. Leung and Phillips studied NAE by different solvents including benzene, toluene and kerosene and found that higher mass transfer rates of bitumen can be achieved when using solvents with higher aromaticity or low boiling points.[9] However, the aromatic solvents can be ruled out due to their odor and toxicity. Wu and Dabros used n-heptane, hexane, cyclopentane and mixtures of n-heptane and cyclopentane in NAE of the Alberta oil sands, and suggested cyclopentane as the best solvent.[10] In their protocol, they utilized centrifugation and filtration to separate mineral solids from the diluted bitumen and recovered solvents remaining in the filtration cake by vacuum evaporation. Bitumen recovery using cyclopentane as the solvent reached 90% after a single stage extraction and can reach above 95% after a three-stages extraction, which were comparable to those achieved by the CHWE process. Studied by Hooshiar and Nikakhtari examined the performance of different classes of light hydrocarbon solvents for NAE process, including aromatics, aliphatics, cylcoalkanes and biologically derived solvents.[11-12] Nikakhtari et al. recommended cyclohexane as the best solvent candidate for NAE based on low fine solids in the produced bitumen and rapid evaporation of cyclohexane from the gangue.

Figure 1. 1 shows a typical flow diagram of NAE process. Briefly, the steps are as follows: (1) batch digestion of oil sands ore and organic solvent in a rotary mixer, (2) sedimentation of the digested oil sands slurry for 30 min, (3) second batch digestion of the sediments in the bottom portion with additional solvent, (4) separation of the supernatant products collected from two stages of batch digestion through a 45-μm aperture sieve, (5) removal of mineral fine solids (< 45 μm fraction) from the supernatant products using the centrifuge at 4000 relative centrifugal force

(RCF) and (6) solvent recovery via a distillation process and recycled upstream to produce the bitumen product. All steps were carried out at room temperature (24 ± 0.5°C) and ambient pressure.

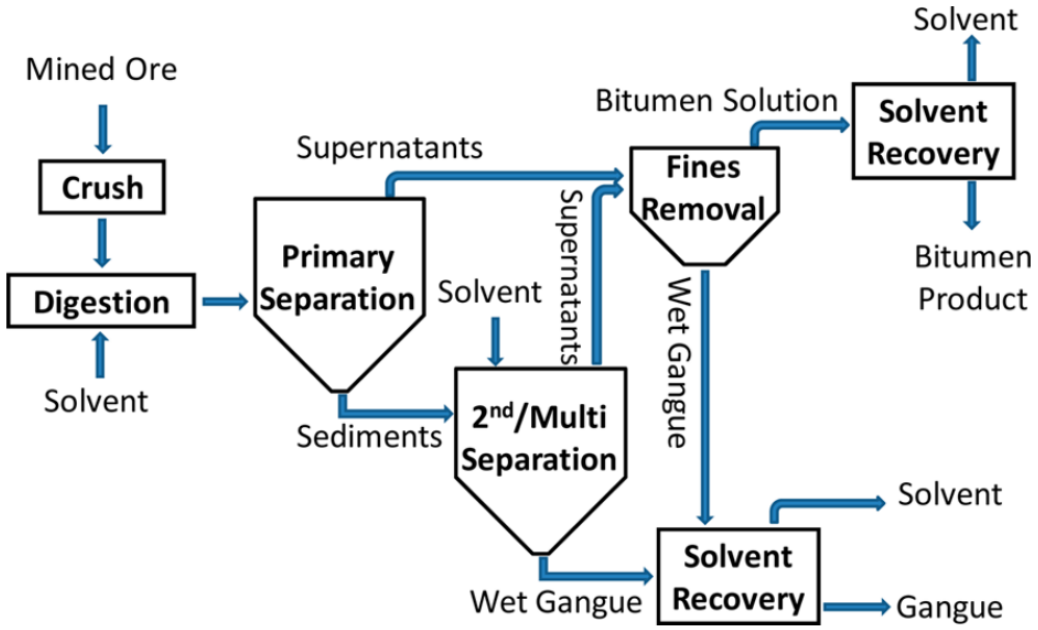

Figure 1. 1 Schematic flow diagram of a typical non-aqueous extraction process.[4]

1.2 Fine solids in NAE bitumen

Currently, no commercial NAE process has been established attributed to some perennial bottlenecks. First, the organic solvent must be recovered from the extraction gangue at high efficiency, aiming to minimize environmental impact of solvent residue and recycle the use of the solvent. Second, the content of fine solids in the bitumen product should be low enough to meet the downstream processing requirements. In the oil sands industry, it is generally recognized that the coarse sands do not cause any problems throughout extraction process, while fine solids are pernicious and detrimental to the quality of bitumen and probably cause some challenging issues in pipeline transportation, upgrading and refinery processes and facilities. The content of fine solids in extracted bitumen depends on several factors such as extraction-separation equipment

and procedure, type and dosage of solvent used, oilsands ore grade as well as content of connate water or added water present in the bitumen-solvent mixture.[13] It was found that the amount of fine solids remaining in the NAE bitumen could be remarkedly increased by removing the connate water from the oilsands ore by oven drying.[13-14] Kumar et al. demonstrated that the polar organic components in bitumen can readily adsorb onto the mineral surface if the brine film breaks.[15] In the NAE process, the step of fine removal from diluted bitumen is always necessary for product purification, as illustrated in Figure 1.1. Unfortunately, even under the optimal technological conditions at present, the NAE bitumen typically contains 0.5-3% fine solids, which is higher than the pipeline specification (0.5 wt%) and even much higher than the requirements of refinery feed (< 0.03 wt%).[16-17] For instance, cyclohexane has been found as a suitable solvent candidate, and bitumen extracted by cyclohexane showed a solid content in bitumen about ~ 1.4 wt%, failing to satisfy the desired standard.[12] Besides, different light hydrocarbon solvents including aromatics, biologically derived solvents and their blends have been compared for extraction of bitumen from Athabasca oil sands, as shown in Table 1.1.

Table 1. 1 Performance of solvents and solvent blends for non-aqueous extraction of oil sands.[12]

Solvent	C % in second tailing	Bitumen recovery, %	C % in centrifuge solids	Weight of centrifuge solids, % of ore
100% Toluene	0.79	96.3 ± 1.1	20.1 ± 2.8	0.07 ± 0.03
70% Toluene/30% *n*-heptane	1.04	94.3 ± 2.3	18.1 ± 6.4	0.16 ± 0.10
50% Toluene/50% *n*-heptane	0.85	95.9[a]	23.6	0.07
30% Toluene/70% *n*-heptane	0.86	95.8 ± 2.5	19.2 ± 6.3	0.63 ± 0.22
20% Toluene/80% *n*-heptane	0.85	95.9	24.4	1.37
Methyl cyclohexane	0.97	94.9	17.0	0.24
Cyclohexane	1.05	94.4 ± 1.7	21.9 ± 1.7	0.11 ± 0.04
Ethylbenzene	1.11	93.8	18.6	0.07
Xylenes	1.16	93.4	20.1	0.08
10% Toluene/90% cyclohexane	1.18	93.2	23.2	0.10
10% Toluene/90% n-heptane	1.27	92.6 ± 3.2	26.9 ± 7.2	2.33 ± 0.64
Isoprene	1.40	91.4 ± 1.5	20.6 ± 1.7	0.38 ± 0.09
Limonene	5.87	53.0	22.3	0.11

1.2.2 Surface properties of fine solids

Recent study on the mineralogy of the centrifuged solids from the bitumen-solvent mixture shows that the fine solids are mainly comprised of silica, kaolinite and illite, and iron minerals.[13]

It has been indicated that the fine mineral solids retained in the NAE bitumen generally possess high mass fraction of carbon content, ranging from ~ 8% to ~ 30% depending on the properties of applied solvents and oilsands ore grade, as shown in Figure 1. 2. The carbon content are mainly contributed by the organic coatings (e.g., bitumen components) on the solids surface.[12] Prior to the surface mining and extraction processes, the mineral solids can be adsorbed by organic components that were originally in the crude oil driven by the surface precipitation and intermolecular interactions involving acid/base attraction, π-π stacking and ion-binding interactions.[18-19] The mined mineral solids could undergo subsequent adsorption of bitumen or asphaltenes from the bitumen-solvent mixture during the extraction process, which therefore increased mass fraction of carton content on the solids surface and renders the solids more hydrophobic. Correspondingly, the contact angles of the fine solids were found to be close to 90º, much higher than those from Soxhlet-extracted ores.[13]

Such organic coatings or bitumen coatings are stubborn and cannot be completely separated from the mineral solids by organic solvents. The wettability of fine solids largely depends on the surface coverage of adsorbed bitumen, consequently affecting the degree of migration of fine solids into bitumen products during the NAE process. Results of X-ray diffraction analysis,[13] time-of-flight secondary ion mass spectroscopy (ToF-SIMS) and X-ray photoelectron spectroscopy (XPS),[20] and AFM force mapping and PeakForce QNM imaging[21] revealed an incomplete and heterogeneous distribution of bitumen coatings or asphaltene coatings on the solids surfaces. Similar to the structure of natural Janus particles,[22] the fine solids with “patchy” bitumen coatings contain both hydrophilic and hydrophobic surfaces, which significantly affect the behavior of the fine solids in organic media.

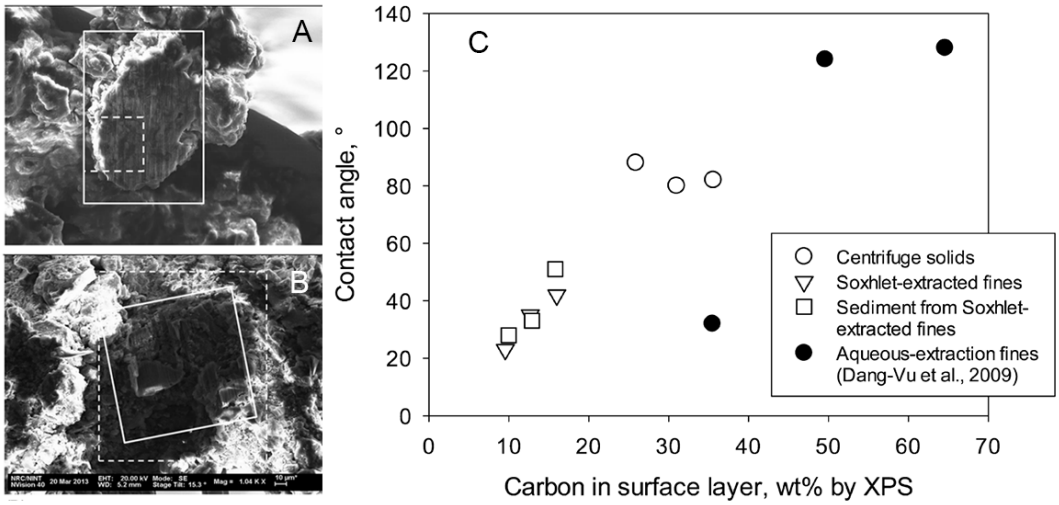

Figure 1. 2 Scanning electron micrographs of fine solids coupled with EDX analysis as shown by the dashed boxes (A) High carbon content (30%) sample from low-fines ore extracted with heptol; (B) Medium carbon content (8%) sample from low-fines ore extracted with cyclohexane. (C) XPS carbon content versus contact angle for centrifuged solids and fines from Soxhlet extracted ores.[13]

A number of experimental studies and computer simulations have been conducted to investigate adsorption behaviors of asphaltenes onto various mineral surfaces.[23-27] It was found that asphaltene adsorption strongly depend on the properties of surrounding organic media and the interfacial chemistry of the mineral surface. Zahabi et al.[24] reported that the concentration of asphaltenes (viz. ratio of oil to solvent) could affect the swelling of asphaltene aggregates in the solution, ultimately influencing constructions of adsorbed asphaltenes on the silica surface. Dorota et al.[28] revealed that the adsorbed mass of asphaltenes to hydrophilic mineral solids was strongly associated with the solubility of asphaltenes in organic solvents and the original size of asphaltene aggregates. In previous studies, a surface analysis technique, quartz crystal microbalance with dissipation (QCM-D), has been widely applied in investigating the adsorption behaviors of bitumen fractions, which offers an effective way to analyze the state of adsorbed species bound to

the solid surfaces, their mass, thickness and viscoelastic properties in real-time with extremely high sensitivity.[29-32]

1.2.1 Interactions of fine solids in oil media

The hydrophobic properties of mineral solids play an important role in forming a stable suspension of fine solids in NAE environments. Many studies on asphaltenes have revealed that the presence of asphaltene layer on the surface of colloids (e.g. mineral solids, emulsion and air bubbles) have a significant impact on the stability of colloids in organic media. Zhang et al. investigated the interaction mechanism of asphaltenes adsorbed on mica surface in heptol (i.e., mixture of toluene and heptane) solvents with assistant of a surface forces apparatus (SFA).[33] They measured a pure repulsion, mainly due to the steric interactions, between two swelling asphaltene surfaces in toluene, which play a critical role in stabilizing the emulsion drops as demonstrated by the micropipet and 4-roll mill fluidic tests. Shi et al. applied the droplet probe atomic force microscopy (AFM) technique to quantitatively analyze the interaction mechanism between water-in-oil (W/O) emulsion droplets with interfacially adsorbed asphaltenes.[34] Unlike the bare water droplets which could readily coalesce with each other in oil, water droplets with interfacial asphaltenes could sterically inhibit droplet coalescence and induce interfacial adhesion during separation of the water droplets.

The stability of the bitumen-coated fine particles suspended in the bitumen-solvent mixture should largely depends on the competition between surface forces such as van der Waals forces, electrostatic forces, and steric interactions among the particle surfaces, solvent media and any water present in the complex organic media. A clear understanding of the interaction mechanisms of the fine solids in the oil sands matrix, and an appropriate design of methods to remove fine

solids from diluted bitumen is required. Surface force measurements between oil sands components in aqueous media using AFM were reported extensively in the literature. A systematic previous study has been conducted to measure forces between bitumen and mineral solids,[35-39] bitumen and bitumen,[40-41] asphaltene and asphaltene,[42-43] and two mineral solids,[44-45] aiming to provide a better understanding of the bitumen extraction process or the flotation process. The direct force measurements in non-aqueous media were mainly performed using SFA.[33, 46-48] AFM force measurements was seldom used for non-aqueous system possibly because the commercial AFM liquid cell could be readily contaminated by the bitumen components in organic solvents. Wang et al. conducted the AFM force measurements between asphaltene surfaces in toluene which was injected into in a specially designed liquid cell well-sealed.[49]

When analyzing the surface forces between oils sands components, van der Waals (VDW) forces are always present and play a critical role in various interfacial phenomena in either aqueous or non-aqueous environments, for while they are not as strong as ionic or covalent bonds. VDW force originates from the electrostatic force between two dipoles which can be attractive and repulsive depending on the properties of two interacting media.[50] Three major components synergistically contribute to the overall VDW interaction including the orientation interaction between two permanent dipoles (Keesom interaction), the induction interaction between a permanent dipole and its induced dipole (Debye interaction), and dispersion interaction between an instantaneous dipole and its induced dipoles (London interaction), all of which vary with the inverse sixth power of the distance. As a non-additive interaction, VDW interaction between two macroscopic bodies across a medium is calculated based on Lifshitz theory which incorporates the influence of surrounding molecules on the interaction between each pair of molecules in the two

interacting bodies.[50] Equation 1.1 illustrates the approximate expression for the VDW interaction per unit area between two flat surfaces 1 and 2 through medium 3.

$$F_{vdw} = -A / 6\pi D^3$$

$$A \approx \frac{3}{4} kT \left(\frac{\varepsilon_1 - \varepsilon_2}{\varepsilon_1 + \varepsilon_3} \right) \left(\frac{\varepsilon_2 - \varepsilon_3}{\varepsilon_2 + \varepsilon_3} \right) + \frac{3h\upsilon_e}{8\sqrt{2}} \frac{(n_1^2 - n_3^2)(n_2^2 - n_3^2)}{\sqrt{(n_1^2 + n_3^2)}\sqrt{(n_2^2 + n_3^2)}\left\{\sqrt{(n_1^2 + n_3^2)} + \sqrt{(n_2^2 + n_3^2)}\right\}} \quad (1.1)$$

where D is the separation between two surfaces, A is the nonretarded Hamaker constant, ε is the dielectric constant, n is the refractive index, k and h are the Boltzmann's and Plank's constants, T is the temperature, υ_e is the main electronic absorption frequency.

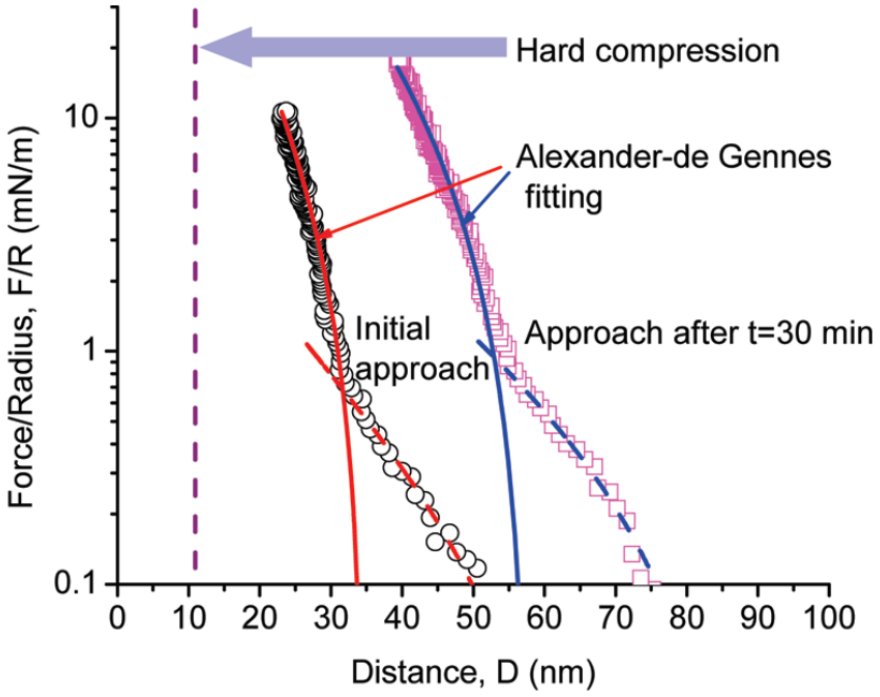

Figure 1. 3 Experimentally measured repulsion forces by SFA and best fitted curves using the AdG theory for approach of two asphaltene films in toluene.[46]

Because of the relatively lower dielectric constants of non-aqueous media as compared to aqueous solutions, the electrostatic interactions are typically negligible in organic solvents (e.g., toluene and cyclohexane) and thereby are not considered when analyzing the

intermolecular and surface forces. Any repulsive interactions observed in organic media could possibly originated from the steric repulsion force which plays a dominate role in the stabilization of colloids in organic media. Steric repulsion was originally used to describe the osmotic repulsion between two polymer-covered surfaces in good solvent medium. When two surfaces approach each other, the outer segments can overlap once the separation is below a few R_g (radius of gyration), and the entropy become unfavorable by confining the polymer chains, leading to a repulsive osmotic force.[51] In the system associated with oil sands, the steric repulsion is mainly attributed to the swelling of asphaltene chains in good solvent (e.g., toluene). The steric repulsive force per unit area between two asphaltene surfaces could be estimated by the Alexander-de Gennes (AdG) steric model, given by Equation (1.2),[50]

$$F_{\text{steric}} \approx \frac{kT}{s^3}\left[\left(2L/D\right)^{9/4} - \left(D/2L\right)^{3/4}\right] for\ D < 2L. \quad (1.2)$$

where T is the absolute temperature, k is the Boltzmann constant, s is the average spacing between two grafted sites, L is length of flexible polymer brush. The first term in Equation 1.2 represents the osmotic repulsion between the coils, while the second term represents the elastic stretch energy of the chains. If $D/2L$ is in the range from 0.2 to 0.9, the preceding pressure can be roughly exponentially expressed,[52]

$$F_{\text{steric}} \approx \frac{100kT}{s^3} e^{-\pi D/L} \quad . \quad (1.3)$$

While the AdG theory was originally developed for the polymer brush with high molecular weight, it has been found to quantitatively account for the forces between asphaltene surfaces in non-aqueous solvents when the asphaltene layer becomes extended and flexible. Figure 1. 3 shows the results of SFA force measurements between two asphaltene films in toluene. The measured steric

force was found to be well described by the AdG theory at short separation distances under high compression forces. Natarajan et al. found that the fitted mean distance between anchoring sites (s) are very close to the size of nanoaggregates of asphaltenes in bulk toluene, and the length of asphaltene layer (L) strongly depends on compression pressure and immersion time of asphaltene films in solvents.[46]

1.3 Removal of fine solids

Owing to the adsorbed organic matters on the surface, fine solids can form the stable suspension in oil media, making it extremely difficult to remove the fine solids by conventional gravitational/centrifugal settling or filtration.[53] During the last decades, some attempts have been made to remove the fine solids suspended in oil media. It is well known that aliphatic solvents such as n-heptane has very low solubility for asphaltenes (i.e., major fraction of bitumen),[54-56] and their use causes asphaltene precipitation which act as bonding bridges among the fine solids.[53, 57-58] As a result, the fine solids will undergo homo-aggregation with the precipitation of asphaltenes. In addition, these solvents can also enhance the particle-particle attraction by modify the parameters of surface force involving in the colloidal system.[33, 46-47] Farnand. et al. found that the use of petroleum ether could lower solid content in naphtha solution of bitumen and accelerate the settling rate of fine solids.[53] They also found that a substantial amount of the solvent was required for the achievement of a relatively low solid content of < 0.5 wt%, which would apparently increase the cost and difficulty in the subsequent operations. The method of hetero-aggregation of fine solids with process aids has been widely used in removing the fine solids during the NAE process. For example, it was found that the addition of ionic liquids (ILs) to mixture of oil sands and organic solvent would significantly lower the solid content in the produced bitumen.[59-63] The

possible reason is that ILs can preferentially wet the solid surface attributed to strong electrostatic attraction between the ILs and minerals, and thereby bitumen coatings can be effectively displaced and liberated from the oil sands.[64-65] The resultant clean solids then can undergo aggregation in ILs, which can be readily removed with ILs because the highly polar ILs are completely immiscible with organic solvent. The drawbacks of use of ILs are mainly associated with their high cost and uncertainty in toxicity to the oil products and the ecological environment.

Since the 1980s, research work has been conducted to investigate the role of small amount of water (typically less than 10%) in agglomerating the fine solids in oil media.[6-8, 66] It was reported that the hydrophilic and relatively clean solids can be physically trapped by the added water and the formation of removable solid-water agglomerates can improve the efficiency of subsequent solids/oil separation. Nonetheless, the added water was unable to wet and capture the hydrophobic bitumen-coated fine solids those account for majority of mineral contaminants in the diluted bitumen. Thereby, the water agglomeration method failed to lower solid content in bitumen to a satisfied level. In addition, addition of too much water would be harmful to the removal of fine solids because the excessive water would facilitate the formation of water-in-oil emulsion stabilized by asphaltenes and fine solids.[13, 67] Switchable-hydrophilicity solvents (e.g., tertiary amines) have been recently used to reduce the hydrophobicity of the fine solids.[68-70] For example, tertiary amines are first protonated in water in the presence of CO_2, which can effectively interaction with active bitumen components adsorbed on minerals to form ion pairs in oil media. However, the dosage of water is quite high in order to generate essential protonated tertiary amines and such aqueous-nonaqueous hybrid extraction inevitably gave rise to the formation of oil-water emulsions.

Flocculation of fine solids by polymers might be another potential remedy to lower solid content, which has been already applied in the demulsification of solid-stabilized emulsions.[71-73] In general, polymer flocculants are able to penetrate through the steric barrier film at the water/oil interface and replace the interfacial species (e.g. asphaltenes and fine solids) on the interface. The typical polymers are non-ionic surfactant, including the polymers having the main components of polyethylene oxide (PEG) and polypropylene oxide (PPG)[71, 74-75] and more eco-friendly polymers such as ethyl cellulose.[76-78] For the removal of fine solids in oil media, the polymer adopted should be interfacial active to effectively bond with functional groups of bitumen coatings. The hydrocarbon chains of the polymer can act as cross bridging to facilitate the aggregation of fine solids, resulting in a formation of large solid flocs.[4] To date, there are no data available on the use of solid flocculation by polymer in the NAE process. In order to explore more effective and economical strategies of removing fine solids from NAE bitumen, it is of vital importance to gain a comprehensive understanding of the surface properties and the stabilization mechanism of fine mineral solids in the organic media.

1.4 Objectives

Developing a NAE process for recovering oil from the oil sands ore without the use of water could eliminate the environmental issues inherent to the Clark hot water extraction (CHWE), such as huge consumption of fresh water and fast accumulation of toxic tailings. Despite many promising results, the considerable amount of fine mineral solids remaining in bitumen product has been a main challenge that the commercialization of the NAE process faces. A deep and comprehensive study of behaviors of fine solids in organic media is of great importance in better understanding a variety of colloidal and interfacial phenomena in NAE process and providing

theoretical guidance to the removal of intractable hydrophobic fine solids from NAE bitumen product. The major objectives of this project are to investigate the surface characteristics (surface heterogeneity, surface wettability and interfacial tension) and underlying interaction mechanism of the bitumen-coated fine solids in complex organic media using several state-of-the-art nanomechanical techniques, such as atomic force microscopic (AFM) and quartz crystal microbalance with dissipation monitoring (QCM-D). The specific objectives are listed as follows.

(1). Characterize the surface properties (surface chemistry, surface wettability and surface heterogeneity) of the indigenous fine solids collected from NAE bitumen extracted with cyclohexane using several complementary techniques to provide a fundamental understanding of behavior of suspended fine particles in organic media.

(2). Unravel the stabilization mechanism of the fine solids with bitumen coatings in different organic solvents (i.e., cyclohexane, heptane and their blends) by investigating the intermolecular and surface interactions between fine solids with bitumen coatings, with implications for an improved understanding of the behaviors of hydrophobic fine solids in NAE process.

(3). Investigate the methods to destabilize the bitumen-coated fine solids in organic media with assistance of chemical additives and water, aiming to explore an effective and facile method of removing the hydrophobic fine solids in organic media during the NAE process.

1.5 Structure of thesis

Chapter 1 introduces the recent advances in the technique of non-aqueous extraction (NAE) of oil sands, the challenges and potential issues of this technique, the surface science in the

colloidal and interfacial phenomena in the organic system during NAE process, and the objectives of this research work.

Chapter 2 describes the experiment methods including lab protocol for collecting fine mineral solids from NAE bitumen extracted by cyclohexane, procedures of preparing model bitumen-coated flat surfaces and bitumen-coated solid particles and working principle of AFM force measurements and QCM-D measurements in organic media.

Chapter 3 demonstrates the characterization results of surface properties of collected indigenous fine solids from the NAE bitumen by virtue of several complementary techniques including XPS, SEM/EDX, AFM force mapping and PeakForce QNM imaging, with implications for a better understanding of behaviors of fine solids in organic media.

Chapter 4 demonstrates the stabilization mechanism of bitumen-coated silica particles in organic media, the effects of interaction forces between fine solids and behaviors of bitumen adsorption on the stability of the solid particles in organic media, and changes in morphology of the adsorbed bitumen layer on solid surface in different organic media.

Chapter 5 illustrates the efficiency of destabilizing and settling bitumen-coated silica particles in cyclohexane with the assistance of additives including small amount of water and amphiphilic polymer PEG-PPG-PEG, and the underlying interaction mechanisms among the bitumen-coated silica surface, water drops and PEG-PPG-PEG in cyclohexane.

Chapter 6 presents the major conclusion and original contributions of this thesis. The future work is also provided.

References

1. Butler, R.; McNab, G.; Lo, H., Theoretical Studies on the Gravity Drainage of Heavy Oil During in-Situ Steam Heating. *Can. J. Chem. Eng.* **1981**, *59*, 455-460.

2. Berkowitz, N.; Speight, J. G., The Oil Sands of Alberta. *Fuel* **1975**, *54*, 138-149.

3. Sheppard, M. C., *Oil Sands Scientist: The Letters of Karl A. Clark, 1920-1949*; University of Alberta, 1989.

4. Lin, F.; Stoyanov, S. R.; Xu, Y., Recent Advances in Nonaqueous Extraction of Bitumen from Mineable Oil Sands: A Review. *Org. Process Res. Dev.* **2017**, *21*, 492-510.

5. Allen, E. W., Process Water Treatment in Canada's Oil Sands Industry: I. Target Pollutants and Treatment Objectives. *Journal of Environmental Engineering and Science* **2008**, *7*, 123-138.

6. Sparks, B.; Meadus, F., A Study of Some Factors Affecting Solvent Losses in the Solvent Extraction—Spherical Agglomeration of Oil Sands. *Fuel Process. Technol.* **1981**, *4*, 251-264.

7. Sparks, B. D.; Meadus, F. W.; Hoefele, E. O., Solvent Extraction Spherical Agglomeration of Oil Sands. Google Patents: 1988.

8. Meadus, F.; Chevrier, P.; Sparks, B., Solvent Extraction of Athabasca Oil-Sand in a Rotating Mill Part 1. Dissolution of Bitumen. *Fuel Process. Technol.* **1982**, *6*, 277-287.

9. Leung, H.; Phillips, C. R., Solvent Extraction of Mined Athabasca Oil Sands. *Ind. Eng. Chem. Fundam.* **1985**, *24*, 373-379.

10. Wu, J.; Dabros, T., Process for Solvent Extraction of Bitumen from Oil Sand. *Energy Fuels* **2012**, *26*, 1002-1008.

11. Hooshiar, A.; Uhlik, P.; Liu, Q.; Etsell, T. H.; Ivey, D. G., Clay Minerals in Nonaqueous Extraction of Bitumen from Alberta Oil Sands: Part 1. Nonaqueous Extraction Procedure. *Fuel Process. Technol.* **2012**, *94*, 80-85.

12. Nikakhtari, H.; Vagi, L.; Choi, P.; Liu, Q.; Gray, M. R., Solvent Screening for Non-Aqueous Extraction of Alberta Oil Sands. *Can. J. Chem. Eng.* **2013**, *91*, 1153-1160.

13. Nikakhtari, H.; Wolf, S.; Choi, P.; Liu, Q.; Gray, M. R., Migration of Fine Solids into Product Bitumen from Solvent Extraction of Alberta Oilsands. *Energy Fuels* **2014**, *28*, 2925-2932.

14. Steinbeck, M.; Schlünder, E.-U., Convective Drying of Porous Material Containing a Partially Miscible Mixture1. *Chemical Engineering and Processing: Process Intensification* **1998**, *37*, 79-88.

15. Kumar, K.; Dao, E.; Mohanty, K., Afm Study of Mineral Wettability with Reservoir Oils. *J. Colloid Interface Sci.* **2005**, *289*, 206-217.

16. Ng, Y. M. S.; Knapper, B.; Kresta, J., Naphtha Based Fungible Bitumen Process. Google Patents: 2014.

17. Pal, K.; Nogueira Branco, L. d. P.; Heintz, A.; Choi, P.; Liu, Q.; Seidl, P. R.; Gray, M. R., Performance of Solvent Mixtures for Non-Aqueous Extraction of Alberta Oil Sands. *Energy Fuels* **2015**, *29*, 2261-2267.

18. Buckley, J.; Liu, Y., Some Mechanisms of Crude Oil/Brine/Solid Interactions. *J. Pet. Sci. Eng.* **1998**, *20*, 155-160.

19. Buckley, J.; Liu, Y.; Monsterleet, S., Mechanisms of Wetting Alteration by Crude Oils. *SPE journal* **1998**, *3*, 54-61.

20. Wang, S.; Liu, Q.; Tan, X.; Xu, C.; Gray, M. R., Study of Asphaltene Adsorption on Kaolinite by X-Ray Photoelectron Spectroscopy and Time-of-Flight Secondary Ion Mass Spectroscopy. *Energy Fuels* **2013**, *27*, 2465-2473.

21. Liu, J.; Wang, J.; Huang, J.; Cui, X.; Tan, X.; Liu, Q.; Zeng, H., Heterogeneous Distribution of Adsorbed Bitumen on Fine Solids from Solvent-Based Extraction of Oil Sands Probed by Afm. *Energy Fuels* **2017**.

22. Walther, A.; Müller, A. H., Janus Particles. *Soft Matter* **2008**, *4*, 663-668.

23. Marczewski, A. W.; Szymula, M., Adsorption of Asphaltenes from Toluene on Mineral Surface. *Colloids Surf., A* **2002**, *208*, 259-266.

24. Zahabi, A.; Gray, M. R.; Dabros, T., Kinetics and Properties of Asphaltene Adsorption on Surfaces. *Energy Fuels* **2012**, *26*, 1009-1018.

25. Xiong, Y.; Li, Z.; Cao, T.; Xu, S.; Yuan, S.; Sjoblom, J.; Xu, Z., Synergistic Adsorption of Polyaromatic Compounds on Silica Surfaces Studied by Molecular Dynamics Simulation. *J. Phys. Chem.* **2018**, *122*, 4290-4299.

26. Xiong, Y.; Cao, T.; Chen, Q.; Li, Z.; Yang, Y.; Xu, S.; Yuan, S.; Sjöblom, J.; Xu, Z., Adsorption of a Polyaromatic Compound on Silica Surfaces from Organic Solvents Studied by Molecular Dynamics Simulation and Afm Imaging. *J. Phys. Chem.* **2017**, *121*, 5020-5028.

27. Wu, G.; He, L.; Chen, D., Sorption and Distribution of Asphaltene, Resin, Aromatic and Saturate Fractions of Heavy Crude Oil on Quartz Surface: Molecular Dynamic Simulation. *Chemosphere* **2013**, *92*, 1465-1471.

28. Dudášová, D.; Silset, A.; Sjöblom, J., Quartz Crystal Microbalance Monitoring of Asphaltene Adsorption/Deposition. *J. Dispersion Sci. Technol.* **2008**, *29*, 139-146.

29. Ekholm, P.; Blomberg, E.; Claesson, P.; Auflem, I. H.; Sjöblom, J.; Kornfeldt, A., A Quartz Crystal Microbalance Study of the Adsorption of Asphaltenes and Resins onto a Hydrophilic Surface. *J. Colloid Interface Sci.* **2002**, *247*, 342-350.

30. Rudrake, A.; Karan, K.; Horton, J. H., A Combined Qcm and Xps Investigation of Asphaltene Adsorption on Metal Surfaces. *J. Colloid Interface Sci.* **2009**, *332*, 22-31.

31. Tavakkoli, M.; Panuganti, S. R.; Vargas, F. M.; Taghikhani, V.; Pishvaie, M. R.; Chapman, W. G., Asphaltene Deposition in Different Depositing Environments: Part 1. Model Oil. *Energy Fuels* **2013**, *28*, 1617-1628.

32. Tavakkoli, M.; Panuganti, S. R.; Taghikhani, V.; Pishvaie, M. R.; Chapman, W. G., Asphaltene Deposition in Different Depositing Environments: Part 2. Real Oil. *Energy Fuels* **2014**, *28*, 3594-3603.

33. Zhang, L.; Shi, C.; Lu, Q.; Liu, Q.; Zeng, H., Probing Molecular Interactions of Asphaltenes in Heptol Using a Surface Forces Apparatus: Implications on Stability of Water-in-Oil Emulsions. *Langmuir* **2016**, *32*, 4886-4895.

34. Shi, C.; Zhang, L.; Xie, L.; Lu, X.; Liu, Q.; He, J.; Mantilla, C. A.; Van den Berg, F. G.; Zeng, H., Surface Interaction of Water-in-Oil Emulsion Droplets with Interfacially Active Asphaltenes. *Langmuir* **2017**, *33*, 1265-1274.

35. Liu, J.; Xu, Z.; Masliyah, J., Studies on Bitumen− Silica Interaction in Aqueous Solutions by Atomic Force Microscopy. *Langmuir* **2003**, *19*, 3911-3920.

36. Liu, J.; Xu, Z.; Masliyah, J., Interaction between Bitumen and Fines in Oil Sands Extraction System: Implication to Bitumen Recovery. *Can. J. Chem. Eng.* **2004**, *82*, 655-666.

37. Long, J.; Zhang, L.; Xu, Z.; Masliyah, J. H., Colloidal Interactions between Langmuir− Blodgett Bitumen Films and Fine Solid Particles. *Langmuir* **2006**, *22*, 8831-8839.

38. Liu, J.; Xu, Z.; Masliyah, J., Role of Fine Clays in Bitumen Extraction from Oil Sands. *AIChE journal* **2004**, *50*, 1917-1927.

39. Zhang, Y.; Ding, M.; Liu, J.; Jia, W.; Ren, S., Studies on Bitumen–Silica Interaction in Surfactants and Divalent Cations Solutions by Atomic Force Microscopy. *Colloids Surf., A* **2015**, *482*, 241-247.

40. Liu, J.; Xu, Z.; Masliyah, J., Colloidal Forces between Bitumen Surfaces in Aqueous Solutions Measured with Atomic Force Microscope. *Colloids Surf., A* **2005**, *260*, 217-228.

41. Liu, J.; Xu, Z.; Masliyah, J., Interaction Forces in Bitumen Extraction from Oil Sands. *J. Colloid Interface Sci.* **2005**, *287*, 507-520.

42. Liu, J.; Zhang, L.; Xu, Z.; Masliyah, J., Colloidal Interactions between Asphaltene Surfaces in Aqueous Solutions. *Langmuir* **2006**, *22*, 1485-1492.

43. Long, J.; Xu, Z.; Masliyah, J. H., Single Molecule Force Spectroscopy of Asphaltene Aggregates. *Langmuir* **2007**, *23*, 6182-6190.

44. Long, J.; Xu, Z.; Masliyah, J. H., Role of Illite–Illite Interactions in Oil Sands Processing. *Colloids Surf., A* **2006**, *281*, 202-214.

45. Li, H.; Long, J.; Xu, Z.; Masliyah, J., Synergetic Role of Polymer Flocculant in Low-Temperature Bitumen Extraction and Tailings Treatment. *Energy Fuels* **2005**, *19*, 936-943.

46. Natarajan, A.; Xie, J.; Wang, S.; Liu, Q.; Masliyah, J.; Zeng, H.; Xu, Z., Understanding Molecular Interactions of Asphaltenes in Organic Solvents Using a Surface Force Apparatus. *J. Phys. Chem.* **2011**, *115*, 16043-16051.

47. Natarajan, A.; Kuznicki, N.; Harbottle, D.; Masliyah, J.; Zeng, H.; Xu, Z., Understanding Mechanisms of Asphaltene Adsorption from Organic Solvent on Mica. *Langmuir* **2014**, *30*, 9370-9377.

48. Wang, J.; van der Tuuk Opedal, N.; Lu, Q.; Xu, Z.; Zeng, H.; Sjöblom, J., Probing Molecular Interactions of an Asphaltene Model Compound in Organic Solvents Using a Surface Forces Apparatus (Sfa). *Energy Fuels* **2011**, *26*, 2591-2599.

49. Wang, S.; Liu, J.; Zhang, L.; Xu, Z.; Masliyah, J., Colloidal Interactions between Asphaltene Surfaces in Toluene. *Energy Fuels* **2008**, *23*, 862-869.

50. Israelachvili, J. N., *Intermolecular and Surface Forces*; Academic press, 2011.

51. Butt, H.-J.; Kappl, M.; Mueller, H.; Raiteri, R.; Meyer, W.; Rühe, J., Steric Forces Measured with the Atomic Force Microscope at Various Temperatures. *Langmuir* **1999**, *15*, 2559-2565.

52. Zhulina, E.; Borisov, O., Structure and Stabilizing Properties of Grafted Polymer Layers in a Polymer Medium. *J. Colloid Interface Sci.* **1991**, *144*, 507-520.

53. Farnand, J.; Meadus, F.; Sparks, B., Removal of Intractable Fine Solids from Bitumen Solutions Obtained by Solvent Extraction of Oil Sands. *Fuel Process. Technol.* **1985**, *10*, 131-144.

54. Brons, G.; Yu, J. M., Solvent Deasphalting Effects on Whole Cold Lake Bitumen. *Energy Fuels* **1995**, *9*, 641-647.

55. Gray, M. R.; Tykwinski, R. R.; Stryker, J. M.; Tan, X., Supramolecular Assembly Model for Aggregation of Petroleum Asphaltenes. *Energy Fuels* **2011**, *25*, 3125-3134.

56. Maqbool, T.; Balgoa, A. T.; Fogler, H. S., Revisiting Asphaltene Precipitation from Crude Oils: A Case of Neglected Kinetic Effects. *Energy Fuels* **2009**, *23*, 3681-3686.

57. Rao, F.; Liu, Q., Froth Treatment in Athabasca Oil Sands Bitumen Recovery Process: A Review. *Energy Fuels* **2013**, *27*, 7199-7207.

58. Kotlyar, L.; Sparks, B.; Woods, J.; Chung, K., Solids Associated with the Asphaltene Fraction of Oil Sands Bitumen. *Energy Fuels* **1999**, *13*, 346-350.

59. Painter, P.; Williams, P.; Lupinsky, A., Recovery of Bitumen from Utah Tar Sands Using Ionic Liquids. *Energy Fuels* **2010**, *24*, 5081-5088.

60. Painter, P.; Williams, P.; Mannebach, E., Recovery of Bitumen from Oil or Tar Sands Using Ionic Liquids. *Energy Fuels* **2009**, *24*, 1094-1098.

61. Pulati, N.; Lupinsky, A.; Miller, B.; Painter, P., Extraction of Bitumen from Oil Sands Using Deep Eutectic Ionic Liquid Analogues. *Energy Fuels* **2015**, *29*, 4927-4935.

62. Li, X.; Sun, W.; Wu, G.; He, L.; Li, H.; Sui, H., Ionic Liquid Enhanced Solvent Extraction for Bitumen Recovery from Oil Sands. *Energy Fuels* **2011**, *25*, 5224-5231.

63. Tourvieille, J.-N.; Larachi, F.; Duchesne, C.; Chen, J., Nir Hyperspectral Investigation of Extraction Kinetics of Ionic-Liquid Assisted Bitumen Extraction. *Chem. Eng. J.* **2017**, *308*, 1185-1199.

64. Hogshead, C. G.; Manias, E.; Williams, P.; Lupinsky, A.; Painter, P., Studies of Bitumen− Silica and Oil− Silica Interactions in Ionic Liquids. *Energy Fuels* **2010**, *25*, 293-299.

65. Li, X.; Wang, J.; He, L.; Sui, H.; Yin, W., Ionic Liquid-Assisted Solvent Extraction for Unconventional Oil Recovery: Computational Simulation and Experimental Tests. *Energy Fuels* **2016**, *30*, 7074-7081.

66. Meadus, F.; Bassaw, B.; Sparks, B., Solvent Extraction of Athabasca Oil-Sand in a Rotating Mill Part 2. Solids—Liquid Separation and Bitumen Quality. *Fuel Process. Technol.* **1982**, *6*, 289-300.

67. Nikakhtari, H.; Pal, K.; Wolf, S.; Choi, P.; Liu, Q.; Gray, M. R., Solvent Removal from Cyclohexane-Extracted Oil Sands Gangue. *Can. J. Chem. Eng.* **2016**, *94*, 408-414.

68. Jessop, P. G.; Phan, L.; Carrier, A.; Robinson, S.; Dürr, C. J.; Harjani, J. R., A Solvent Having Switchable Hydrophilicity. *Green Chemistry* **2010**, *12*, 809-814.

69. Holland, A.; Wechsler, D.; Patel, A.; Molloy, B. M.; Boyd, A. R.; Jessop, P. G., Separation of Bitumen from Oil Sands Using a Switchable Hydrophilicity Solvent. *Can. J. Chem.* **2012**, *90*, 805-810.

70. Sui, H.; Xu, L.; Li, X.; He, L., Understanding the Roles of Switchable-Hydrophilicity Tertiary Amines in Recovering Heavy Hydrocarbons from Oil Sands. *Chem. Eng. J.* **2016**, *290*, 312-318.

71. Atta, A. M.; Fadda, A. A.; Abdel-Rahman, A. A.-H.; Ismail, H. S.; Fouad, R. R., Application of New Modified Poly (Ethylene Oxide)-Block-Poly (Propylene Oxide)-Block-Poly (Ethylene Oxide) Copolymers as Demulsifier for Petroleum Crude Oil Emulsion. *J. Dispersion Sci. Technol.* **2012**, *33*, 775-785.

72. Peña, A. A.; Hirasaki, G. J.; Miller, C. A., Chemically Induced Destabilization of Water-in-Crude Oil Emulsions. *Ind. Eng. Chem. Res.* **2005**, *44*, 1139-1149.

73. Hirasaki, G. J.; Miller, C. A.; Raney, O. G.; Poindexter, M. K.; Nguyen, D. T.; Hera, J., Separation of Produced Emulsions from Surfactant Enhanced Oil Recovery Processes. *Energy Fuels* **2010**, *25*, 555-561.

74. Pensini, E.; Harbottle, D.; Yang, F.; Tchoukov, P.; Li, Z.; Kailey, I.; Behles, J.; Masliyah, J.; Xu, Z., Demulsification Mechanism of Asphaltene-Stabilized Water-in-Oil Emulsions by a Polymeric Ethylene Oxide–Propylene Oxide Demulsifier. *Energy Fuels* **2014**, *28*, 6760-6771.

75. Xu, Y.; Wu, J.; Dabros, T.; Hamza, H.; Venter, J., Optimizing the Polyethylene Oxide and Polypropylene Oxide Contents in Diethylenetriamine-Based Surfactants for Destabilization of a Water-in-Oil Emulsion. *Energy Fuels* **2005**, *19*, 916-921.

76. Feng, X.; Xu, Z.; Masliyah, J., Biodegradable Polymer for Demulsification of Water-in-Bitumen Emulsions. *Energy Fuels* **2008**, *23*, 451-456.

77. Feng, X.; Wang, S.; Hou, J.; Wang, L.; Cepuch, C.; Masliyah, J.; Xu, Z., Effect of Hydroxyl Content and Molecular Weight of Biodegradable Ethylcellulose on Demulsification of Water-in-Diluted Bitumen Emulsions. *Ind. Eng. Chem. Res.* **2011**, *50*, 6347-6354.

78. Feng, X.; Mussone, P.; Gao, S.; Wang, S.; Wu, S.-Y.; Masliyah, J. H.; Xu, Z., Mechanistic Study on Demulsification of Water-in-Diluted Bitumen Emulsions by Ethylcellulose. *Langmuir* **2009**, *26*, 3050-3057.

Chapter 2 Experimental Methodologies

2.1 Collection of fine solids

To study the surface properties of the fine solids, the fine solid particles were collected from the Athabasca oil sands using the protocol reported elsewhere.[1-2] Figure 2.1 shows a brief schematic of the protocol. Details on the procedure are summarized as follows: (1) 150 g Athabasca oil sands and 100 g cyclohexane were mixed for 10 min in a Teflon bottle mounted on a rotary mixer (60 rpm, Rotator drive STR4, Stuart Scientific); (2) the oil sands slurry was allowed to settle for 30 min in a graduated cylinder; (3) the first supernatant was withdrawn by siphoning and the sediment in the bottom portion was mixed with additional 50 g cyclohexane by the same method; (4) the second supernatant product was separated from the slurry through a 45-μm aperture sieve (ASTM E-11 Standard test sieve no 325, Fisher Scientific Co., USA); (5) the tailings retained on the sieve was rinsed with 2 batches of 50 g cyclohexane and the third supernatant was collected as the liquid passing through the sieve and (5) the second and third supernatants were combined (including fine solids and bitumen-solvent mixture) and then centrifuged (Avanti J-30I centrifuge, Beckman Coulter, Mississauga, ON) at 4000 relative centrifugal force (RCF) for 1 h to recover the fine solids from the supernatants. The collected fine solids were then thoroughly rinsed with toluene to remove the weakly adsorbed bitumen by placing the solids in a Millipore filter (0.22 μm pore-sized). This rinsing step was repeated until the filtrate became colorless. All steps were carried out at room temperature (24 ± 0.5°C) and ambient pressure.

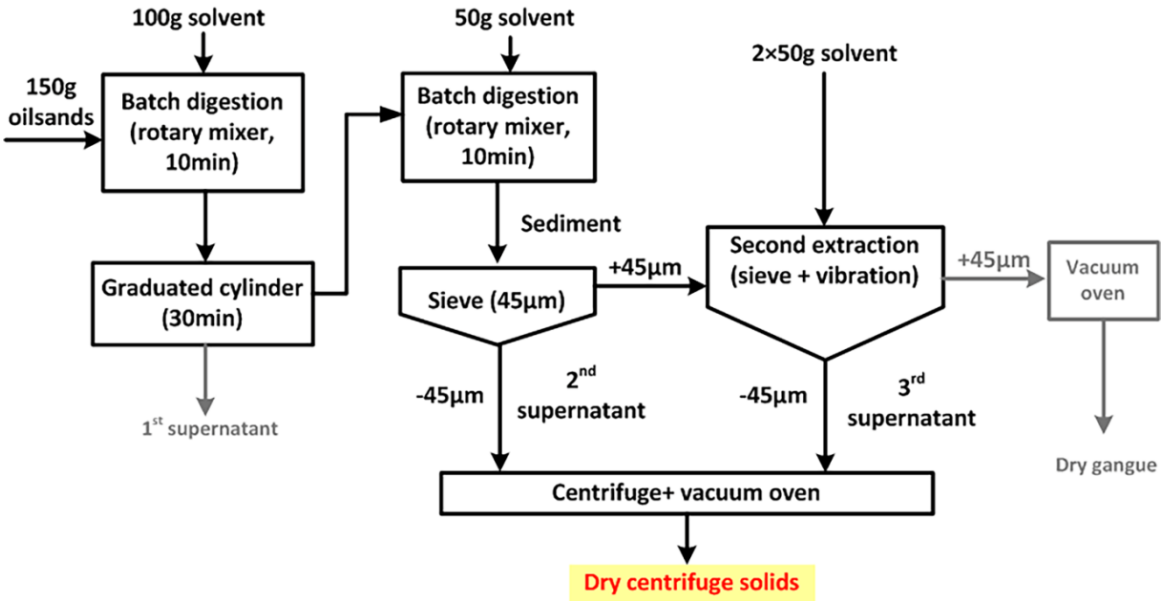

Figure 2. 1 Schematic of lab protocol for collecting fine mineral solids from oil sands using the non-aqueous extraction method.

2.2 Preparation of bitumen-coated solid substrate and particles

Both the flat bitumen-coated solid substrate and bitumen-coated solid particles were prepared by a dip-coating method. Prior to the dip-coating, a bitumen/cyclohexane solution (0.1 wt%) was prepared by diluting Athabasca bitumen with cyclohexane under ambient conditions. The bitumen solution was sonicated for 10 min to separate any large aggregates of bitumen apart. For the flat bitumen-coated solid surface, a clean silica wafer (~ 1×1 cm^2) was treated by UV/ozone to remove any organic contaminants on the silica surface, then immersed in the bitumen/cyclohexane solution for 10 min, thoroughly rinsed with both cyclohexane to remove any weakly adsorbed bitumen and blow-dried with nitrogen. For the bitumen-coated solid solids, the preparation procedure was a modified method according to the literature.[3] Briefly, about 10 g silica solid particles were dispersed in the bitumen/cyclohexane solution and the mixture was sonicated for 5 min to separate

any solids aggregates apart. Then the mixture was agitated for 10 min using a magnetic stirrer (1000 rpm) to allow the adsorption of bitumen onto the silica solid particles. The resulting solids were thoroughly washed in cyclohexane using repeatedly centrifugation (4000 rpm) to remove non-adsorbing bitumen or loose deposit from the solids surface. The centrifuged solids were collected and dried under fume hood over 48 h.

2.3 AFM force measurement

AFM has emerged as a practical tool to study interfacial force between two colloidal surfaces across a medium especially when that force comes to dispersing colloids in a liquid.[4-7] During the force measurement, the AFM probe was driven to approach the bottom surface and then started to retract from the surface until a pre-set deflection of the cantilever was reached. A plot of the deflection versus the displacement of the z-piezo device is obtained in each AFM measurement. The deflection of the cantilever is monitored by detecting the position of a laser beam reflected from cantilever onto a photo detector. Force between the probe and the bottom surface is converted from the deflection of the cantilever using Hooke's law. Although the AFM force measurement cannot provide the absolute probe-sample separation distance, it can measure the relative changes in the probe-sample separation between the base of the AFM probe and the base of the substrate. The schematic of typical AFM setup is shown in Figure 2. 2. The scanner is composed of three piezo components to control both the horizontal (x and y) and vertical (z) movement of the sample.

To measure forces more quantitatively and sensitively, the colloidal probe technique of AFM was first introduced in 1991. Ducker et al.[8] attached a silica microsphere to the end of AFM cantilever and Butt et al.[9] used glass beads. Then a direct force measurement between a single

microsphere and a flat surface could be determined. Up to now, numerous microsphere materials such as silica, zirconia, polymer and cellulose have been applied to produce colloidal probes in various colloidal systems.[10-13] In this work, silica microsphere was used as the colloidal probe to interact with bottom flat surface in organic solvents. The silica microsphere was glued to the end of a tipless AFM cantilever using an Epoxy adhesive under the integrated optical microscope of AFM. Details of preparing the colloidal probe have been given elsewhere.[14]

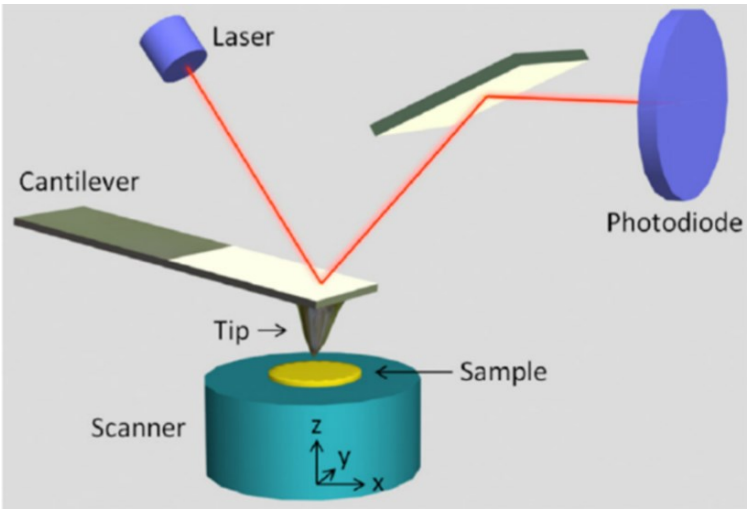

Figure 2. 2 Schematic illustration of working principle of AFM.[15]

2.4 QCM-D measurements

QCM-D is a nanoscale technique for analyzing surface phenomenon in real-time including thin film formation, interactions and reactions. A typical QCM-D sensor consists of a thin quartz crystal sandwiched between a pair of electrodes and have a fundamental resonance frequency of 5 MHz. Application of an alternating voltage results in the oscillation of the sensor at its resonance frequency. Since the driving voltage is intermittently switched off, the decay of the oscillation in time is monitored and the frequency *f* and the energy dissipation *D* of the freely oscillating sensor are extracted from the decay curve. Figure 2. 3 shows the QCM-D instrument used in this work

and working principle of the sensor as a sensitive balance. When a thin film is adsorbed to the sensor, the frequency decreases, which is proportional to the mass of the adhering layer if the film is thin and rigid. The mass of the rigid film can be calculated using the Sauerbrey relation:[16]

$$\Delta m = -\frac{C\Delta f}{n} \tag{2.1}$$

where Δm is adsorbed mass, Δf is the frequency shift, n = 1, 3, 5, 7, 9, 11 is the order number of harmonic overtones of the crystal sensor, C = 17.7 ng/(Hz·cm2) is the constant for a 5 MHz crystal sensor. It is also possible to estimate the thickness of the adhering layer:

$$d_{eff} = \frac{\Delta m}{\rho_{eff}} \tag{2.2}$$

where ρ_{eff} is the effective density of the adhering layer. When the film is soft and viscous, the Sauerbrey equation is not applicable. In that case, the viscoelastic and structural properties including the adsorbed mass can be obtained by measuring both frequencies and dissipations at multiple overtones according to the Voigt viscoelastic model incorporated in the Q-sensor software.

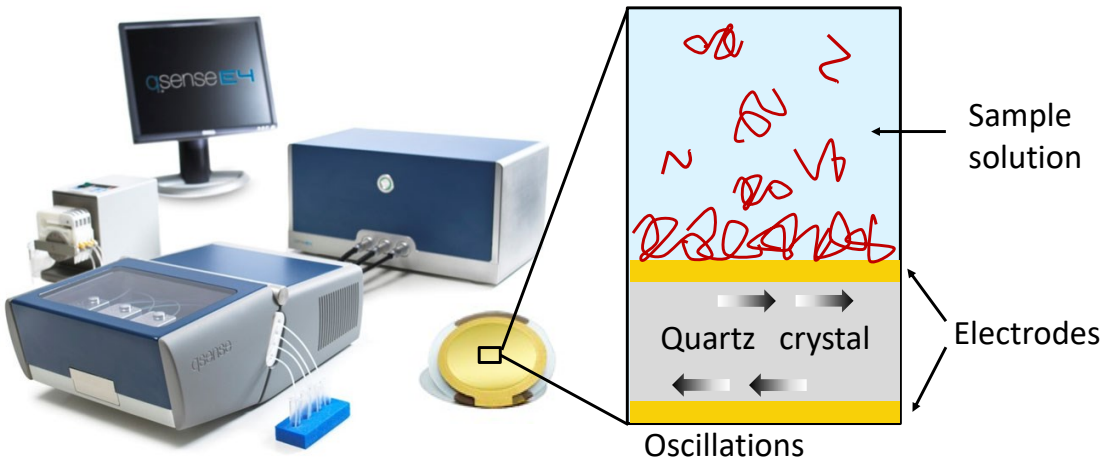

Figure 2. 3 QCM-D system and sensing principle.

Reference

1. Hooshiar, A.; Uhlik, P.; Liu, Q.; Etsell, T. H.; Ivey, D. G., Clay Minerals in Nonaqueous Extraction of Bitumen from Alberta Oil Sands: Part 1. Nonaqueous Extraction Procedure. *Fuel processing technology* **2012**, *94*, 80-85.

2. Nikakhtari, H.; Wolf, S.; Choi, P.; Liu, Q.; Gray, M. R., Migration of Fine Solids into Product Bitumen from Solvent Extraction of Alberta Oilsands. *Energy Fuels* **2014**, *28*, 2925-2932.

3. Jin, Y.; Liu, W.; Liu, Q.; Yeung, A., Aggregation of Silica Particles in Non-Aqueous Media. *Fuel* **2011**, *90*, 2592-2597.

4. Butt, H.-J.; Cappella, B.; Kappl, M., Force Measurements with the Atomic Force Microscope: Technique, Interpretation and Applications. *Surface science reports* **2005**, *59*, 1-152.

5. Cui, X.; Shi, C.; Xie, L.; Liu, J.; Zeng, H., Probing Interactions between Air Bubble and Hydrophobic Polymer Surface: Impact of Solution Salinity and Interfacial Nanobubbles. *Langmuir* **2016**, *32*, 11236-11244.

6. Xie, L.; Wang, J.; Shi, C.; Huang, J.; Zhang, H.; Liu, Q.; Liu, Q.; Zeng, H., Probing Surface Interactions of Electrochemically Active Galena Mineral Surface Using Atomic Force Microscopy. *J. Phys. Chem. C* **2016**, *120*, 22433-22442.

7. Cui, X.; Shi, C.; Zhang, S.; Xie, L.; Liu, J.; Jiang, D.; Zeng, H., Probing the Effect of Salinity and Ph on Surface Interactions between Air Bubbles and Hydrophobic Solids: Implications for Colloidal Assembly at Air/Water Interfaces. *Chemistry–An Asian Journal* **2017**, *12*, 1568-1577.

8. Ducker, W. A.; Senden, T. J.; Pashley, R. M., Direct Measurement of Colloidal Forces Using an Atomic Force Microscope. *nature* **1991**, *353*, 239.

9. Butt, H.-J., Measuring Electrostatic, Van Der Waals, and Hydration Forces in Electrolyte Solutions with an Atomic Force Microscope. *Biophysical Journal* **1991**, *60*, 1438-1444.

10. Hogshead, C. G.; Manias, E.; Williams, P.; Lupinsky, A.; Painter, P., Studies of Bitumen− Silica and Oil− Silica Interactions in Ionic Liquids. *Energy Fuels* **2010**, *25*, 293-299.

11. Pedersen, H. G.; Bergström, L., Forces Measured between Zirconia Surfaces in Poly (Acrylic Acid) Solutions. *Journal of the American Ceramic Society* **1999**, *82*, 1137-1145.

12. Nalaskowski, J.; Drelich, J.; Hupka, J.; Miller, J. D., Preparation of Hydrophobic Microspheres from Low-Temperature Melting Polymeric Materials. *Journal of adhesion science and technology* **1999**, *13*, 1-17.

13. Carambassis, A.; Rutland, M. W., Interactions of Cellulose Surfaces: Effect of Electrolyte. *Langmuir* **1999**, *15*, 5584-5590.

14. Wang, J.; Li, J.; Xie, L.; Shi, C.; Liu, Q.; Zeng, H., Interactions between Elemental Selenium and Hydrophilic/Hydrophobic Surfaces: Direct Force Measurements Using Afm. *Chem. Eng. J.***2016**, *303*, 646-654.

15. Zeng, G.; Duan, Y.; Besenbacher, F.; Dong, M., Nanomechanics of Amyloid Materials Studied by Atomic Force Microscopy. In *Atomic Force Microscopy Investigations into Biology-from Cell to Protein*, InTech: 2012.

16. Sauerbrey, G., Verwendung Von Schwingquarzen Zur Wägung Dünner Schichten Und Zur Mikrowägung. *Zeitschrift für physik* **1959**, *155*, 206-222.

Chapter 3 Heterogeneous Distribution of Adsorbed Bitumen on Fine Solids from Non-aqueous Extraction of Oil Sands

3.1. Introduction

The oil sands deposits in Alberta is the world's third-largest oil reserve.[1] Extraction of bitumen from oil sands ores is of vital importance in the oil production process. The current economical water-based extraction of oil sands, however, requires excessive fresh water usage, almost all of which ends up in toxic extraction tailings.[2-3] Extraction of oil sands using organic solvents has been considered as a potential alternative to the water-based extraction because it is capable of dramatically decreasing the need for fresh water and eliminating the challenging tailings issue resulted from the water extraction process.[4-9] Nevertheless, non-aqueous extraction process has not been commercialized despite the research efforts over the past two decades. One major problem impeding its industrial application is that considerable amounts of fine solids, several μm or less in size, can stably suspend in the bitumen-solvent mixture and migrate into the extracted bitumen products.[7] The presence of these fine solids renders the bitumen product unsuitable for pipeline transport and as refinery feed.[10-14]

Adsorbed organics on fine solids are believed to play an important role in the stability of fine solids in the complex organic media.[15] Previous studies show that bitumen components can strongly adsorb onto rock reservoirs and clays mostly due to physical adsorption (though chemical binding might be also present for some specific components), making the mineral solids more oil-wet.[16-18] The wettability of fine solids largely depends on the surface coverage of adsorbed bitumen,

consequently affecting the interactions of these fine particles and the degree of migration of fine solids into bitumen products during the non-aqueous extraction process.[19] It has been hypothesized in previous reports that the distribution of adsorbed bitumen on mineral particles is discontinuous.[10, 20] Thus, characterizing the surface properties of fine mineral solids and the distribution of adsorbed organics on surfaces of these solid particles has attracted consideration attention. The average wettability of these mineral particles was characterized by contact angle measurement.[19] Other analytic techniques such as time-of-flight secondary ion mass spectroscopy (ToF-SIMS)[21-22] and X-ray photoelectron spectroscopy (XPS)[23-24] have been also used to characterize the surface properties of the mineral solid particles. Nevertheless, characterizations of the particle surfaces and verification of heterogeneous distribution of adsorbed bitumen on fine solids still remain incomplete for the development of non-aqueous extraction process for the oil sands industry.

Atomic force microscope (AFM) is a useful technique for characterizing the distinct structures,[25-26] patterns[27-28] or functional sites[29-31] along with their distributions on various material surfaces in a wide range of research fields. AFM force mapping method was applied to characterize the distribution of specific molecular recognition sites on living cells by probing ligand-receptor interaction forces through a functionalized tip.[32-33] The AFM nanomechanical mapping in the so-called PeakForce quantitative nanomechanics (QNM) mode enables measurements of mechanical properties of materials at nano-scale, which can help distinguish the distribution of different material components on the surfaces. Lohse et al.[34] and Cui et al [35] have used the PeakForce QNM technique to characterize the distribution of nanobubbles or nanodroplets generated on hydrophobic substrates by distinguishing soft structures from the rigid substrates in terms of nano-mechanical properties. These previous studies suggest the applicability of AFM in characterizing

the distribution of adsorbed bitumen on the surface of mineral solids in the non-aqueous extraction process of oil sands.

In this work, the fine mineral solids were collected from the non-aqueous extraction process of Althabasca oil sands. Cyclohexane was used as the solvent for the extraction experiment due to its good performance with high bitumen recovery, high evaporation rate from extracted sands and low solids content in the recovered bitumen, , as reported previously.[7] The chemical compositions of solid surfaces were characterized using XPS and energy dispersive X-ray spectroscopy (EDX), and the wettability of solids was determined by contact angle measurements using Washburn method. The particle surfaces and distribution of adsorbed organics on fine solid particles were studied using PeakForce QNM imaging and AFM force mapping by characterizing the nano-mechanical properties and hydrophobicity across the mineral surfaces. This work provides useful insights into the surface properties and the interaction mechanism of the fine solids suspended in bitumen from the non-aqueous extraction process of oil sands, which is of both fundamental and practical importance for the oil industry.

3.2. Materials and experimental methods

3.2.1 Materials

The oil sands ore samples were rich-grade Athabasca oil sands ore provided by Syncrude Canada Ltd. The ore has 13.5 wt% bitumen, 3.0 wt% water, 11.2 wt% fine solids, and almost 70 wt% coarse sands. ACS grade cyclohexane (Fisher Scientific, Canada) was used as the solvent in the non-aqueous extraction process of oil sands. UV curing adhesive (Norland optical adhesive 81, Norland Products, Inc., NJ) was used for fixing centrifuged fine solids on the glass slide. Athabasca bitumen provided by Syncrude Canada Ltd was used to prepare bitumen coating as the model

sample. Silicon wafer with 0.5 μm thermal oxide (silica) (nanoFAB, University of Alberta) was used as the substrate of model samples. Octadecyltrichlorosilane (OTS) ($C_{18}H_{37}SiCl_3$, 95%, ACROS Organics) was used to prepare the hydrophobized AFM tip.

3.2.2. Collection of fine solids from oil sands

The protocol used in this work for the solvent extraction of bitumen from oil sands ores follows a reported procedure by Nikakhtari et al.[7] Details on collecting fine mineral solids from solvent-extracted bitumen can be found elsewhere,[9, 19] and the collection procedure used in this work are presented in Figure 2.1 and in section 2.1.

3.2.3. Particle size measurements

A laser diffraction particle size analyzer (Mastersizer 3000, Malvern Instruments) was used to determine the particle size distribution of centrifuged fine solids in terms of volume fraction. Small amount of fine solids sample (~ 0.5 g) was dispersed in cyclohexane and used for size distribution measurements.

3.2.4. Contact angle measurements

The hydrophobicity of the fine mineral solids was determined by contact angle measurement using a force tensiometer (Sigma700/701, Biolin Scientific) through the Washburn method.[36] Briefly, the fine solids were packed into an open-ended column with the bottom in contact with a probing liquid, which was water in this case. Due to the capillary force, the water rose in the column, obeying the relationship of equation 3.1,

$$t = \frac{\eta}{C_1 \rho^2 \gamma \cos\theta} M^2 \tag{3.1}$$

where t is the time after contact and M is the mass of water absorbed into the packed column. From the value of the slope $\eta/C_1\rho^2\gamma\cos\theta$, the contact angle θ can be determined with the known parameters of the liquid viscosity η, density ρ, surface tension γ and a material constant characteristic of solid sample C_1 which can be calibrated through measurements by applying a total wetting liquid, i.e. $\theta = 0°$.

3.2.5. Surface analysis of elemental composition

Scanning electron microscope (SEM) coupled with EDX (with a typical detection depth of several micrometers) was applied to characterize the surface chemical composition of the fine mineral solids. The chemical composition of fine solid surfaces was also characterized by X-ray photoelectron spectroscopy (XPS) (Kratos Axis 165) with Al Ka radiation (with a typical detection depth of several nanometers), operated at 12 mA, 14 kV. High-resolution spectra of C 1s, S 2p and N 1s regions were acquired with a pass energy of 40 eV and a dwell time of 160 ms, of which the peak fitting was performed by CasaXPS software.

3.2.6. Preparation of model samples

A 0.1 wt% bitumen/cyclohexane solution was prepared by diluting Athabasca bitumen with cyclohexane under ambient conditions. Bitumen surface was prepared by spin-coating 3-4 drops of bitumen solution on a clean silica wafer (~ 1×1 cm^2) with a layer of ~ 500 nm silica, which was later dried in vacuum overnight to evaporate residual solvent. The coated bitumen layer and the bare silica substrate without bitumen coating were used as the model samples in the AFM experiments.

3.2.7. PeakForce QNM AFM imaging

PeakForce QNM imaging, an operation mode of Dimension Icon AFM (Bruker, Santa Barbara, CA), is capable of mapping the nano-mechanical properties of material surfaces by acquiring and analyzing the force-separation curves simultaneously with topographic imaging.[37-39] By controlling the force (peak force) that the tip applies to the sample, PeakForce QNM imaging mode is able to acquire images with high spatial resolution. Prior to the AFM experiment, the fine solids were dispersed onto a layer of UV adhesive casted on a glass slide which was pre-cured by exposing to UV light for 4 min. The dispersed particle samples on a glass slide were viewed by the camera of the integrated optical microscope of AFM, with a typical microscopic view shown in Figure 3.1.

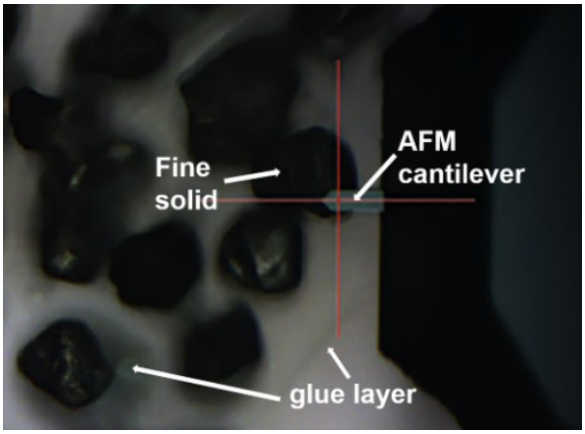

Figure 3. 1. Top view of the AFM tip and particle samples taken by the camera of the integrated optical microscope of AFM. The red cross indicates the location of the AFM tip.

Topography and mechanical properties of fine solid surfaces were recorded simultaneously in PeakForce QNM mode in air, with humidity of about 20% and temperature of 22 ºC, under which the possible capillary effect on AFM measurements could be neglected.[40] In this work, for the same type of AFM measurements, AFM mapping was conducted on the different locations of different particles to confirm the reproducibility of the data, and representative results are shown.

Figure 3.2 gives an example of the force-separation curve illustrating the types of mechanical properties that can be obtained. The adhesion force is the maximum force required to separate the AFM tip and the sample surface in the retraction curve. The deformation represents the penetration or indentation of the tip into the sample surface. The modulus information of solid sample is calculated using the Derjaguin-Muller-Toropov (DMT) model[41] that is applied to fit the retraction force-separation curve (the blue dash line in Figure 3.2).

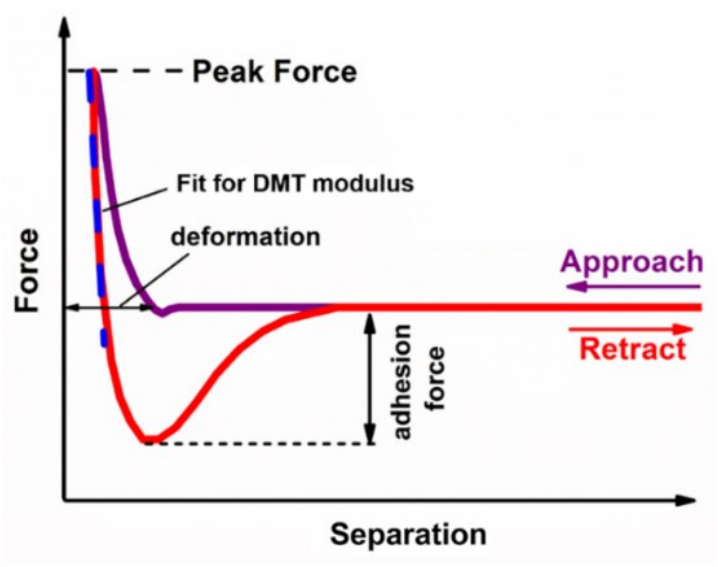

Figure 3. 2. Typical force–separation curve obtained during AFM imaging by PeakForce QNM.

DMT contact mechanics model takes the adhesion between the tip and the surface into account and its equation is given by:

$$F_{\text{tip}} = \frac{4}{3} E^* \sqrt{Rd^3} + F_{adh} \tag{3.2}$$

where F_{tip} is the force applied on the tip, F_{adh} is the adhesion force, R is the tip radius, d is instantaneous deformation of the sample, and E^* is the reduced Young's modulus. The relation between E^* and the sample's Young's modulus is given by:

$$E^* = \left[\frac{1-v_t^2}{E_t} + \frac{1-v_s^2}{E_s} \right]^{-1} \tag{3.3}$$

where v_t and E_t are the AFM tip's Poisson's ratio and Young's modulus, respectively, v_s and E_s are the sample's Poisson's ratio and Young's modulus, respectively. In this study, silicon nitride AFM cantilevers were used for the PeakForce QNM imaging on fine solid surfaces with a scan rate of 1 Hz. The spring constants of the cantilevers were determined using the Hutter and Bechhoefer method.[42] A typical cantilever has a spring constant of k = 42 N/m.

3.2.8. AFM force mapping in water

The surface hydrophobicity heterogeneity of fine solids was also characterized by AFM force mapping in water. Surface mapping of topography and adhesion force on fine solids was acquired using MPF-3D AFM (Asylum Research, Santa Barbara, CA). When the AFM tip was brought close to the sample surface, the deflection of cantilever was detected by a laser beam as a function of tip-sample separations and then converted to force using the Hooke's law. By using the AFM tip to raster-scan the sample surface, AFM force mapping can collect the force-separation curve at each pixel point of the image viewed.[43] AFM cantilevers, hydrophobized by a self-assembled monolayer of OTS following a procedure reported previously,[44-46] were applied to conduct the force mapping on fine solid surfaces. Briefly, the AFM cantilever was immersed in a freshly prepared hot piranha solution (a 3:1 (v/v) mixture of 98% H_2SO_4 and 30% H_2O_2) until no visible bubbles were released, followed by rinsing thoroughly with Milli-Q water and drying with N_2 flow. Then, the AFM cantilever was immediately transferred into a solution of 2.0 mM OTS in a 4:1 (v/v) mixture of hexane and chloroform for 24 h. Finally, the tip was rinsed thoroughly with chloroform and dried with N_2 flow.

The interactions between the AFM tip and the solid surface were analyzed by the theoretical model of classical Derjaguin-Landau-Verwey-Overbeek (DLVO) model,[47] which consists of electrical double layer forces (F_{edl}) and van der Waals forces (F_{vdW}) as given by equation 3.4 and equation 3.5, respectively:

$$F_{edl} = 4\pi\varepsilon_0\varepsilon\psi_1\psi_2(a_0e^{-\kappa D} - a_1e^{-\kappa L_1}) - 2\pi\varepsilon_0\varepsilon(\psi_1^2 + \psi_2^2)(a_2e^{-2\kappa D} - a_3e^{-2\kappa L_1}) + \frac{4\pi\varepsilon_0\varepsilon\kappa}{\tan\alpha}[b_1\psi_1\psi_2e^{-\kappa L_1} + b_2\frac{\psi_1^2 + \psi_2^2}{2}e^{-2\kappa L_1}] \quad (3.4)$$

$$F_{vdW} = \frac{A_{123}}{6}[\frac{R + D - 2L_1}{L_1^2} - \frac{R - D}{D^2}] - \frac{A}{3\tan^2\alpha}(\frac{1}{L_1} + \frac{R\sin\alpha\tan\alpha - D - R(1-\cos\alpha)}{2L_1^2}) \quad (3.5)$$

where ψ is the surface potential, ε the relative permittivity of medium, ε_0 the permittivity of vacuum, κ^{-1} the Debye length, R the tip radius, α the geometric angle for the spherical cap at the tip end, D the separation distance between the tip and the sample surface, A_{132} the Hamaker constant for the tip and the sample surface interacting across water, subscripts 1 and 2 refer to the tip and the sample surface, respectively. Other parameters are given by $L_1 = D + R(1-\cos\alpha)$, $a_0 = \kappa R - 1$, $a_1 = \kappa R\cos\alpha - 1$, $a_2 = a_0 + 0.5$, *and* $a_3 = a_1 + 0.5$. When the sample surface is hydrophobic, the additional hydrophobic interaction (F_{hb}) [48-49] should be included in the overall surface force to modify the DLVO model, as most commonly described by an empirical exponential expression:

$$F_{hb} = RCe^{-\frac{D}{D_0}} \quad (3.6)$$

where C is the pre-exponential constant and D_0 is the decay length of the hydrophobic interaction.

3.3 Results and Discussion

3.3.1. Size distribution of fine solids

Figure 3.3 shows the size distribution of the fine solids measured by the Malvern Mastersizer 3000. The peak of size distribution located at ~ 30 μm and the volume average particle size was 25 μm, indicating that majority of the solid particles was smaller than 45 μm. One possibility for the presence of small portion of solid particles larger than 45 μm could be due to the aggregation of small particles.

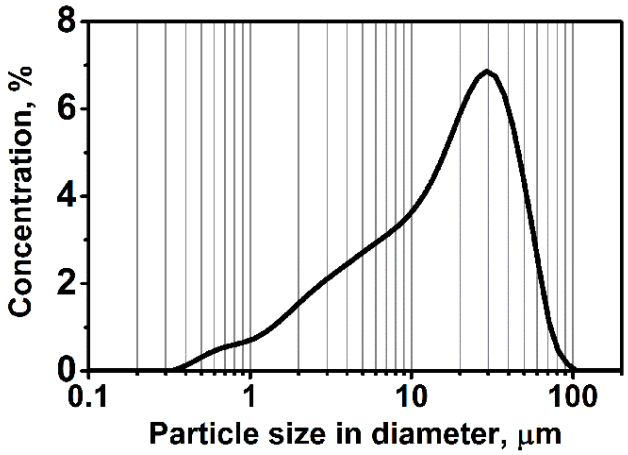

Figure 3. 3. Size distribution of the fine solid particles in terms of volume fraction which were collected using a protocol illustrated in Figure 2.1.

3.3.2 Verification of bitumen adsorbed on fine solids

The composition of solids particle surface was characterized by EDX analysis. It is evident from Table 3.1 that, the fine solids were mainly composed of silica (quartz) and aluminosilicate (clay) due to the high concentrations of oxygen (O), silicon (Si) and aluminum (Al). Other trace elements potassium (K), iron (Fe) and magnesium (Mg) could be assigned to the minor inorganic components such as pyrite, feldspar and magnesium carbonate. Figure 3.4A-D shows the SEM image of fine solids and EDX maps of main elements: O, Si and Al. The distributions of O and Si

were clearly observed through the field of view, and Al was not continuously distributed, suggesting that the aluminosilicate domains were surrounded by silica. High concentration of carbon (C) and small amounts of sulfur (S) were also detected, which could be attributed to either the mineral components (e.g. magnesium carbonate and pyrite) or the organic components (e.g. hydrocarbon) due to adsorbed bitumen. In the EDX mapping in Figure 3.4E-H, low concentration S was observed throughout the field of view in conjunction with Fe, indicating the presence of pyrite. When comparing the elemental maps of C and Mg, distributions of these two elements were not well matched, suggesting that C was mainly assigned to the organic deposits from bitumen. However, due to the low spatial resolution of EDX mapping, the EDX results could not provide the precise distribution of bitumen adsorbed on solid particle surface.

Table 3.1. Atomic percentage of different elements characterized by EDX of fine solids

Element	C	O	Si	Al	S	K	Fe	Mg
Atomic%	38.45	52.07	8.49	0.82	0.06	0.04	0.03	0.04

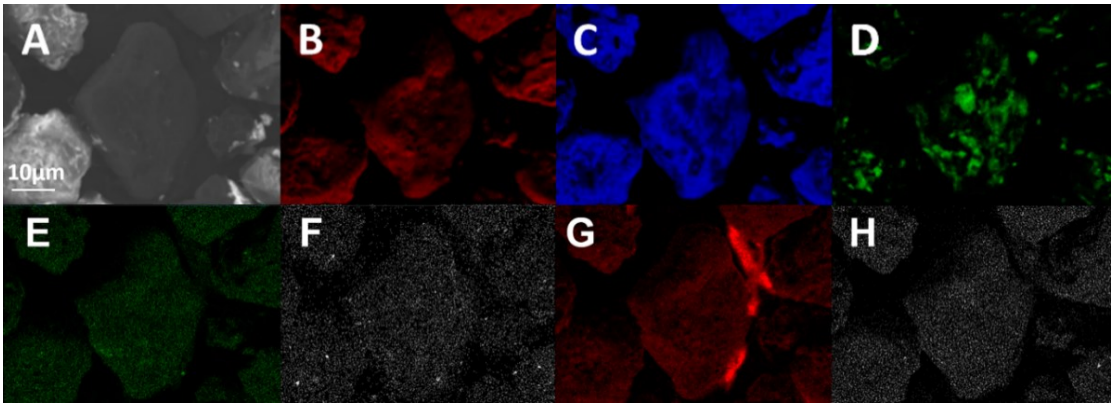

Figure 3. 4. (A)SEM secondary electron image of fine solids and EDX elemental maps of (B) O, (C) Si, (D) Al, (E) S, (F) Fe, (G) C and (H) Mg on fine solids.

XPS analysis was also applied to characterize the elemental composition and chemical state of the outer-most surface (a few nm) of the fine solids. The concentrations of major elements detected are summarized in Table 3.2, and the high-resolution electron binding energy spectra of C 1s, S 2p and N 1s were illustrated in Figure 3.5. It was noticed that C was highly concentrated (65.70 at%) on fine solid surfaces. The C 1s spectrum was deconvoluted into two peaks at 284.8 eV and 286.3 eV binding energy, respectively. The first peak was assigned to carbon in the aliphatic or aromatic C-H environment and the second one was assigned to C in the C-O environment (Figure 3.5A).[50-51] The concentrations of elements sulfur (S) and nitrogen (N), important heteroatoms in bitumen components, were 1.91 at% and 1.04 at% respectively on the fine solids surface. The S 2p spectrum was composed of two components S $2p_{3/2}$ at 165.2 eV and S $2p_{1/2}$ at 164.0 eV, assigned to the presence of thiophenic sulfur and sulfide (Figure 5B).[52-54] The N 1s spectrum at 398.7 eV and 400.2 eV was the characteristic of pyridinic and pyrrolic type nitrogen, respectively (Figure 5C).[52, 55] Therefore, it was evident from EDX and XPS analysis that bitumen was adsorbed on the surfaces of fine solids.

Table 3.2. Surface elemental analysis of fine solids by XPS

Element	C 1s	S 2p	N 1s	Si 2p	Al 2p	O 1s
Atomic%	65.70	1.91	1.04	8.04	4.01	19.3

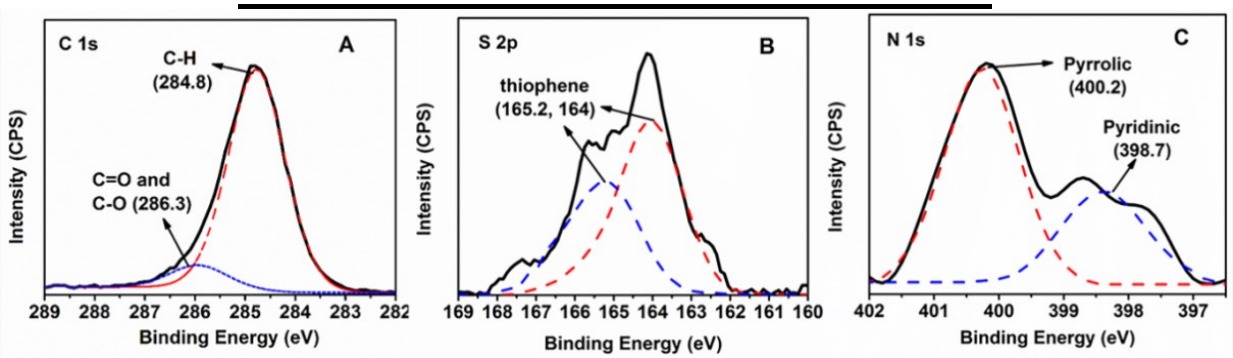

Figure 3. 5. (A) C 1s, (B) S 2p and (C) N 1s XPS spectra for fine solids with peak fit.

In addition to the above elements, Si, Al and O, representing silica and aluminosilicate, were also detected on the outer-most surface of the fine solids, with an abundance of 8.04 at%, 4.01 at% and 19.3 at%, respectively. The detected concentration of O was significantly higher than that detected in bitumen or asphaltene (0.88-5.9 at%) reported previously,20, 56 indicating that the detected O was mainly from the mineral components. The appearance of Si, Al and O suggested that a portion of solid surfaces might be exposed mineral materials without bitumen coating. The other possibility was that the detected Si, Al and O could be attributed to the mineral substrate beneath a thin layer (<10 nm) of adsorbed bitumen. To better characterize the distribution of bitumen adsorbed on fine solids, AFM technique was applied to probe the surface properties of fine solids, such as topography and interaction force behaviors.

3.3.3 Heterogeneity of nano-mechanical properties of fine solids

3.3.3.1 Force behaviors of bare mineral surface and bitumen layer

Interaction forces of bare mineral surface (i.e. bare silica) and bitumen layer coated on silica, as model surfaces, were studied by AFM. Figure 3.6A shows the topography image of the bare silica substrate, which is very smooth and has no visible feature. Figure 3.6B shows the topographic image of bitumen layer coated on silica substrate, which is composed of many self-associated bitumen aggregates[57-58] uniformly deposited on the surface, similar to previous results reported in the literature.[59] The interactions between the AFM tip and model surfaces were investigated by measuring the force-separation curves in air, as shown in Figure 3.6C (silica substrate) and Figure 3.6D (bitumen layer on silica substrate). In AFM force measurements, “jump-in” behavior could be observed when the tip was brought to approach the sample surface (blue curve), indicating that attraction (i.e. van de Waals interaction) between the two surfaces

drove the AFM tip to attach to the sample surface. During retraction (red curve) adhesion was measured and the AFM tip was suddenly detached from the sample surface corresponding to a so-called "jump-out" phenomenon.

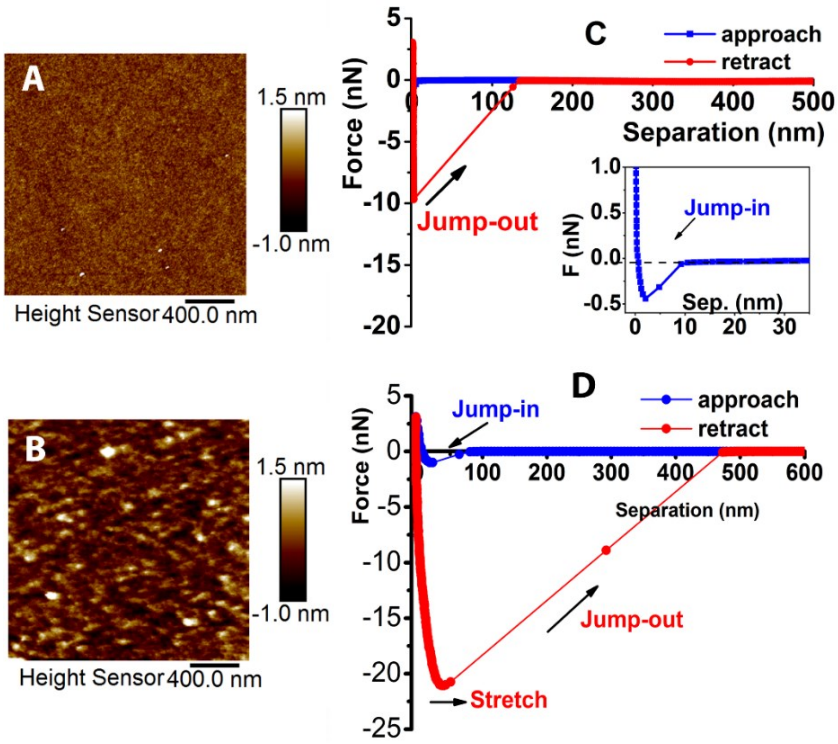

Figure 3. 6. Topographic AFM image of (A) bare silica substrate and (B) bitumen layer coated on silica substrate (~30 nm), and corresponding typical force-separation curves obtained on the surface of (C) bare silica substrate (D) bitumen layer (blue curve for approach, and red curve for retraction).

For the bare silica substrate (Figure 3. 6C), during approach the repulsive force after the "jump-in" behavior increased drastically as the tip was further lowered down and compressed against the bare silica substrate (inset of Figure 3. 6C); during retraction, adhesion was measured, showing a steep and sudden "jump-out" behavior. These interaction features on the force-separation curve suggest that the tip experienced a hard contact with the silica surface. In

comparison, for the bitumen coating surface (Figure 3.6D), the "jump-in" behavior was followed by a mild increase in the repulsive force because the bitumen surface was relatively soft and underwent a large deformation as the tip contacted with and was further compressed against the bitumen surface. Figure 3.6D also shows that the "jump-out" phenomenon in the bitumen coating case occurred at a much longer separation distance (around 35 nm) than that of the bare silica case (around 0 nm, Figure 3.6C), showing a long-range stretching behavior during the retraction process. Such stretching behavior was generally found to be a typical feature for retraction force curves when AFM tip was interacting with soft polymers or flexible aggregates.[60] Here, the stretching behavior was believed to be caused by the extension of bitumen aggregates due to the strong attraction between the bitumen layer and the AFM tip. Once the cantilever spring force reached the critical value (i.e. adhesion force), the AFM tip was detached from the stretched bitumen aggregates and the tip jumped apart from the bitumen surface.

By comparing the force curves of the bare silica case and bitumen coating case, it was noted that the measured adhesion on bitumen coating was much higher than that of silica substrate under the same applied force. The deformation of silica surface (~ 0.9 nm) was almost negligible as compared with that of the bitumen coating (~ 8 nm). Based on equation 3.2, the DMT moduli values of silica and bitumen layer could be calculated to be 1.3 GPa and 0.1 GPa, respectively. It should be noted that due to the limitation of the cantilever stiffness and the small indentation depth, the DMT modulus fitted through the PeakForce QNM software might not quantitatively match the bulk modulus values of materials measured at macroscale. Taking the bare silica case as an example, the relative modulus obtained here was about 1.3 GPa, which was much lower than the reported values of silica (74 ± 2 GPa) from 150 nm of indentation depth with sharp diamond as the indenter.[61] Nevertheless, the apparent contrast of relative moduli calculated, combined with

the information on adhesion, deformation and force curves, could still clearly distinguish the model bitumen surface from the bare silica surface. In addition, these nanoscale mechanical properties and interaction behaviors could be used as references to help determine the distribution of adsorbed bitumen on fine solids in the PeakForce QNM imaging (discussed below).

3.3.2. PeakForce QNM imaging over fine solids in Air

Fine solid particle was imaged by PeakForce QNM to provide information on the topography, adhesion, deformation and DMT modulus as illustrated in Figure 3.7A-D. The topography image (Figure 3.7A) shows that the imaged area (3 × 3 μm) of the solid surface was uniform except for a few protrusions, which however could not tell much more information on the distribution of adsorbed bitumen. The notable contrasts in channels of mechanical properties (Figure 3.7B-D) indicated the presence of different materials on the imaged area. Based on the results obtained on model silica substrate and bitumen layer, in Figure 3.7B, the high adhesion region highlighted by the red dash line should correspond to the adsorbed bitumen, while the low adhesion region highlighted in green dash line should correspond to the mineral surface. The region between the red dash line zone and the green dash line zone was believed to be mineral surface with a very thin layer (e.g. nm thickness) of adsorbed bitumen. This conclusion could be further supported by the DMT modulus and deformation results in the two regimes (i.e., adsorbed bitumen exhibited larger deformation but lower DMT modulus than mineral surface), as shown in Figure 3.7C and 3.7D.

More detailed deformation and modulus information of the fine mineral solid on the imaged area was shown in Figure 3.7E-F. The deformation values of adsorbed bitumen and mineral surface can be clearly viewed by the cross-section analysis (Figure 3.7E), which were ~10

nm (red line) and ~1 nm (green line), respectively. This result was consistent with deformation values on model samples by the force-distance curve measurements in Figure 3.6. Very recently, Lorenzoni et al.[62] found that surface deformation is the key parameter in determining the DMT modulus calculated by the PeakForce software, and modulus value of material surface remains constant under the same deformation condition. Herein, the modulus histogram graph according to the modulus mapping (Figure 3.7C) was ploted with Gaussian fitting (Figure 3.7F). Two separated peaks located at 0.2 GPa (sharp peak) and 1.8 Gpa (broad peak) were contributed by the adsorbed bitumen and the exposed mineral surface, respectively, matching the relative moduli on model samples in Figure 3.6.

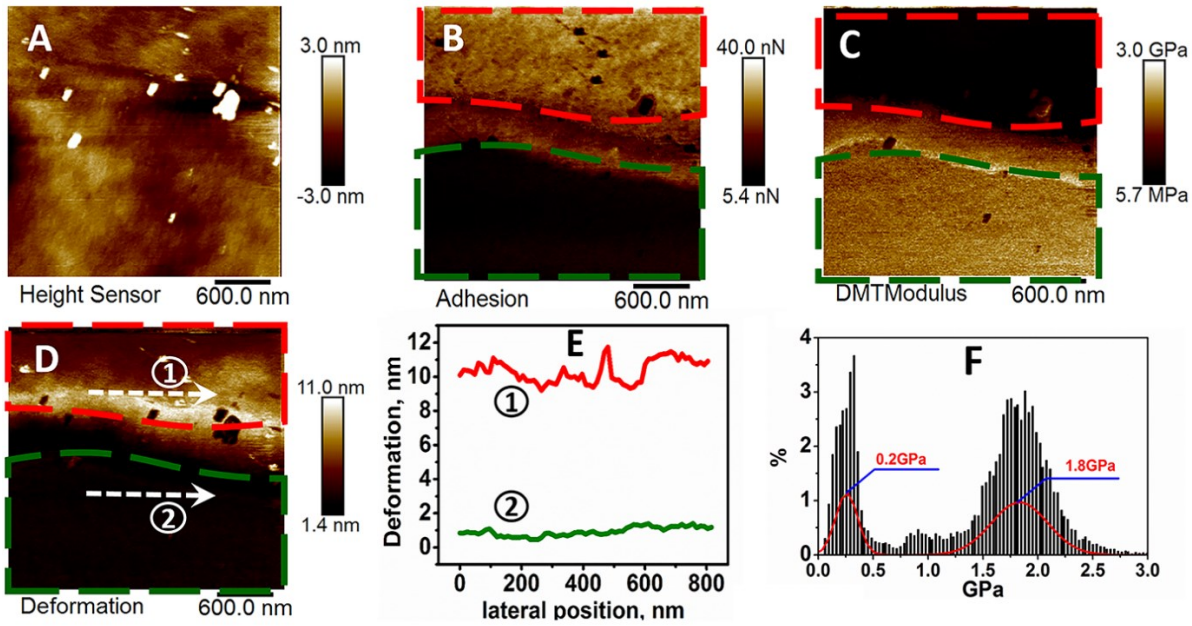

Figure 3. 7. Representative maps (3 × 3 μm) of (A) topography, (B) adhesion force, (C) DMT modulus and (D) deformation obtained on a solid particle surface by PeakForce QNM in air, (E) cross-section analysis of deformation corresponding to the white dash line in panel (D), and (F) histogram of modulus map with Gaussian fittings.

3.3.4 Heterogeneity of surface hydrophobicity of fine solids

Recent study by Nikakhtari et al.[19] reported that the water contact angle of centrifuged fine solids from bitumen product was in the range of 80-88º, which was significantly higher than the Soxhlet extracted fine solids (23-42º) but lower than bitumen (92-98º).[63] In this work, using the Washburn method, the water contact angle of the collected fine solids was determined to be 88.8 ± 0.9º, which agrees with the water contact angle (80-88º) on the compressed particle bed measured using the sessile drop method.[19] The result of contact angle measurement suggested that adsorbed bitumen could increase the surface hydrophobicity of fine mineral solids. Therefore, hydrophobicity at nanoscale could be another parameter to characterize the distribution of bitumen adsorbed on fine mineral solids.

Previous studies showed that the hydrophobic attraction dominated between a hydrophobic AFM tip and the hydrophobic sample surface, while was absent on the hydrophilic surface.[45] Through AFM force mapping in water, the distribution of hydrophobic domains across fine solid surfaces was studied in this work. Figure 3. 8 shows the topography image and adhesion force mapping of fine solid surfaces in water probed by a hydrophobized AFM tip. The topography image (Figure 3. 8A) could not provide direct and convincing evidence of heterogeneous distribution of adsorbed bitumen on mineral particle surface; however, the notable contrast of adhesion force in Figure 3.8B indicated the presence of surface material heterogeneity on the imaged area, and distinguished interaction behaviors of tip-sample at different regimes across the solid surface (viz. the regimes with brighter colors showed higher adhesion).

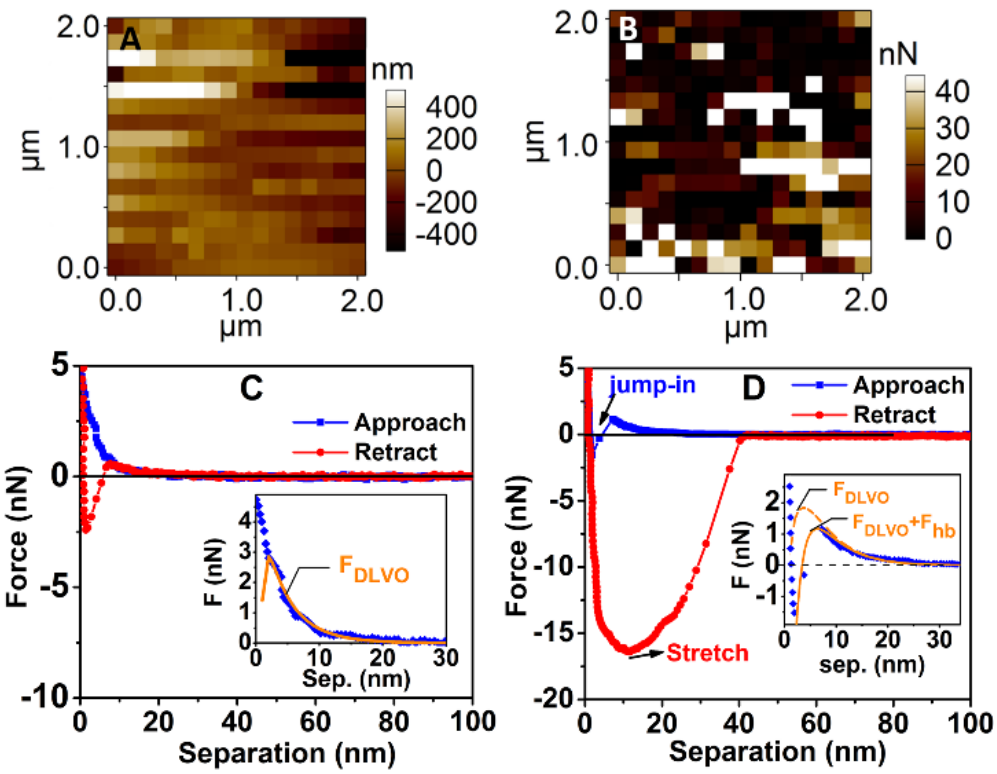

Figure 3. 8. Images of (A) topography and (B) adhesion force of fine solid surfaces characterized by AFM force mapping in water using a hydrophobized Si_3N_4 tip, respectively, and force-separation curves obtained on (C) the dark and (D) bright regions in panel (B), respectively.

The typical force-separation curve obtained on the dark regime of the force mapping (Figure 3.8B) was shown in Figure 3.8C. No obvious "jump-in" behavior occurred as the tip approached the sample surface, and a long-range repulsion starting at ~ 30 nm was observed and increased gradually with approaching. During retraction, the steep and sudden "jump-out" behavior indicated that AFM tip experienced a hard contact with the sample surface in the dark regime. In comparison, the force-separation curve recorded on the bright regime, as shown in Figure 3.8D, exhibited a sudden "jump-in" behavior where the interaction force drastically turned from repulsion to attraction during approach. In addition, a much stronger adhesion force accompanied by the stretching behavior was observed when the AFM tip was separated from the

sample surface, indicating that the material on the bright regime was relatively soft. Based on these interaction features, the bright regimes are assigned to hydrophobic domains with adsorbed bitumen and the dark regimes are believed to the more hydrophilic mineral domains.

To further analyze the force-separation curves, DLVO and modified DLVO models as given by Equation (4) - (6) were applied to fit the approach force curves (blue lines). For the mineral surface regime, the approach force-separation curve could be well fitted by the classical DLVO model (orange solid curve), as shown in the inset of Figure 3.8C, with fitted surface potentials ψ_1 = -80 mV, ψ_2 = -70 mV for AFM tip and mineral surface, respectively. In this case, the effective Hamaker constant A_{132} = 1.13 × 10^{-20} J was calculated by the combining relation $A_{132} \approx (\sqrt{A_{11}} - \sqrt{A_{33}})(\sqrt{A_{22}} - \sqrt{A_{33}})$,[64] where A_{11}, A_{22} and A_{33} are the Hamaker constants for AFM tip, mineral surface (i.e. silica as the representative) and water interacting with the identical phase across vacuum, respectively. The fitted value of ψ_1 = -80 mV for AFM tip surface hydrophobized by OTS was consistent with previous report.65 Thus, the same surface potential value of ψ_1 was used in fitting the interaction between adsorbed bitumen and the OTS-hydrophobized tip (discussed below). The fitted value of ψ_2 = -70 mV for mineral surface agreed with the reported surface potential of silica surface in pure water at pH = 5.6,[66] which was consistent with the XPS results that the majority of mineral composition of fine solids was silica.

For the adsorbed bitumen, the approach force-separation curve could not be well fitted by the classical DLVO model, and the attractive hydrophobic interaction was consequently considered in this case. The inset curves in Figure 3. 8D illustrated that the force curve can be well fitted by the modified DLVO model by including the hydrophobic interaction, with calculated A_{132} = 6.86×10^{-21} J and fitted parameters ψ_2 = -90 mV, C = -20.4 mN/m and D_0 = 1.6 nm. The fitted ψ_2 = -90 mV for the adsorbed bitumen was comparable to the experimental values of bitumen layer

in water reported elsewhere.[47] The pre-exponential factor C is associated with the change in the surface (interfacial) free energy of the system during the interaction process. In this work, the C was theoretically determined to be -20.4 mN/m. D_0 is the characteristic parameter describing the decaying behavior of the hydrophobic interaction with the separation between the two interacting hydrophobic surfaces. Here, D_0 was theoretically fitted to be 1.6 nm, also falling in the range of the reported decay length of hydrophobic interaction varying from ~ 1.0 nm to several nm for different hydrophobic solid systems.[46, 49, 67] The "jump-in" behavior during approach due to hydrophobic attraction, enhanced adhesion and "stretching" behavior during separation have clearly confirmed the presence of bitumen adsorbed on bright regimes on particle surface in Figure 3. 8B. The above results have further demonstrated that AFM force mapping on fine mineral solids in water is capable of distinguishing adsorbed bitumen from the exposed mineral surface.

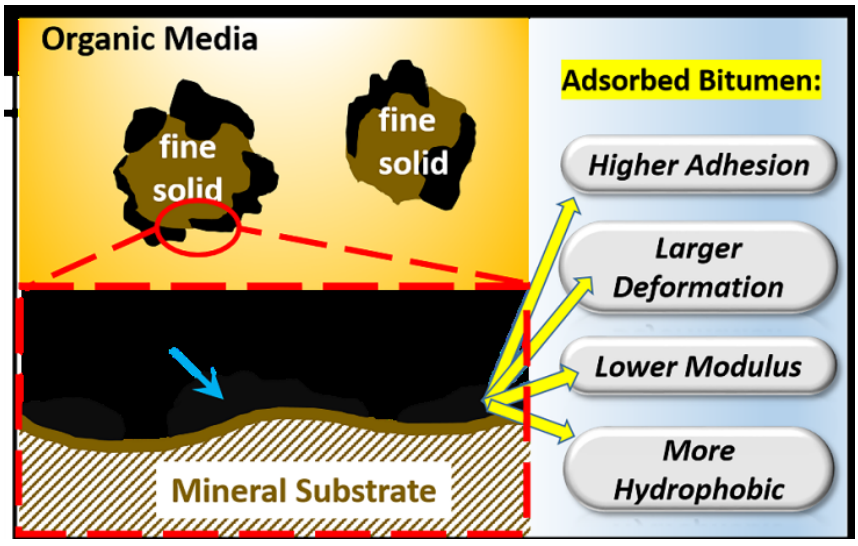

Figure 3. 9. Schematic of characterizing distribution of bitumen adsorbed on fine mineral solids by AFM technique.

3.4. Conclusions

Bitumen adsorbed on mineral solids plays an important role in the stability of these solid particles in oil product in oil sands production. In this study, the surface properties of fine mineral solids collected from the non-aqueous extraction of Athabasca oil sands were characterized by several complementary techniques. Elemental analysis and contact angle measurements on the surfaces of fine solids showed a strong signature of adsorbed bitumen that was found to partially (instead of completely) cover the solid surfaces. The distribution of adsorbed bitumen on fine solid surfaces was further characterized using AFM techniques by probing nano-mechanical properties (i.e. adhesion, deformation and DMT modulus) and surface hydrophobicity of fine solids, respectively (as illustrated in Figure 3.9). To study nano-mechanical properties of bitumen-adsorbed fine solids, interaction features on force-separation curves were first obtained on model surfaces (i.e. bare silica substrate and bitumen layer) and used as references. AFM force measurements showed that the bitumen layer had a stretching behavior with AFM tip during separation accompanied with higher adhesion, larger deformation and lower modulus as compared to that for bare silica surface under the same conditions. Based on these observations, regimes with and without adsorbed bitumen on fine solid surfaces were successfully identified and distinguished using the PeakForce QNM imaging in air, demonstrating that adsorbed bitumen was heterogeneously distributed on mineral surfaces. Such heterogeneity was further confirmed by AFM force mapping using a hydrophobized AFM tip on fine solids in water. The force-separation profiles obtained on relative hydrophilic mineral regimes could be well fitted by the classical DLVO theory, while additional hydrophobic interaction should be included for the interaction on more hydrophobic domains (due to the presence of bitumen adsorbed on mineral surface). The hydrophobic attraction between hydrophobized AFM tip and adsorbed bitumen led to an obvious

"jump in" behavior during approach and relatively long-range "stretching" during separation, with significantly enhanced adhesion as compared to that on more hydrophilic mineral regimes in the AFM force mapping. This work has provided a facile and useful methodology for characterizing the surface properties of bitumen adsorbed fine solids in oil production, which can be readily extended to the characterization of other solids with heterogeneous surface properties. Our results have clearly demonstrated the heterogeneous distribution of bitumen adsorbed on mineral particles (Figure 3.9), with important implications for better understanding the interaction mechanisms of solid particles suspended in bitumen products in oil production.

References

1. Czarnecki, J.; Radoev, B.; Schramm, L. L.; Slavchev, R., On the Nature of Athabasca Oil Sands. *Adv. Colloid Interface Sci.* **2005**, *114*, 53-60.

2. Wang, S.; Zhang, L.; Yan, B.; Xu, H.; Liu, Q.; Zeng, H., Molecular and Surface Interactions between Polymer Flocculant Chitosan-G-Polyacrylamide and Kaolinite Particles: Impact of Salinity. *J. Phys. Chem. C* **2015**, *119*, 7327-7339.

3. Allen, E. W., Process Water Treatment in Canada's Oil Sands Industry: Ii. A Review of Emerging Technologies. *J. Environ. Eng. Sci.* **2008**, *7*, 499-524.

4. Hanson, D. O.; Sherk, F. T., Solvent Extraction of Tar Sand. Google Patents: 1979.

5. Funk, E. W.; May, W. G.; Pirkle Jr, J. C., Solvent Extraction Process for Tar Sands. Google Patents: 1982.

6. Wang, T.; Zhang, C.; Zhao, R.; Zhu, C.; Yang, C.; Liu, C., Solvent Extraction of Bitumen from Oil Sands. *Energy Fuels* **2014**, *28*, 2297-2304.

7. Nikakhtari, H.; Vagi, L.; Choi, P.; Liu, Q.; Gray, M. R., Solvent Screening for Non-Aqueous

Extraction of Alberta Oil Sands. *Can. J. Chem. Eng.* **2013**, *91*, 1153-1160.

8. Meadus, F.; Bassaw, B.; Sparks, B., Solvent Extraction of Athabasca Oil-Sand in a Rotating Mill Part 2. Solids-Liquid Separation and Bitumen Quality. *Fuel Process. Technol.* **1982**, *6*, 289-300.

9. Hooshiar, A.; Uhlik, P.; Liu, Q.; Etsell, T. H.; Ivey, D. G., Clay Minerals in Nonaqueous Extraction of Bitumen from Alberta Oil Sands: Part 1. Nonaqueous Extraction Procedure. *Fuel Process. Technol.* **2012**, *94*, 80-85.

10. Bensebaa, F.; Kotlyar, L. S.; Sparks, B. D.; Chung, K. H., Organic Coated Solids in Athabasca Bitumen: Characterization and Process Implications. *Can. J. Chem. Eng.* **2000**, *78*, 610-616.

11. Osacky, M.; Geramian, M.; Ivey, D. G.; Liu, Q.; Etsell, T. H., Mineralogical and Chemical Composition of Petrologic End Members of Alberta Oil Sands. *Fuel* **2013**, *113*, 148-157.

12. Wang, S.; Chung, K.; Masliyah, J. H.; Gray, M. R., Toluene-Insoluble Fraction from Thermal Cracking of Athabasca Gas Oil: Formation of a Liquid-in-Oil Emulsion That Wets Hydrophobic Dispersed Solids. *Fuel* **1998**, *77*, 1647-1653.

13. Chaisoontornyotin, W.; Haji-Akbari, N.; Fogler, H. S.; Hoepfner, M. P., Combined Asphaltene Aggregation and Deposition Investigation. *Energy Fuels* **2016**, *30*, 1979-1986.

14. Abdallah, D.; Al-Basry, A. H.; Zwolle, S.; Grutters, M.; Huo, Z.; Stankiewicz, A. In *Asphaltene Studies in on-Shore Abu Dhabi Oil Fields, Part Ii: Investigation and Mitigation of Asphaltene Deposition-a Case Study*, Abu Dhabi International Petroleum Exhibition and Conference, Society of Petroleum Engineers: 2010.

15. Jin, Y.; Liu, W.; Liu, Q.; Yeung, A., Aggregation of Silica Particles in Non-Aqueous Media. *Fuel* **2011**, *90*, 2592-2597.

16. Farnand, J.; Meadus, F.; Sparks, B., Removal of Intractable Fine Solids from Bitumen Solutions Obtained by Solvent Extraction of Oil Sands. *Fuel Process. Technol.* **1985**, *10*, 131-144.

17. Pernyeszi, T.; Patzko, A.; Berkesi, O.; Dékány, I., Asphaltene Adsorption on Clays and Crude Oil Reservoir Rocks. *Colloids Surf., A* **1998**, *137*, 373-384.

18. Liu, X.; Yan, W.; Stenby, E. H.; Thormann, E., Release of Crude Oil from Silica and Calcium Carbonate Surfaces: On the Alternation of Surface and Molecular Forces by High-and Low-Salinity Aqueous Salt Solutions. *Energy Fuels* **2016**, *30*, 3986-3993.

19. Nikakhtari, H.; Wolf, S.; Choi, P.; Liu, Q.; Gray, M. R., Migration of Fine Solids into Product Bitumen from Solvent Extraction of Alberta Oilsands. *Energy Fuels* **2014**, *28*, 2925-2932.

20. Wang, S.; Liu, Q.; Tan, X.; Xu, C.; Gray, M. R., Study of Asphaltene Adsorption on Kaolinite by X-Ray Photoelectron Spectroscopy and Time-of-Flight Secondary Ion Mass Spectroscopy. *Energy Fuels* **2013**, *27*, 2465-2473.

21. Tu, Y.; Kingston, D.; Kung, J.; Kotlyar, L. S.; Sparks, B. D.; Chung, K. H., Adsorption of Pentane Insoluble Organic Matter from Oilsands Bitumen onto Clay Surfaces. *Pet. Sci. Technol.* **2006**, *24*, 327-338.

22. Sparks, B.; Kotlyar, L.; O'Carroll, J.; Chung, K., Athabasca Oil Sands: Effect of Organic Coated Solids on Bitumen Recovery and Quality. *J. Pet. Sci. Eng.* **2003**, *39*, 417-430.

23. Durand, C.; Beccat, P., Use of Xps for Reservoir Sandstone Wettability Evaluation. Application to Kaolinite and Illite. *J. Pet. Sci. Eng.* **1998**, *20*, 259-265.

24. Abdallah, W. A.; Taylor, S. D., Study of Asphaltenes Adsorption on Metallic Surface Using Xps and Tof-Sims. *J. Phys. Chem. C* **2008**, *112*, 18963-18972.

25. Guo, S.; Akhremitchev, B. B., Packing Density and Structural Heterogeneity of Insulin Amyloid Fibrils Measured by AFM Nanoindentation. *Biomacromolecules* **2006**, *7*, 1630-1636.

26. Quist, A.; Doudevski, I.; Lin, H.; Azimova, R.; Ng, D.; Frangione, B.; Kagan, B.; Ghiso, J.; Lal, R., Amyloid Ion Channels: A Common Structural Link for Protein-Misfolding Disease. *Proc. Natl. Acad. Sci. U.S.A.* **2005**, *102*, 10427-10432.

27. Pauli, A.; Grimes, R.; Beemer, A.; Turner, T.; Branthaver, J., Morphology of Asphalts, Asphalt Fractions and Model Wax-Doped Asphalts Studied by Atomic Force Microscopy. *Int. J. Pavement Eng.* **2011**, *12*, 291-309.

28. Schön, P.; Bagdi, K.; Molnár, K.; Markus, P.; Pukánszky, B.; Vancso, G. J., Quantitative Mapping of Elastic Moduli at the Nanoscale in Phase Separated Polyurethanes by AFM. *Eur. Polym. J.* **2011**, *47*, 692-698.

29. Jogikalmath, G.; Stuart, J.; Pungor, A.; Hlady, V., Adhesion Mapping of Chemically Modified and Poly (Ethylene Oxide)-Grafted Glass Surfaces. *Colloids Surf., A* **1999**, *154*, 53-64.

30. Huang, Y.-W.; Gupta, V. K., A Spr and AFM Study of the Effect of Surface Heterogeneity on Adsorption of Proteins. *J. Chem. Phys.* **2004**, *121*, 2264-2271.

31. Dufrêne, Y. F.; Martínez-Martín, D.; Medalsy, I.; Alsteens, D.; Müller, D. J., Multiparametric Imaging of Biological Systems by Force-Distance Curve-Based AFM. *Nat. Methods* **2013**, *10*, 847-854.

32. Hinterdorfer, P.; Dufrêne, Y. F., Detection and Localization of Single Molecular Recognition Events Using Atomic Force Microscopy. *Nat. Methods* **2006**, *3*, 347-355.

33. Dupres, V.; Menozzi, F. D.; Locht, C.; Clare, B. H.; Abbott, N. L.; Cuenot, S.; Bompard, C.; Raze, D.; Dufrêne, Y. F., Nanoscale Mapping and Functional Analysis of Individual Adhesins on Living Bacteria. *Nat. Methods* **2005**, *2*, 515-520.

34. Lohse, D.; Zhang, X., Surface Nanobubbles and Nanodroplets. *Rev. Mod. Phys.* **2015**, *87*, 981.

35. Cui, X.; Shi, C.; Xie, L.; Liu, J.; Zeng, H., Probing Interactions between Air Bubble and Hydrophobic Polymer Surface: Impact of Solution Salinity and Interfacial Nanobubbles. *Langmuir* **2016**, *32*, 11236-11244.

36. Neirinck, B.; Van Deursen, J.; Van der Biest, O.; Vleugels, J., Wettability Assessment of Submicrometer Alumina Powder Using a Modified Washburn Method. *J. Am. Ceram. Soc.* **2010**, *93*, 2515-2518.

37. Pittenger, B.; Erina, N.; Su, C., Quantitative Mechanical Property Mapping at the Nanoscale with Peakforce Qnm. *Application Note Veeco Instruments Inc* **2010**.

38. Nahar, S.; Schmets, A.; Schitter, G.; Scarpas, A. In *Quantitative Nanomechanical Property Mapping of Bitumen Micro-Phases by Peak-Force Atomic Force Microscopy*, 12th ISAP Conference on 30 Asphalt Pavements, 2014.

39. Sababi, M.; Kettle, J.; Rautkoski, H.; Claesson, P. M.; Thormann, E., Structural and Nanomechanical Properties of Paperboard Coatings Studied by Peak Force Tapping Atomic Force Microscopy. *ACS Appl. Mater. Interfaces* **2012**, *4*, 5534-5541.

40. Xiao, X.; Qian, L., Investigation of Humidity-Dependent Capillary Force. *Langmuir* **2000**, *16*, 8153-8158.

41. Maugis, D., *Contact, Adhesion and Rupture of Elastic Solids*; Springer Science & Business Media, 2013; Vol. 130.

42. Hutter, J. L.; Bechhoefer, J., Calibration of Atomic-Force Microscope Tips. *Rev. Sci. Instrum.* **1993**, *64*, 1868-1873.

43. Green, N. H.; Allen, S.; Davies, M. C.; Roberts, C. J.; Tendler, S. J.; Williams, P. M., Force Sensing and Mapping by Atomic Force Microscopy. *TrAC, Trends Anal. Chem.* **2002**, *21*, 65-74.

44. Sung, M. M.; Kluth, G. J.; Maboudian, R., Formation of Alkylsiloxane Self-Assembled

Monolayers on Si_3n_4. *J. Vac. Sci. Technol. A* **1999**, *17*, 540-544.

45. Headrick, J. E.; Berrie, C. L., Alternative Method for Fabricating Chemically Functionalized AFM Tips: Silane Modification of Hf-Treated Si3n4 Probes. *Langmuir* **2004**, *20*, 4124-4131.

46. Wang, J.; Li, J.; Xie, L.; Shi, C.; Liu, Q.; Zeng, H., Interactions between Elemental Selenium and Hydrophilic/Hydrophobic Surfaces: Direct Force Measurements Using AFM. *Chem. Eng. J.* **2016**, *303*, 646–654.

47. Drelich, J.; Long, J.; Yeung, A., Determining Surface Potential of the Bitumen-Water Interface at Nanoscale Resolution Using Atomic Force Microscopy. *Can. J. Chem. Eng.* **2007**, *85*, 625-634.

48. Israelachvili, J.; Pashley, R., Measurement of the Hydrophobic Interaction between Two Hydrophobic Surfaces in Aqueous Electrolyte Solutions. *J. Colloid Interface Sci.* **1984**, *98*, 500-514.

49. Donaldson Jr, S. H.; Røyne, A.; Kristiansen, K.; Rapp, M. V.; Das, S.; Gebbie, M. A.; Lee, D. W.; Stock, P.; Valtiner, M.; Israelachvili, J., Developing a General Interaction Potential for Hydrophobic and Hydrophilic Interactions. *Langmuir* **2014**, *31*, 2051-2064.

50. Ren, S.; Dang-Vu, T.; Zhao, H.; Long, J.; Xu, Z.; Masliyah, J., Effect of Weathering on Surface Characteristics of Solids and Bitumen from Oil Sands. *Energy Fuels* **2008**, *23*, 334-341.

51. Liu, G.; Wu, S.; van de Ven, M.; Molenaar, A.; Besamusca, J., Characterization of Organic Surfactant on Montmorillonite Nanoclay to Be Used in Bitumen. *J. Mater. Civ. Eng.* **2010**, *22*, 794-799.

52. Abdallah, W.; Taylor, S., Surface Characterization of Adsorbed Asphaltene on a Stainless Steel Surface. *Nucl. Instrum. Methods Phys. Res., Sect. B* **2007**, *258*, 213-217.

53. Horgnies, M.; Darque-Ceretti, E.; Fezai, H.; Felder, E., Influence of the Interfacial Composition on the Adhesion between Aggregates and Bitumen: Investigations by Edx, Xps and Peel Tests. *Int. J. Adhes. Adhes.* **2011**, *31*, 238-247.

54. Zhao, S.; Kotlyar, L.; Woods, J.; Sparks, B.; Hardacre, K.; Chung, K., Molecular Transformation of Athabasca Bitumen End-Cuts During Coking and Hydrocracking. *Fuel* **2001**, *80*, 1155-1163.

55. Rudrake, A.; Karan, K.; Horton, J. H., A Combined Qcm and Xps Investigation of Asphaltene Adsorption on Metal Surfaces. *J. Colloid Interface Sci.* **2009**, *332*, 22-31.

56. Long, J.; Zhang, L.; Xu, Z.; Masliyah, J. H., Colloidal Interactions between Langmuir-Blodgett Bitumen Films and Fine Solid Particles. *Langmuir* **2006**, *22*, 8831-8839.

57. Yarranton, H. W., Asphaltene Self-Association. *J. Dispersion Sci. Technol.* **2005**, *26*, 5-8.

58. Sedghi, M.; Goual, L.; Welch, W.; Kubelka, J., Effect of Asphaltene Structure on Association and Aggregation Using Molecular Dynamics. *J. Phys. Chem. B* **2013**, *117*, 5765-5776.

59. Kumar, K.; Dao, E.; Mohanty, K., AFM Study of Mineral Wettability with Reservoir Oils. *J. Colloid Interface Sci.* **2005**, *289*, 206-217.

60. Zahabi, A.; Gray, M. R.; Dabros, T., Heterogeneity of Asphaltene Deposits on Gold Surfaces in Organic Phase Using Atomic Force Microscopy. *Energy Fuels* **2012**, *26*, 2891-2898.

61. Chen, B.; Evans, J. R., Elastic Moduli of Clay Platelets. *Scripta Mater.* **2006**, *54*, 1581-1585.

62. Lorenzoni, M.; Evangelio, L.; Verhaeghe, S.; Nicolet, C. l.; Navarro, C.; Pérez-Murano, F., Assessing the Local Nanomechanical Properties of Self-Assembled Block Copolymer Thin Films by Peak Force Tapping. *Langmuir* **2015**, *31*, 11630-11638.

63. Vargha-Butler, E.; Potoczny, Z.; Zubovits, T.; Budziak, C.; Neumann, A., Surface Tension

of Bitumen from Contact Angle Measurements on Films of Bitumen. *Energy Fuels* **1988**, *2*, 653-656.

64. Israelachvili, J. N., *Intermolecular and Surface Forces: Revised Third Edition*; Academic press, 2011.

65. Ducker, W. A.; Xu, Z.; Israelachvili, J. N., Measurements of Hydrophobic and Dlvo Forces in Bubble-Surface Interactions in Aqueous Solutions. *Langmuir* **1994**, *10*, 3279-3289.

66. Hartley, P. G.; Larson, I.; Scales, P. J., Electrokinetic and Direct Force Measurements between Silica and Mica Surfaces in Dilute Electrolyte Solutions. *Langmuir* **1997**, *13*, 2207-2214.

67. Zeng, H.; Shi, C.; Huang, J.; Li, L.; Liu, G.; Zhong, H., Recent Experimental Advances on Hydrophobic Interactions at Solid/Water and Fluid/Water Interfaces. *Biointerphases* **2016**, *11*, 018903.

Chapter 4 Understanding the Stabilization Mechanism of Bitumen-coated Fine Solids in Organic Media

4.1. Introduction

The technology of non-aqueous extraction (NAE) of oil sands, using organic solvents to liberate and dissolve bitumen from oil sands ore, was first explored in the 1960s to avoid the environmental issues associated with hot water extraction process, such as substantial fresh water consumption, high thermal energy cost and rapid accumulations of toxic tailing ponds.[1] Since then, great efforts have been devoted to examine the extraction performances of the NAE process including bitumen recovery from the oil sands, solvent recovery from the extraction gangue, and fine solids removal from the bitumen product.[2-6] Many modified approaches have been proposed to improve the NAE progress, such as solvent extraction spherical agglomeration,[7-8] ionic liquid assisted solvent extraction[9-10] and switchable hydrophilicity solvent extraction.[11-12] Nonetheless, the NAE technology has not been implemented beyond pilot scale over last four decades, and one pressing challenge lies in the migration of considerable amounts of fine solids into the produced bitumen. Even under the optimal technological conditions at present, the content of the fine solids residing in the produced bitumen is generally far beyond the pipeline specification (0.5 wt%) and refinery feed (0.03 wt%), making the product unqualified for the downstream operations.[3, 13-14] In order to explore effective and economical strategies to reduce solids content in NAE bitumen, it is of vital importance to gain a comprehensive understanding of the stabilization mechanism of fine solids in the organic media.

The stabilization mechanism of the fine solids in organic media should be closely related to the interfacial properties of mineral solids. The fine mineral solids retained in the NAE bitumen generally possess high mass fraction of carbon content, ranging from ~ 17.0% to ~ 26.9% depending on the properties of applied solvents, which are assigned to the organic materials adsorbed on the solids surface.[2, 15] Prior to the surface mining and extraction processes, the mineral solids can be adsorbed by organic components that were originally in the crude oil driven by the surface precipitation and intermolecular interactions involving acid/base attraction, π-π stacking and ion-binding interactions.[16-18] The mined mineral solids could undergo subsequent adsorption of bitumen components during the extraction process, which therefore renders the solids more oleophilic. Such bitumen coating is stubborn and cannot be completely separated from the mineral solids using organic solvents. Many previous studies on the stabilization of emulsion drops during petroleum processing have revealed that the presence of interfacial adsorbed bitumen components (e.g., asphaltene) can sterically inhibit coalescence of emulsion droplets.[19-21] It is reasonable to expect that adsorbed bitumen on mineral solid surfaces should also play an important role in forming a stable suspension of fine solids in the NAE process. Nanomechanical techniques, such as atomic force microscope (AFM) and surface force apparatus (SFA), offer effective ways to understand behaviors of bitumen components and mineral solids in oil sands processing. With the assistance of colloidal probe AFM, interaction behaviors between bitumen and different mineral solid surface (e.g., silica, kaolinite and montmorillonite) in aqueous media have been systematically studied.[22-24] The direct force measurements in non-aqueous media were mainly conducted using SFA.[25-27]

A number of experimental studies and computer simulations have been conducted to investigate adsorption behaviors of crude oil onto various materials.[28-32] The adsorption of bitumen

onto mineral surface strongly depends on the properties of surrounding organic media and the interfacial chemistry of the surface. Zahabi et al.[33] reported that the concentration of asphaltenes (viz. ratio of oil to solvent) could affect the swelling of asphaltene aggregates in the solution, ultimately influencing constructions of adsorbed asphaltenes on the silica surface. Dorota et al.[34] revealed that the adsorbed mass of asphaltenes to hydrophilic mineral solids was highly related to the solubility of asphaltenes in organic solvents and the original size of asphaltene aggregates. A surface analysis technique, quartz crystal microbalance with dissipation (QCM-D), has been applied in investigating the adsorption characteristics of bitumen fractions on solid surfaces. QCM-D technique can provide both qualitative and quantitative information of adsorbed species, including adsorbed mass, thickness and viscoelastic properties in real-time with extremely high sensitivity.[34-36] For an instance, Serkan et al.[37] quantified adsorption affinity of naphthenic acids to mineral surfaces based on the adsorption free energies ($\Delta G°$) calculated in QCM-D measurements.

Despite these reported results, there are no available data on either the adsorption behaviors of bitumen onto fine solids or the mechanism of interactions between the bitumen-coated fine solids involved in the NAE process. Currently, cyclohexane has been recognized as the most promising solvent because it exhibits high efficiency in solvent recovery with relative low solids content in bitumen product, while n-heptane is considered as a poor solvent as it normally has low bitumen recovery.[14] Therefore, these two typical solvents were of interest in this present work and their effects on the stability of bitumen-coated fine solids were systematically investigated. Notably, QCM-D was employed to elucidate the adsorption behaviors of bitumen onto the mineral solid surface (i.e., silica in this work), and colloidal probe AFM was utilized to quantify the inter-particle interactions in the related organic media, respectively. In addition, a series of

sedimentation tests for bitumen-coated silica particles was conducted to macroscopically analyze the effects of bitumen adsorption and inter-particle forces on the stability of fine solids in organic media.

4.2. Materials and experimental methods

4.2.1. Materials

Athabasca bitumen was provided by Syncrude Canada Ltd and contains ~ 0.6 wt% solid. Cyclohexane and n-heptane (both Certified ACS grade, > 99%) were purchased from Fisher Scientific, Canada. The quartz crystal sensor coated with 50 nm silicon dioxide (QSX 303) was purchased from Biolin Scientific, Sweden. Toluene (HPLC grade) and sodium dodecyl sulfate (SDS, 99% purity) were purchased from Fisher Scientific. Silicon wafer with 0.5 μm thermal oxide (i.e., silica) film was purchased from NanoFab, University of Alberta. Silica microspheres (diameter ~ 5 μm) and silica solid particles (diameter ~ 0.5-10 μm) were purchased from Sigma-Aldrich, Canada. All solvents were used as received without further purification.

4.2.2. Preparation of mixed solvents and bitumen solutions

The mixed organic solvents cyclohexane-heptane were prepared by mixing cyclohexane and heptane with different volume fraction of cyclohexane (φ_c) ranging from 1 to 0. The Athabasca bitumen sample was diluted in toluene at a 1:1 mass ratio and centrifuged at 9000 RCF for 1 h to eliminate any remaining contained fine solids. After centrifugation, toluene was evaporated from the supernatant and the dried sample was considered solid-free-bitumen. The pretreated bitumen was then dissolved in cyclohexane-heptane (φ_c = 1.00, 0.90, 0.75, 0.60 and 0.50) to prepare diluted bitumen solutions at a concentration of 0.1 wt%, followed by 10 min sonication to completely

dissolve the bitumen. The achieved bitumen solutions are denoted as bitumen/cyclohexane-heptane henceforth. Prior to each adsorption experiment or dip-coating preparation, the bitumen solutions were sonicated for another 10 min.

The asphaltene precipitation onset of our bitumen system was determined using UV-vis spectroscopy. The working mechanism and procedure details can be found elsewhere.[43] A brief measurements protocol is summarized as follows: (1) preparing 0.1 wt% bitumen/cyclohexane-heptane solution with different volume fraction of cyclohexane (φ_c), 1, 0.9, 0.8, etc, (2) sonicating the bitumen solution and allowing it undisturbed, (3) centrifuging the mixture at 4000 rpm for 15 min, (4) diluting about 0.5 mL of the supernatant liquid with 4 mL of cyclohexane and (5) measuring its absorbance of UV-vis at 400 nm with cyclohexane as the reference. The absorbance of UV-vis as a function of φ_c are plotted as shown in Figure 4. 1. The precipitation onset is defined as the data point where absorbance values suffer a sudden drop. In this system, the precipitation onset happens at the intersection of two straight dash lines, which was determined to be $\varphi_c = 0.74$ for 0.1 wt% bitumen solutions.

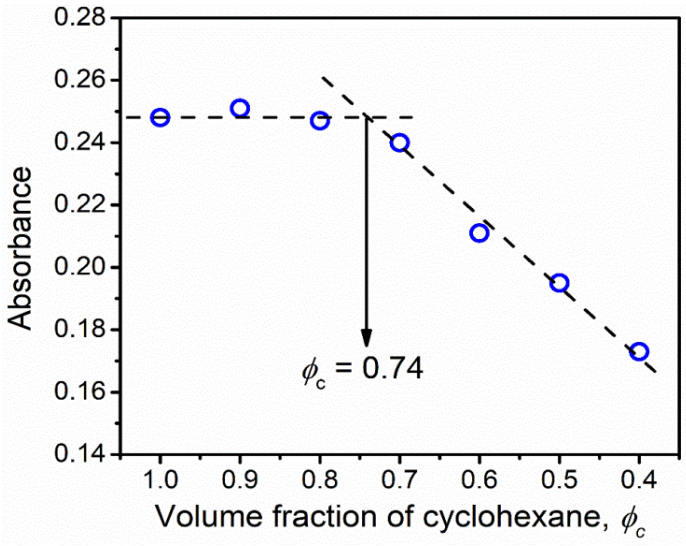

Figure 4. 1. Asphaltene precipitation onset measurements for bitumen sample using an absorbance of UV-vis at 400 nm wavenumber.

4.2.3. AFM force measurements and AFM imaging

All the AFM experiments were performed on a Dimension Icon AFM (Bruker, Santa Barbara, CA). A colloidal probe AFM technique was applied to directly measure interaction forces between two solids surfaces in organic media, as illustrated in Figure 4. 2. Details of preparing the colloidal probe have been given elsewhere.[38-40] Briefly, a silica microsphere was glued to the end of a tipless AFM cantilever using an Epoxy adhesive under the integrated optical microscope of AFM. The diameters of the colloidal probes can be determined by the scanning electron microscopy (SEM). In this work, the silica probe was either clean or coated with bitumen by a dip-coating method. Specifically, the silica probe was treated by UV/ozone to remove any contaminants on the silica surface, then immersed in the bitumen/cyclohexane solution for 10 min, thoroughly rinsed with both cyclohexane and heptane, and blow-dried with nitrogen. The bottom silica substrate with bitumen coating was prepared using the same dip-coating method.

The AFM force measurements were conducted in a fluid cell where the pristine or bitumen-coated silica probe interacted with the bottom bitumen-coated silica surface in cyclohexane-heptane with φ_c ranging from 1 to 0. During the force measurement, the AFM probe was driven to approach the bottom surface and then started to retract from the surface until a pre-set deflection of the cantilever was reached. A plot of the deflection versus the displacement of the z-piezo device is obtained in each AFM measurement. The deflection of the cantilever is monitored by detecting the position of a laser beam reflected from cantilever onto a photo detector. Force between the probe and the bottom surface is converted from the deflection of the cantilever using Hooke's law. A triangular silicon nitride AFM cantilever with spring constant of 0.06-0.35 N/m was used in the force measurements. All the AFM force measurements under each condition were repeated for at

least three times using independently prepared substrate surfaces and colloidal probes in order to ensure the reproducibility and reliability of the results.

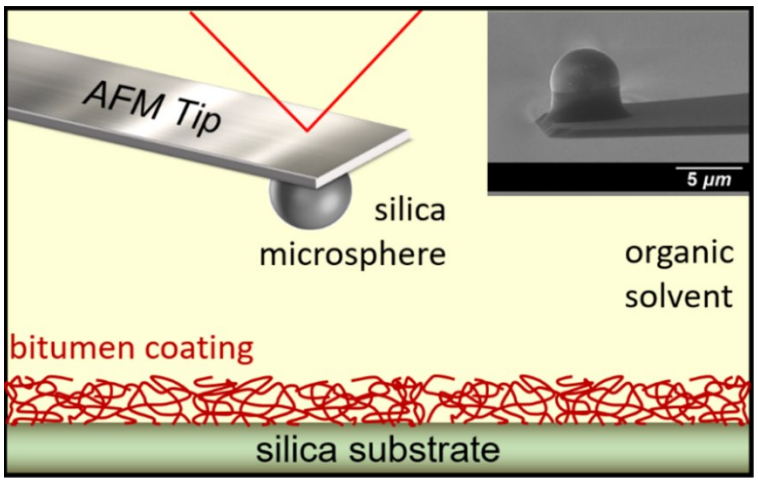

Figure 4. 2. Experimental setup of the colloidal probe AFM. Insert: typical SEM photomicrograph of a silica colloidal probe.

AFM imaging was conducted in the tapping mode to probe topographic characteristics of the quartz crystal sensors collected after the adsorption process in QCM-D measurements. The morphologic changes of adsorbed bitumen in different organic solvents were also probed by AFM imaging in a fluid cell. Rectangular silicon nitride AFM cantilever with spring constant of 5 N/m were used for all AFM imaging.

4.2.4. QCM-D measurements on bitumen adsorption to silica surfaces

Before running each QCM-D experiment, the quartz crystals, the flow module and connecting tubes were thoroughly cleaned to eliminate the effect of any contaminations on the characterization results. The cleaning steps followed a procedure reported previously.[41] The QCM-D experiments started from injecting a bitumen-free solvent (i.e., cyclohexane or cyclohexane-heptane mixtures) to the flow module containing a silica-coated quartz crystal sensor. The system was then considered as stable when the frequency shift of the sensor became less than ± 1 Hz

within 5 min, after which the bitumen/cyclohexane-heptane solution was injected to the flow module at constant rate (0.35 mL/min). During the QCM-D measurements, two parameters, frequency and dissipation, of the crystal sensor were monitored simultaneously in real-time. Frequency is related to the mass of adsorbed species, which can be calculated using Sauerbrey relation[41-42] as shown in equation 4.1,

$$\Delta m = -\frac{C\Delta f}{n} \tag{4.1}$$

where Δm is adsorbed mass, Δf is the frequency shift, n = 1, 3, 5, 7, 9, 11 is the order number of harmonic overtones of the crystal sensor, C = 17.7 ng/(Hz·cm^2) is the constant for a 5 MHz crystal sensor. However, the Sauerbrey relation is only valid for a thin and rigid adsorbed film which shows all harmonics overlay in Δf responses and small dissipation shifts (ΔD) (i.e., $\Delta D/\Delta f \ll 0.4 \times 10^{-6}$ Hz^{-1}).[43] Dissipation shift reveals the rigidity and viscoelasticity of adsorbed film, which is monitored by recording the response of the oscillating sensor that has been vibrated at its resonance frequency, as defined in equation 4.2,[34]

$$D = \frac{E_{lost}}{2\pi E_{stored}} \tag{4.2}$$

where E_{lost} is the energy lost during one oscillation cycle and E_{stored} is the total energy stored in the oscillator.

4.2.5. Sedimentation tests for bitumen-coated silica particles

The bitumen-coated silica particles were prepared by mixing 2 g of clean silica solid particles (diameter about ~ 0.5-10 μm) with 40 mL of 0.1 wt% bitumen/cyclohexane-heptane solutions. The mixture was sonicated for 5 min to suspend the silica particles, agitated for 10 min using a magnetic stirrer (1000 rpm) and thoroughly washed through repeatedly centrifugation

(4000 rpm) to remove non-adsorbing bitumen fractions. The centrifuged solid particles were collected and dried in a fume hood for 48 hours. The resulting bitumen-coated silica particles showed particle size ~ 1-3 μm in diameter measured by dynamic light scattering (DLS). The degree of bitumen adsorption was estimated by Diffuse Reflectance Infrared Fourier Transform Spectroscopy (DRIFTS). The silica solids were placed in a sample unit for diffuse reflectance and were scanned 32 times with a resolution of 4 cm^{-1}. The diffuse radiation is reflected and converted by the detector into absorbance spectra using the single beam of bare silica solids as the background.

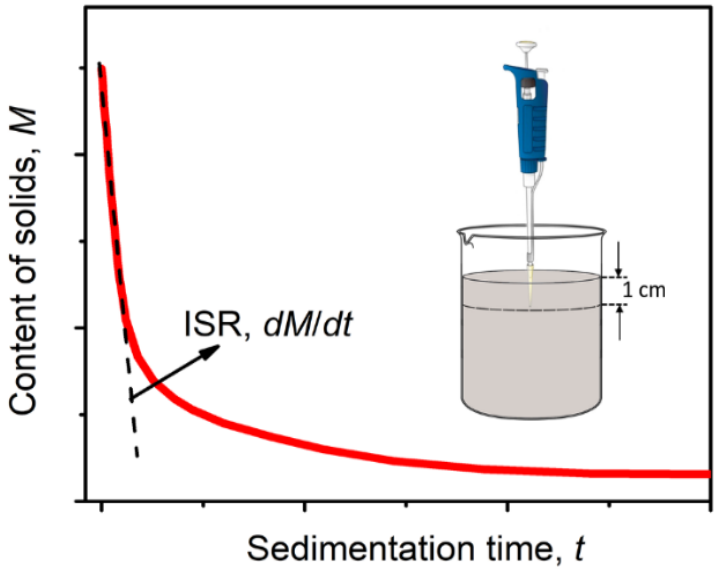

Figure 4. 3. Schematic of typical sedimentation test for bitumen-treated silica solids and initial settling rate (ISR) calculation via plotting the initial slope of the sedimentation curve.

Steps of the sedimentation tests have been reported previously.[44] Briefly, a suspension of bitumen-treated silica (~ 3500 ppm) in cyclohexane-heptane was homogenized through vigorous magnetic stir (1000 rpm) at ambient temperature. The time was defined as $t = 0$ once the stir ceased and the settling started. At different time intervals, 1 mL suspension sample was collected at a depth of 1 cm from the free surface. The collected samples were dried in a fume hood and the mass

of the dried solids (M, mg) versus time (t, s) was illustrated in Figure 4. 3. In this work, the stability of the solid particles in organic solvents was qualitatively demonstrated by the initial sedimentation rate (ISR) presented by the initial slope of the sedimentation curve (dM/dt) and the solids content (M_s) in the supernatant after settling for 30 min.

4.3. Results and discussion

4.3.1. AFM force measurements

4.3.1.1 Interactions between a pristine solid and a bitumen-coated solid

To start with, interactions between a pristine silica microsphere and a bitumen-coated flat silica surface in two different organic solvents (i.e., cyclohexane and heptane) were investigated using the colloidal probe AFM technique, and the typical force-separation profiles were displayed in Figure 4. 4. Clearly, when the silica probe gradually approached the bitumen surface in cyclohexane (Figure 4. 4A), a repulsion was measured and grew increasingly stronger especially at the separation $\leqslant \sim 3$ nm. During the retraction process, the silica-bitumen interaction kept repulsive before the two solids surfaces got separated. Considering that cyclohexane is a good solvent for bitumen, the measured strongly repulsive interaction force indicates that the bitumen layer tended to extend and swell enormously in cyclohexane, and the resulting strong steric force prevented the silica probe from attaching onto the bitumen-coated silica surface. Besides, a notable hysteresis between the approach and retraction force curves was observed, which could arise from the energy dissipation due to the deformation of the sample surface under external force,[45-46] which also implies that the bitumen layer should be swollen and flexible in cyclohexane.

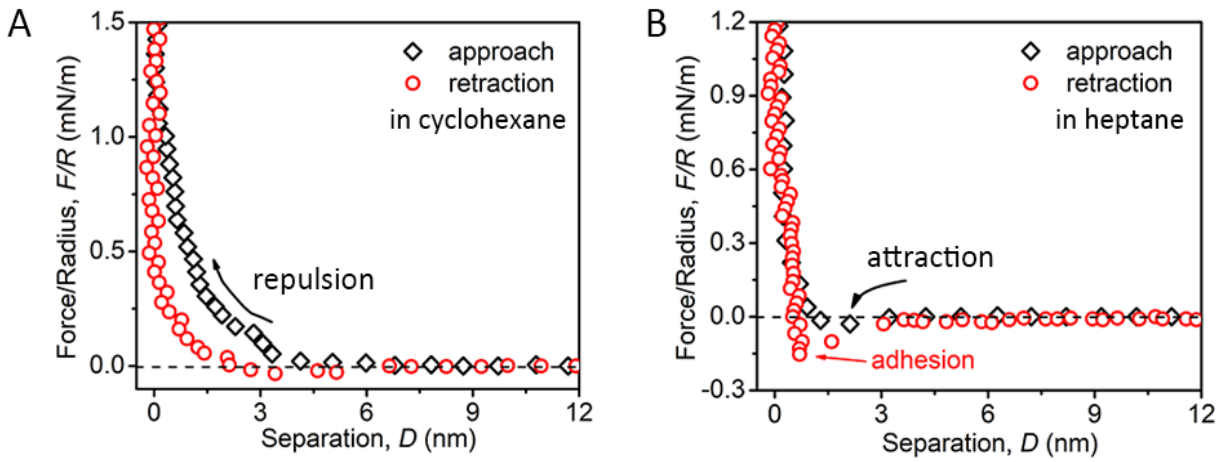

Figure 4. 4. Measured interaction forces between the silica probe and the bitumen-coated silica surface in (A) cyclohexane and (B) heptane, respectively. The square black and circular red symbols represent the data measured during the approach and retraction processes, respectively.

In contrast, the measured interaction force between the silica probe and the bitumen-coated surface in heptane showed remarkably different features (Figure 4. 4B). Specifically, a weak attraction instead of the strong repulsion was detected during the approach process when the separation was smaller than 3 nm, which was due to the van der Waals (VDW) attraction between the two surfaces. With the silica probe further approaching, the interaction force turned repulsive and the strength increased sharply after the probe came into contact with the bitumen surface. This phenomenon could be highly associated with the fact that the bitumen layer tended to shrink in heptane which is a typical poor solvent for bitumen components (e.g., asphaltene), resulting in a much weaker steric force that cannot inhibit the silica probe from attaching onto the bitumen-coated surface. In the retraction curve, the repulsive region first exhibited a roughly linear relationship with the separation and almost fully overlapped with that of the approach curve, indicating that the bitumen layer should be much more rigid in heptane than in cyclohexane. Afterwards, a noticeable adhesion denoted by the distinct “jump-out” feature in the force curve

was measured, manifesting that the probe was suddenly released from the bitumen surface. Such adhesion force could arise from VDW interaction between the two surfaces as well as a binding configuration between the silica surface and heteroatoms (e.g., N, O and S) in bitumen.[47] The adhesion force was negligible in cyclohexane possibly due to the dominated steric repulsive force which could prevent the silica probe from intimately attaching onto the bitumen-coated surface and overcome the van der Waals interactions. These striking discrepancies in the AFM force measurement results suggest that the organic solvent plays a critical role in modulating the interactions involving the bitumen-coated mineral surfaces.

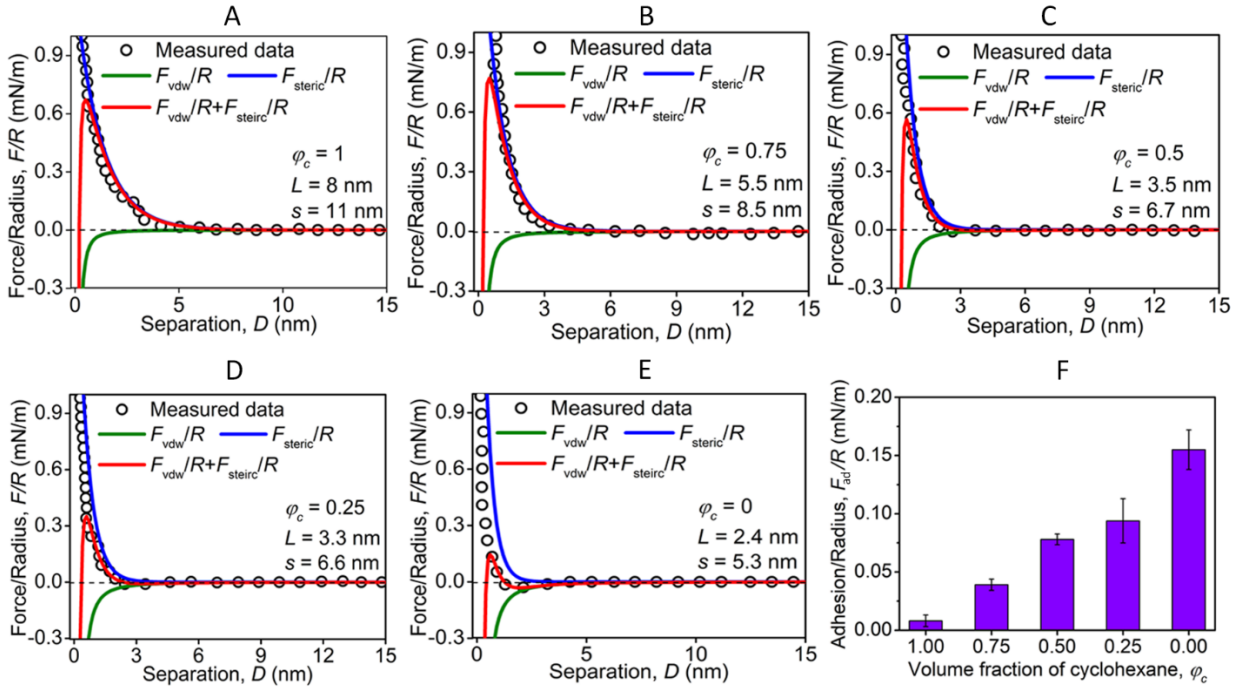

Figure 4. 5. (A-E) Theoretical analysis results (solid curve) of the measured interaction forces (circular black symbol) during the approach process between the silica probe and the bitumen-coated silica surface in cyclohexane-heptane with cyclohexane volume fraction φ_c = 1.00, 0.75, 0.50, 0.25 and 0.00, respectively. (F) Summary of the normalized adhesion F_{ad}/R results from about 10 independent force measurements for each solvent condition.

Interactions between the silica probe and the bitumen-coated silica surface were systematically measured in cyclohexane-heptane in order to gain more insights into the effects of the organic solvents on the interfacial interactions. The circular black symbol in Figure 4. 5A-E present the measured forces during the approach processes with volume fraction of cyclohexane φ_c = 1.00, 0.75, 0.50, 0.25 and 0.00, respectively. Notably, both the range and the magnitude of the repulsive force decreased gradually with φ_c declining, until a weak attraction was observed in pure heptane (φ_c = 0). Figure 4. 5F shows the statistical values of the normalized adhesion forces in different cases measured from the corresponding retraction curves, which can be correlated to the interactions and the stability of fine solids in organic media. With φ_c decreasing, the normalized adhesion F_{ad}/R was much strengthened from ~ 0.008 mN/m to ~ 0.155 mN/m, illustrating an obvious improvement in the affinity of silica surface to bitumen.

To theoretically analyze the interaction mechanisms of fine solids in organic media, two kinds of surface forces should be taken into consideration, i.e., VDW force and steric repulsive force. In order to make the quantification results reliable, the bitumen-coated silica surface was thoroughly rinsed with both cyclohexane and heptane prior to the AFM force measurements so that the depletion effect arising from the dissolution of the non-adsorbed bitumen components in the fluid could be eliminated.[48-49] Because of the relatively low dielectric constant of the organic solvents, the electrical double layer (EDL) force could be negligible in this study. Here, the VDW force (F_{vdw}) between a spherical particle and a flat surface is given by equation 4.3,[48]

$$F_{vdw} = -A_{132}R / 6D^2 \tag{4.3}$$

where R is the particle radius, D is the particle-surface separation, A_{132} is the Hamaker constant for media 1 and 2 interacting across medium 3 and is estimated according to equation 4.4,

$$A_{132} = (\sqrt{A_{11}} - \sqrt{A_{33}})(\sqrt{A_{22}} - \sqrt{A_{33}}) \tag{4.4}$$

where A_{11}, A_{22} and A_{33} are the Hamaker constants between two identical media 1, 2 and 3 interacting across vacuum, respectively. In this work, 1, 2 and 3 denote the silica, bitumen and organic solvent, respectively. The values of A_{11} and A_{22} have been well documented to be 6.3×10^{-20} J [48] and 6.0×10^{-20} J,[22] respectively. The values of A_{33} for cyclohexane and heptane were reported to be 5.40×10^{-20} and 4.50×10^{-20},[48,52] and the calculated values of A_{33} and A_{132} in different organic solvents were listed in Table 4.1. It is evident that A_{132} remained positive across all investigated cases, which demonstrated that the VDW force between silica and bitumen remained attractive in the mixed solvent cyclohexane-heptane. As φ_c was lowered from 1.00 to 0.00, A_{132} gradually increased from 2.34×10^{-22} J to 1.27×10^{-21} J, indicating that the VDW force was strengthened in sequence. The steric force (F_{steric}) between the pristine silica probe and the bitumen-coated silica surface could be estimated by Alexander-de Gennes steric model,[50-51] given by equation 4.5,

$$\frac{F_{steric}}{R} = \frac{50kTL}{s^3} e^{-2\pi D/L} \tag{4.5}$$

where T is the absolute temperature, k is the Boltzmann constant, s is the average spacing between two grafted points of bitumen chains, L is the length of bitumen chains.

Table 4. 1. Values of Hamaker constant for VDW forces in cyclohexane-heptane.

φ_c	A_{33}[a] (J)	A_{132} (J)	A_{232} (J)
1.00	5.40×10^{-20}	2.34×10^{-22}	1.58×10^{-22}
0.75	5.18×10^{-20}	4.06×10^{-22}	3.01×10^{-22}
0.50	4.95×10^{-20}	6.40×10^{-22}	5.04×10^{-22}
0.25	4.73×10^{-20}	9.20×10^{-22}	7.54×10^{-22}
0.00	4.50×10^{-20}	1.27×10^{-21}	1.08×10^{-21}

a. A_{33} is a function of φ_c and calculated by $A_{33}(\varphi_c) = \varphi_c \times A_{33}(\varphi_c = 1) + (1 - \varphi_c) \times A_{33}(\varphi_c = 0)$.[31]

The values of L and s in different systems were obtained by theoretically fitting the measured interaction forces between the AFM probes and the flat surfaces during the approach processes. In Figure 4. 5A-E, the green and blue curves are the theoretically reconstructed force-separation profiles of the VDW and steric forces, respectively, and the red curve denotes the integration of these two surface forces, which is in good agreement with the measured force data at separations greater than 1 nm. At very small separations, i.e., less than 1 nm, the measured repulsive forces grow increasingly stronger, which are found to be inconsistent with the attractive force predicted by the theoretical model. Such discrepancy could be attributed to the surface roughness[65] or small protrusions from the bitumen/silica interface[23] which led to steric repulsion at small separation distances. To be specific, the quantified L and s were found to sequentially decrease from ~ 8.0 nm to ~ 2.4 nm and from ~ 11.0 nm to ~ 5.3 nm, respectively, when φ_c was continuously lowered from 1 to 0. The synchronous reduction in L and s illustrated that the surface morphology of adsorbed bitumen layer was very sensitive to the variation in surrounding solvents, which in turn influenced the strength of inter-particle interactions. In cyclohexane, the fully extended bitumen layer exhibited strong and long-ranged steric repulsive force against the silica probe. However, the addition of heptane into solvents could inhibit swelling of bitumen layer and cause the shrink and collapse of the bitumen layer (viz. low values of L and s). In pure heptane, the collapsed bitumen layer would undergo interdigitation and formed nanoaggregates, as probed by AFM imaging in Figure 4. 6B. Meanwhile, the contribution of VDW force to the overall interaction monotonically increased with the higher content of heptane, which could also account for the ascending trend in the bitumen-silica adhesion in Figure 4. 5F.

The morphology changes of bitumen film coated on silica surface in organic solvent were characterized by AFM imaging. In cyclohexane (Figure 4. 6A), the bitumen film was molecularly

smooth (R_q = 0.30 nm) with many small self-associated bitumen nanoaggregates over the viewed surface. In contrast, the bitumen film in heptane (Figure 4. 5B) showed many large aggregates on the surface which could be attributed to interdigitation and bridging behaviors of collapsed bitumen layer. As a result, surface roughness of the bitumen surface in heptane was slightly increased (R_q = 0.60 nm).

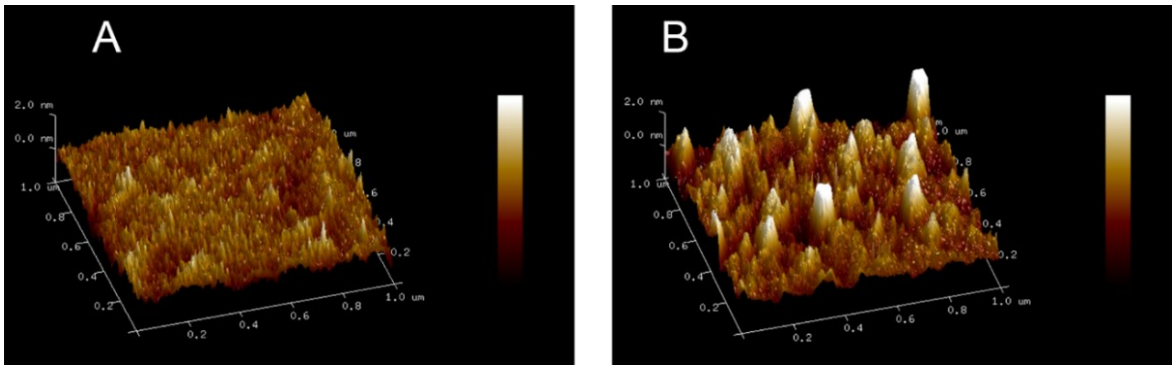

Figure 4. 6. 3D AFM height images (1 × 1 μm^2) of immobilized bitumen layer in (A) cyclohexane and (B) heptane.

4.3.1.2. Interactions between two bitumen-coated solids

The interactions between a bitumen-coated silica probe and the bitumen-coated silica surface in cyclohexane-heptane were also quantitatively investigated. Figure 4. 7A-E show the corresponding force-separation curves during the approach processes in the mixed solvent of φ_c = 1.00, 0.75, 0.50, 0.25 and 0.00. Similar to the silica-bitumen case mentioned above, both the range and magnitude of the repulsive force between two bitumen surfaces gradually decreased with decreasing φ_c. However, under the same solvent condition, the bitumen-bitumen repulsion possessed a much longer range than the silica-bitumen repulsion, which could be reasonably attributed to the extra bitumen layer coated on the silica probe. For instance, the initial separation

of the measured repulsive force almost doubled, increasing from ~ 8 nm for the silica-bitumen case to ~ 16 nm for the bitumen-bitumen case in pure cyclohexane.

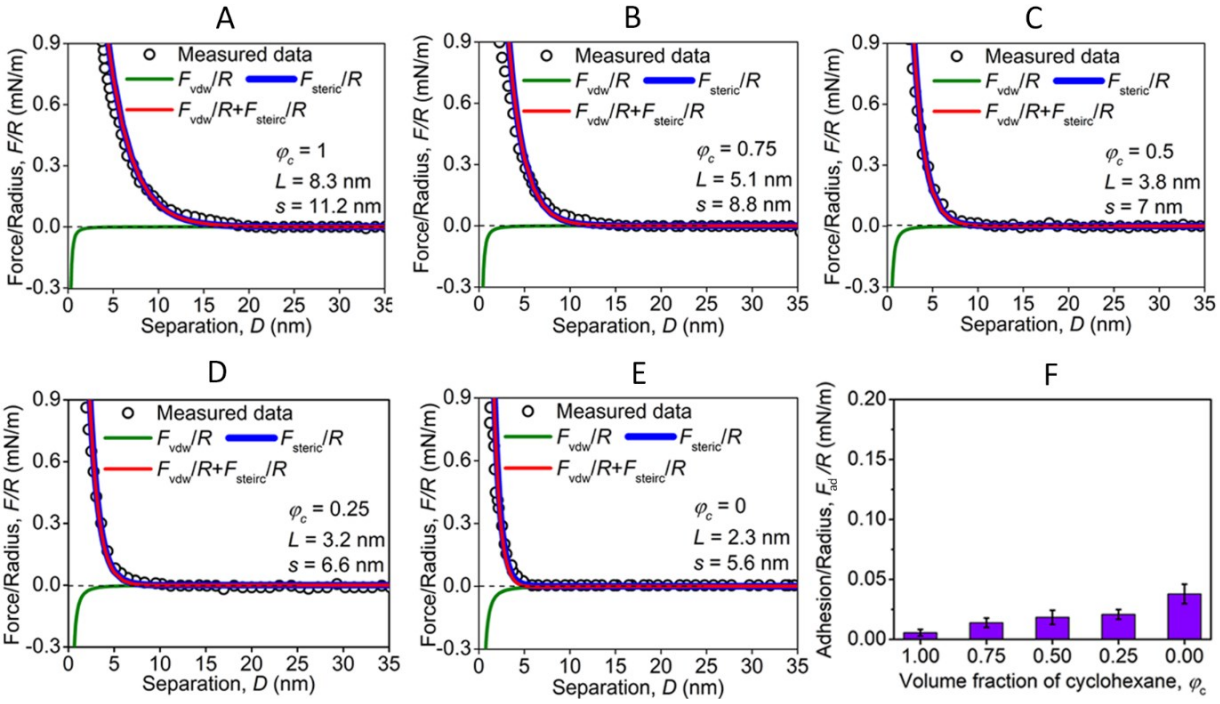

Figure 4. 7. (A-E) Theoretical analysis results (solid curve) of the measured interaction forces (open symbol) during the approach process between the bitumen-coated silica sphere and the bitumen-coated silica surface in cyclohexane-heptane with φ_c = 1.00, 0.75, 0.50, 0.25 and 0.00, respectively. (F) Summary of the normalized adhesion F_{ad}/R results from about 10 independent force measurements for each solvent condition.

Several modifications were applied for quantifying the VDW and steric forces in analyzing the surface forces between two bitumen surfaces. Table 4.1 shows the calculated Hamaker constants A_{232} for the symmetric bitumen-bitumen VDW force, which were also positive but slightly smaller than A_{132} in the corresponding cases. The steric force was estimated using the Alexander-de Gennes steric model for the symmetric case to account for the increased thickness of two bitumen layers, as shown in equation 4.6,[48, 53-54]

$$\frac{F_{steric}}{R} = \frac{200kTL}{s^3} e^{-\pi D/L} \quad (6)$$

It is noticeable that the force-separation profile of the steric force almost completely overlaps with that of the overall force, indicating the dominant role of steric repulsion between two bitumen surfaces. When φ_c was lowered from 1 to 0, the fitted L consequently decreased from ~ 8.3 nm to ~ 2.3 nm and s decreased from ~ 11.2 nm to ~ 5.6 nm, respectively. These values were consistent with those in the corresponding silica-bitumen cases. Figure 4. 7F shows the adhesion forces between two bitumen surfaces measured in cyclohexane-heptane, which were noticeably weaker than those measured for silica-bitumen. Even in the pure heptane, adhesion force for bitumen-bitumen was only ~ 0.038 mN/m, almost three times small than that for silica-bitumen under the same solvent condition, which was mainly due to the enhanced steric interactions of two bitumen layers. Such weak adhesion force is likely contributed by the interdigitation and bridging behaviors between two bitumen surfaces after being brought into contact. In a cyclohexane-rich solvent, bitumen chains strongly repel each other and do not become easily interdigitated or bridged, resulting in a negligible adhesion force.[48] The strong steric repulsion combined with extremely weak adhesion force between two bitumen surfaces should play a critical role in the stable suspension of bitumen-coated fine solids in the NAE environment.

4.3.2 Bitumen adsorption behaviors

Figure 4. 8 shows an example of frequency and dissipation changes of the silica sensor (overtones n = 3, 5, 7, 9 and 11, respectively) recorded in the QCM-D experiment for bitumen adsorption. The background solvent, i.e., cyclohexane in this case, was first introduced to flush the crystal sensor to obtain a stable baseline for measurements (regime I). Then, cyclohexane was switched to the 0.1 wt% bitumen/cyclohexane solution (regime II), and immediate drop in

frequency and rise in dissipation were observed synchronously, indicating a fast adsorption of bitumen onto the sensor surface at the initial state. After the rapid initial adsorption, bitumen continued adsorbing onto the surface at a lower rate considering the relatively milder frequency and dissipation changes with time. Finally, the sensor was flushed with cyclohexane again to remove any weakly adsorbed bitumen, resulting in a slight increase in frequency (regime III). For each overtone number, the ΔD values were high and spreading of the overtones was observed in Δf and ΔD responses, indicating that the adsorbed bitumen layer showed a viscoelastic behavior[43, 55]. Therefore, the Sauerbrey equation (Eq. (1)) is not applicable in this case. However, by measuring both frequencies and dissipations at multiple overtones according to the Voigt viscoelastic model incorporated in the Q-sensor software, the viscoelastic and structural properties including the adsorbed mass can be characterized.

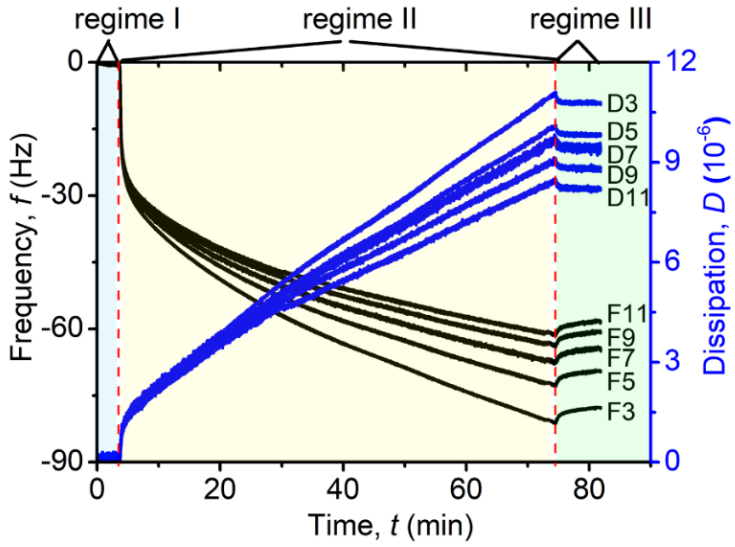

Figure 4. 8. An example of frequency (black) and dissipation (blue) changes of a silica sensor during the QCM-D measurements for bitumen adsorption.

Moreover, QCM-D experiments of the bitumen adsorption in different cyclohexane-heptane solvents (φ_c = 0.90, 0.75, 0.60 and 0.50, respectively) were conducted. It is worth

mentioning that bitumen solutions with φ_c < 0.50 could undergo a significant phase separation mainly because of the asphaltene precipitation in poor solvents and therefore were not examined in QCM-D experiments. The real-time mass of adsorbed bitumen onto the silica surface in different bitumen/cyclohexane-heptane solutions were calculated using the Voigt viscoelastic model. Frequencies and dissipations at overtone n = 3, 5 and 7 were selected for modelling, and the results are exhibited in Figure 4. 9. During the initial time (Figure 4. 9A), the adsorption process started from a period in which the amount of adsorbed mass was a linear function of time, which means that the adsorption process was controlled by adsorption kinetics.[43, 55] In other words, the bitumen-silica interactions are dominant at the initial adsorption stage. This period was quite short and ranged from 2-30 s depending on the properties of surrounding solvents. The rates of adsorption at initial scale (viz. initial slope) were calculated to be about 70, 127 and 218 mg/m^2·min at φ_c = 1, 0.9 and 0.75, respectively, suggesting the stronger bitumen-silica interactions with lower φ_c, which was consistent with the AFM force measurements results. However, when φ_c was further lowered from 0.75 to 0.5, the initial adsorption rate reduced significantly to about 17.6 mg/m^2·min, which looks contradictory to the AFM results. It is worth noting that the drastic change occurred at φ_c = 0.75 which was very close to the asphaltene precipitation onset (φ_c = 0.74) of the bitumen solutions (Figure 4. 1). Therefore, it is reasonable to speculate that after the precipitation onset the concentration of some bitumen fractions (e.g., asphaltenes) dissolved in solution was highly reduced, significantly inhibiting the opportunity for bitumen fractions to interact with the silica surface. As a result, the global adsorption rate of bitumen reduced although bitumen-silica interaction was strong.

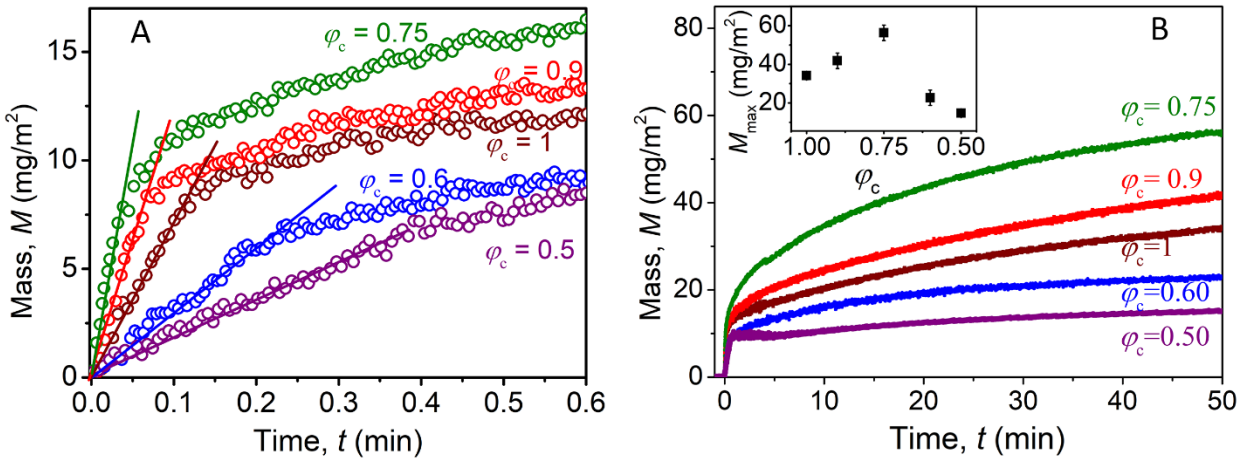

Figure 4. 9. (A) Mass of adsorbed bitumen onto the silica sensor at initial time from 0.1 wt% bitumen/cyclohexane-heptane solutions with varying φ_c, where open symbols and solid lines represent experimental data and initial adsorption slope, respectively. (B) Mass of adsorbed bitumen during the whole adsorption process. Inset: mass determined at t = 50 min.

After the initial process, the bitumen-bitumen interactions should play the main role in the adsorption kinetics. Previous studies revealed that the transport of asphaltenes to the quartz sensor at long time became more complicated and may be affected by multiple processes, such as aggregation, deposition, precipitation, diffusion and advection.[33, 55-56] These processes should be taken into consideration in this study besides the adsorption kinetics. Figure 4. 8B shows the changes of adsorbed mass during the whole adsorption process. With $\varphi_c > 0.5$ no saturation plateau of the mass curve was observed within the experimental time, suggesting a continuous adsorption process of bitumen which was possibly multilayered on the silica surface.[33, 57] When φ_c was lowered to 0.5, the bitumen adsorption got saturated on the silica surface without any further mass changes after t = 10 min. At each time point, the adsorbed mass was found to increase with φ_c decreasing from 1 to 0.75 but was in turn decreased by further reducing φ_c from 0.75 to 0.5. For

instance, at t = 50 min the maximum mass of adsorbed bitumen occurred as φ_c = 0.75 (inset of Figure 4. 9B).

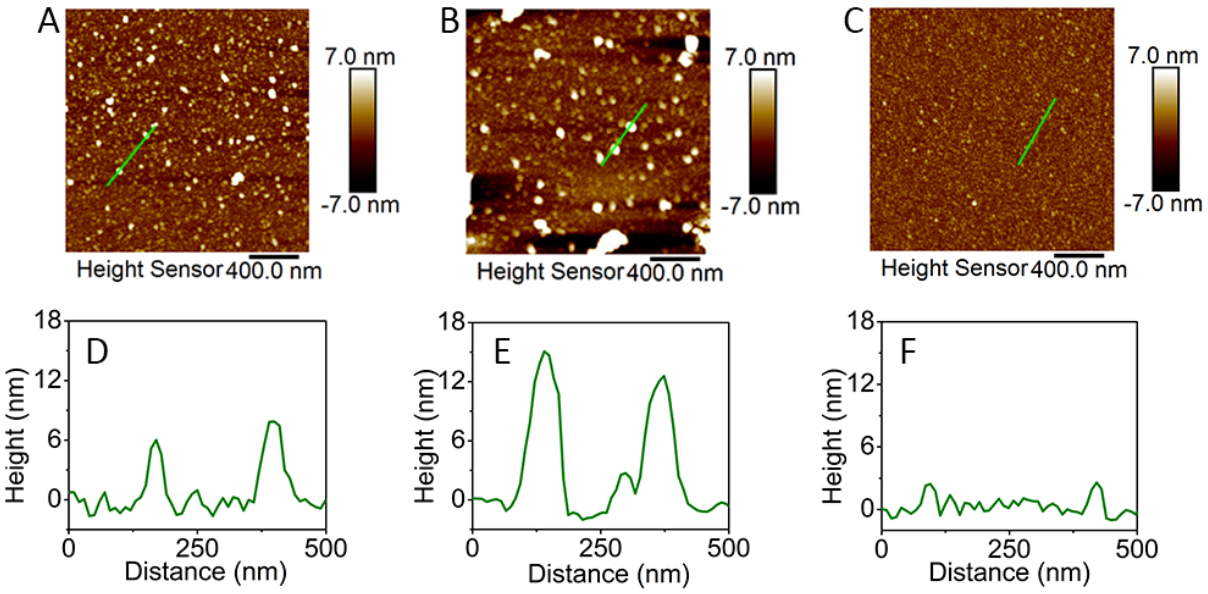

Figure 4. 10. Surface topography (2 × 2 μm^2) of the silica sensors that have been flushed by bitumen/cyclohexane-heptane solution in QCM-D measurements with (A) φ_c = 1, (B) φ_c = 0.75 and (C) φ_c = 0.5. Cross-section analysis plots along green lines in topography panels with (D) φ_c = 1, (E) φ_c = 0.75 and (F) φ_c = 0.5.

Figure 4. 10 shows the surface topography of the quartz crystal sensor at t = 50 min tracked by AFM imaging immediately. In the case of φ_c = 1, spherical bitumen nanoaggregates with the height of 6-8 nm was observed on the silica surface (Figure 4. 10A and 4. 10D). When φ_c was lowered to 0.75, similar but larger spherical nanoaggregates formed (11-13 nm in height) and some irregular bitumen nanoaggregates with the height of 20-40 nm also displayed on the surface (Figure 4. 10B and 4.10E). Correspondingly, the surface roughness (R_q) was measured to be 1.50 nm and 4.00 nm for φ_c = 1 and 0.75, respectively. Unlike these two cases, the adsorbed bitumen

layer in the case of φ_c = 0.5 was relatively smooth with R_q = 0.50 nm and the average height of bitumen nanoaggregates drastically reduced to about 3 nm (Figure 4. 10C and 4. 10F).

The topography changes of adsorbed bitumen on the surface revealed the distinct bitumen morphologies present in bulk solutions. Before the asphaltene precipitation onset ($\varphi_c > 0.74$), some bitumen fractions such as asphaltenes were well dissolved but could still readily form primary self-assembly nanoaggregates through VDW interaction, π-π stacking[58] and polymerization-like association "reactions",[59] contributing to the main constituent of the adsorbed bitumen layer. Adding heptane slightly increased concentrations of insoluble asphaltenes present in solution, which could enhance the deposition of asphaltenes to the surface.[60] Simultaneously, increasing contents of heptane (viz. decrease φ_c) could promote growth of both soluble and insoluble asphaltene aggregates in size possibly due to the stronger VDW attraction among bitumen fractions.[61] Whereas, after the precipitation onset ($\varphi_c < 0.74$), the poor solubility of asphaltenes in heptane-rich environments triggered the generation of large asphaltene particles. Under constant temperature and constant flow rate, such large asphaltene particles would have a lower diffusion rate than the primary aggregates or even small molecules of asphaltenes.[43, 62] As a result, the large aggregated particles could be immediately flushed away from the flow module without adsorption or deposition because of inertia of convective transfer. That's why, with $\varphi_c < 0.75$, the adsorbed mass suffered a drastic decrease and the surface of adsorbed bitumen layer became relatively smooth and flat. The results of QCM-D experiments provide the evidence on the effects of organic solvents on the adsorbed mass and surface morphologies of bitumen film on the mineral solids.

4.3.3. Sedimentation tests

The sedimentation test on the macroscopic scale was monitored for the bitumen-treated silica solids to analyze contributions of bitumen adsorption behaviors and particle-particle interactions to the stability of fine solids in organic media. Hence, two scenarios of batch tests were conducted: (1) preparing bitumen-coated fine solids in different bitumen/cyclohexane-heptane solutions (φ_c = 1.00, 0.90, 0.75, 0.6 and 0.50) and settling these solids in pure cyclohexane; (2) preparing bitumen-coated fine solids in the bitumen/cyclohexane solution and settling these solids in the mixed solvent cyclohexane-heptane (φ_c = 1.00, 0.75, 0.5, 0.25 and 0.00). All the treated silica solids were centrifuged in cyclohexane to remove any non-adsorbing bitumen fractions or weakly adsorbed bitumen from the solids.

In the first scenario, structures of bitumen-coated solids were analyzed by infrared spectroscopy, which showed typical characteristic peaks of asphaltenes reported elsewhere.[63] The degree of adsorption of bitumen on the silica solids was quantified by the peak intensity (PI) of methylene group (-CH_2-) on the solids surface demonstrated by infrared spectroscopy, as shown in Figure 4. 11. Peaks located at 2959, 2928 and 2856 cm^{-1} are assigned to the stretching aliphatic bands ($\nu(CH_3 + CH_2)$) (Figure 4. 11A), and peaks at 1076 and 798 cm^{-1} reflect Si-O-Si band and Si-OH deformation band, respectively (Figure 4. 11B).[64] The positive absorbance bands $\nu(CH_3 + CH_2)$ indicated the presence of bitumen coating on the solid surfaces, and the negative absorbance bands of Si-O-Si and Si-OH indicated the loss of outmost silica surface of solid particles due to bitumen adsorption. The peak intensity (PI) of these feature bands was measured from the absorbance spectra detected under all solvent conditions, as shown in Figure 4. 11C. It was noticed that the increase in PI of hydrocarbon bands (CH_2, CH_3) was always accompanied with the reduction in PI of silica bands (Si-O-Si, Si-OH), demonstrating that the higher degree of bitumen

adsorption on the solid particles would result in the smaller exposed surface area of silica. It was also found that the changes of CH_2 intensity showed the order: PI (φ_c = 0.75) > PI (φ_c = 0.9) > PI (φ_c = 1) > PI (φ_c = 0.6) > PI (φ_c = 0.5), which was consistent with the order in the adsorbed mass of bitumen on the silica sensor revealed by QCM-D experiments: Mass (φ_c = 0.75) > Mass (φ_c = 0.9) > Mass (φ_c = 1) > Mass (φ_c = 0.6) > Mass (φ_c = 0.5) (Figure 4. 11D). Therefore, the CH_2 intensity was used as the indicator of degree of adsorption of bitumen on the silica particles.

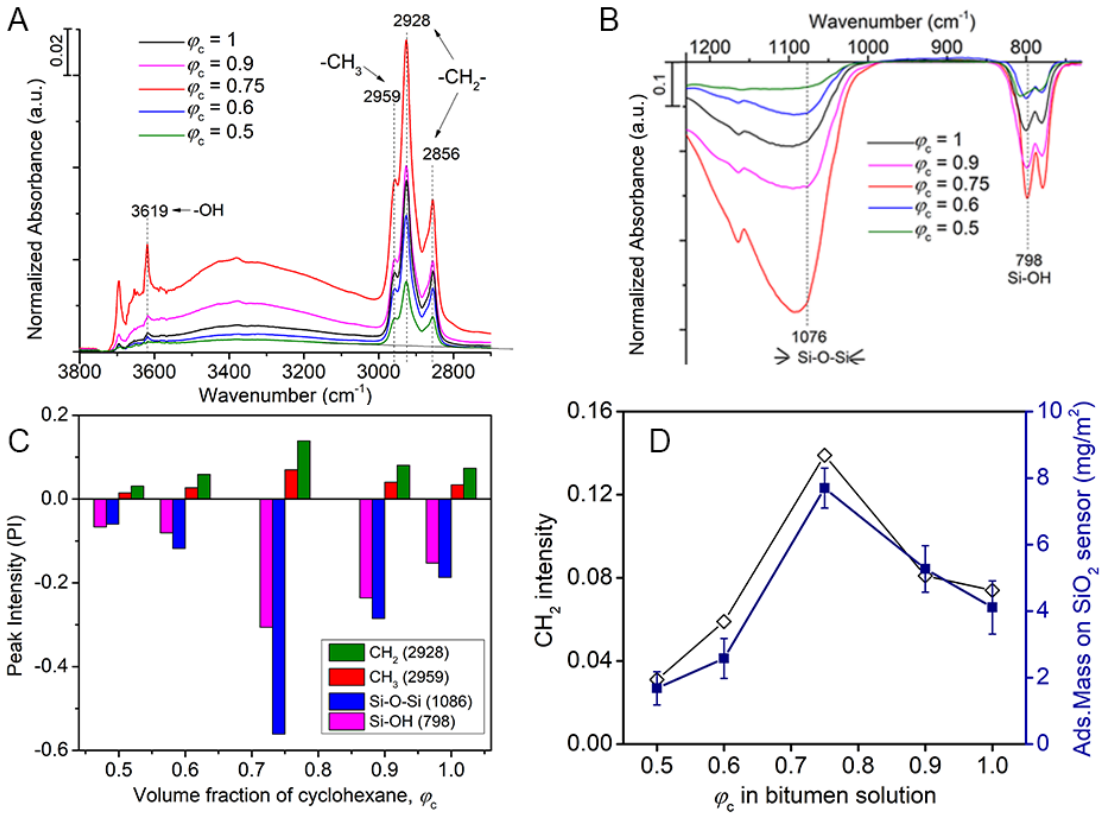

Figure 4. 11. Absorbance spectra of silica solids treated by different bitumen/cyclohexane-heptane solutions with varied volume fraction of cyclohexane (φ_c) corresponding to the regions between (A) 2700 -3800 cm^{-1} and (B) 700 - 1300 cm^{-1}. (C) Measured peak intensity (PI) of feature bands CH_2, CH_3, Si-O-Si and Si-OH, and (D) PI of CH_2 (black symbol) and adsorbed mass of bitumen on the QCM-D sensor at t = 50 min (blue symbol).

Figure 4. 12A shows the settling performance of the silica solids with different degree of bitumen adsorption (scenario 1). With the degree of adsorption increasing, the ISR showed a slowly increment and always kept below 10 mg/s, which indicates an ineffective role of adsorption degree in the initial settling process. At long settling time, it was found that the bitumen-coated fine solids could not completely settle out and the content of residual solids in the supernatant at t = 30 min slightly increased from ~ 400 ppm to ~ 500 ppm when the degree of adsorption was raised from 1.0 to 4.6. This result suggested that the higher degree of bitumen adsorption could stabilize the suspended fine solids possibly due to the stronger repulsion between solid particles.

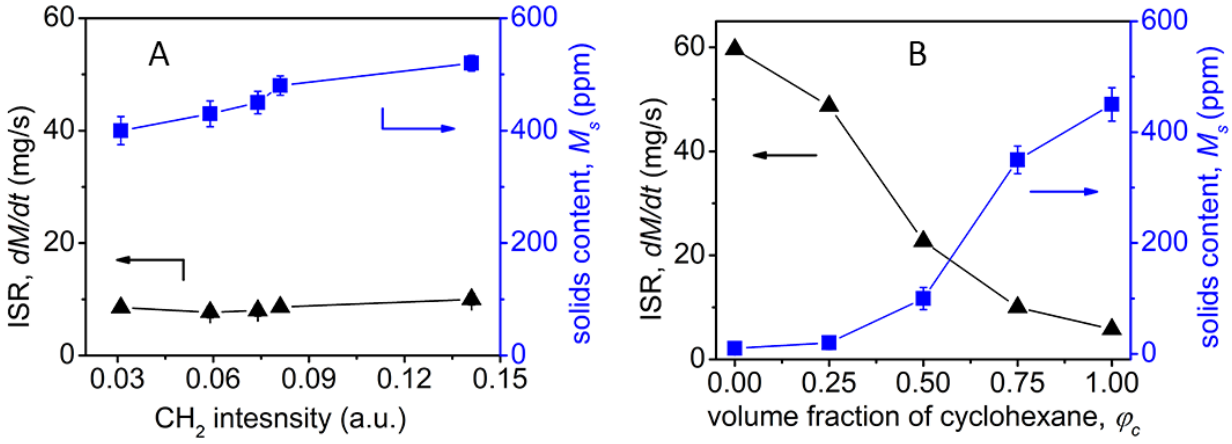

Figure 4. 12. Data on initial settling rate (ISR) and residual solids content collected in the sedimentation tests (A) as a function of the degree of adsorption of bitumen on the solids and (B) as a function of φ_c in the sedimentation solvent cyclohexane-heptane.

Figure 4. 12B shows the effects of organic solvents on the settling performances of the treated solids with the same degree of bitumen adsorption (scenario 2). A noticeable increment in ISR was observed with φ_c declining. The ISR in pure heptane (~ 59 mg/s) was almost 10 times larger than that in pure cyclohexane (~ 6 mg/s). With prolonged settling time, the solids content was significantly reduced from ~ 450 ppm to a negligible value via adjusting φ_c from 1 to 0. Both low ISR or high solids content in cyclohexane should be attributed to the strong and long-ranged

steric repulsion between bitumen-coated fine solids, suggesting the formation of a stable suspension of fine solids in cyclohexane. When the fine solids came into contact during the magnetic stir, the weak adhesion between two contact particles in cyclohexane was not comparable to the shear forces of stirring that can tear solids apart. In comparison, the high ISR and extremely low solids content in heptane indicated the effective particle-particle interactions, which enhanced the formation of solids aggregates and destabilize the fine solids in the suspension.

4.4. Conclusions

In this study, the interaction forces between a silica microsphere and a flat silica substrate either clean or coated with bitumen were measured using a colloidal probe AFM in the mixture of cyclohexane and heptane. A steric repulsion between the silica microsphere and bitumen-coated silica surface was observed in pure cyclohexane caused by the extension of bitumen chains in good solvent. Such steric repulsion was gradually weakened with lower volume fraction of cyclohexane (φ_c) and finally turned to a weak attraction in the pure heptane. The range and magnitude of the steric repulsion were further enhanced in a symmetric system where both two silica surfaces were coated with bitumen layer. The theoretical model, sum of VDW force and steric force, agreed well with the force-separation profiles measured during the approach process. The adhesion force required to separate two contact solid surfaces was found to increase with decreasing φ_c.

QCM-D was applied to characterize the adsorption behaviors of bitumen on a simulated silica surface in diluted bitumen/cyclohexane-heptane solutions with varying φ_c. The results showed that the degree of adsorption of bitumen at initial time was mainly controlled by the interactions between bitumen and silica surface, while at long time was synchronously affected by the diffusion, aggregation, deposition and convection processes. The diffusion of bitumen fractions

from the organic media to the silica surface was strongly related to the morphology of bitumen in solution. Before the precipitation onset, generation of primary bitumen nanoaggregates contributed to the bitumen deposition to the solid surface and were the main constituent of the adsorbed bitumen layer. The adsorbed mass and the initial adsorption rate of bitumen increased with lowering φ_c due to the growth of primary aggregates. After the precipitation onset, large aggregate particles of bitumen were formed which could be immediately flushed away from the flow module without deposition or adsorption to the surface, resulting in the notable decrease in both adsorption mass and initial adsorption rate of bitumen.

The stability of bitumen-coated silica particles was evaluated using semi-empirical sedimentation tests with the effects of surrounding organic solvents and the degree of bitumen adsorption on solids surface. The results showed that both the ISR and the content of residual silica solids in the supernatant were significantly influenced by surrounding organic solvents that could mediate particle-particle interactions. The bitumen-coated silica particles were quite stable in cyclohexane due to the presence of bitumen coating on the solids surface which produced the steric repulsion between two particles, resulting in the low ISR value (~ 6 mg/s) and high solids content (~ 450 ppm). The increase in the degree of bitumen adsorption could further slightly increase the content of residual solids (~ 500 ppm) remained in the supernatant. The findings in this work provide useful insights into the fundamental understanding of stabilization mechanisms of fine solids in organic media from the NAE process.

Reference

1. West, R. C., Non-Aqueous Process for the Recovery of Bitumen from Tar Sands. Google Patents: 1964.

2. Nikakhtari, H.; Vagi, L.; Choi, P.; Liu, Q.; Gray, M. R., Solvent Screening for Non-Aqueous Extraction of Alberta Oil Sands. *Can. J. Chem. Eng.* **2013**, *91*, 1153-1160.

3. Pal, K.; Nogueira Branco, L. d. P.; Heintz, A.; Choi, P.; Liu, Q.; Seidl, P. R.; Gray, M. R., Performance of Solvent Mixtures for Non-Aqueous Extraction of Alberta Oil Sands. *Energy Fuels* **2015**, *29*, 2261-2267.

4. Leung, H.; Phillips, C. R., Solvent Extraction of Mined Athabasca Oil Sands. *Ind. Eng. Chem. Fundam.* **1985**, *24*, 373-379.

5. Wu, J.; Dabros, T., Process for Solvent Extraction of Bitumen from Oil Sand. *Energy Fuels* **2012**, *26*, 1002-1008.

6. Hooshiar, A.; Uhlik, P.; Liu, Q.; Etsell, T. H.; Ivey, D. G., Clay Minerals in Nonaqueous Extraction of Bitumen from Alberta Oil Sands: Part 1. Nonaqueous Extraction Procedure. *Fuel Process. Technol.* **2012**, *94*, 80-85.

7. Sparks, B.; Meadus, F., A Study of Some Factors Affecting Solvent Losses in the Solvent Extraction—Spherical Agglomeration of Oil Sands. *Fuel Process. Technol.* **1981**, *4*, 251-264.

8. Meadus, F.; Bassaw, B.; Sparks, B., Solvent Extraction of Athabasca Oil-Sand in a Rotating Mill Part 2. Solids—Liquid Separation and Bitumen Quality. *Fuel Process. Technol.* **1982**, *6*, 289-300.

9. Painter, P.; Williams, P.; Mannebach, E., Recovery of Bitumen from Oil or Tar Sands Using Ionic Liquids. *Energy Fuels* **2009**, *24*, 1094-1098.

10. Williams, P.; Lupinsky, A.; Painter, P., Recovery of Bitumen from Low-Grade Oil Sands Using Ionic Liquids. *Energy Fuels* **2010**, *24*, 2172-2173.

11. Holland, A.; Wechsler, D.; Patel, A.; Molloy, B. M.; Boyd, A. R.; Jessop, P. G., Separation of Bitumen from Oil Sands Using a Switchable Hydrophilicity Solvent. *Can. J. Chem.* **2012**, *90*, 805-810.

12. Jessop, P. G.; Phan, L. N.; Carrier, A. J.; Resendes, R.; Wechsler, D., Switchable Hydrophilicity Solvents and Methods of Use Thereof. Google Patents: 2013.

13. Bensebaa, F.; Kotlyar, L. S.; Sparks, B. D.; Chung, K. H., Organic Coated Solids in Athabasca Bitumen: Characterization and Process Implications. *Can. J. Chem. Eng.* **2000**, *78*, 610-616.

14. Nikakhtari, H.; Wolf, S.; Choi, P.; Liu, Q.; Gray, M. R., Migration of Fine Solids into Product Bitumen from Solvent Extraction of Alberta Oilsands. *Energy Fuels* **2014**, *28*, 2925-2932.

15. Liu, J.; Wang, J.; Huang, J.; Cui, X.; Tan, X.; Liu, Q.; Zeng, H., Heterogeneous Distribution of Adsorbed Bitumen on Fine Solids from Solvent-Based Extraction of Oil Sands Probed by Afm. *Energy Fuels* **2017**.

16. Buckley, J.; Liu, Y., Some Mechanisms of Crude Oil/Brine/Solid Interactions. *J. Pet. Sci. Eng.* **1998**, *20*, 155-160.

17. Liu, Q.; Dong, M.; Asghari, K.; Tu, Y., Wettability Alteration by Magnesium Ion Binding in Heavy Oil/Brine/Chemical/Sand Systems—Analysis of Electrostatic Forces. *J. Pet. Sci. Eng.* **2007**, *59*, 147-156.

18. Tian, C.; Lu, Q.; Liu, Y.; Zeng, H.; Zhao, Y.; Zhang, J.; Gupta, R., Understanding of Physicochemical Properties and Formation Mechanisms of Fine Particular Matter Generated from Canadian Coal Combustion. *Fuel* **2016**, *165*, 224-234.

19. Shi, C.; Zhang, L.; Xie, L.; Lu, X.; Liu, Q.; He, J.; Mantilla, C. A.; Zeng, H., Surface Interaction of Water-in-Oil Emulsion Droplets with Interfacially Active Asphaltenes. *Langmuir* **2017**, *33*, 1265-1274.

20. Shi, C.; Zhang, L.; Xie, L.; Lu, X.; Liu, Q.; Mantilla, C. A.; van den Berg, F. G.; Zeng, H., Interaction Mechanism of Oil-in-Water Emulsions with Asphaltenes Determined Using Droplet Probe Afm. *Langmuir* **2016**, *32*, 2302-2310.

21. Jian, C.; Poopari, M. R.; Liu, Q.; Zerpa, N.; Zeng, H.; Tang, T., Reduction of Water/Oil Interfacial Tension by Model Asphaltenes: The Governing Role of Surface Concentration. *J. Phys. Chem. B* **2016**, *120*, 5646-5654.

22. Liu, J.; Xu, Z.; Masliyah, J., Role of Fine Clays in Bitumen Extraction from Oil Sands. *AlChE J.* **2004**, *50*, 1917-1927.

23. Liu, J.; Xu, Z.; Masliyah, J., Studies on Bitumen− Silica Interaction in Aqueous Solutions by Atomic Force Microscopy. *Langmuir* **2003**, *19*, 3911-3920.

24. Liu, J.; Xu, Z.; Masliyah, J., Interaction between Bitumen and Fines in Oil Sands Extraction System: Implication to Bitumen Recovery. *Can. J. Chem. Eng.* **2004**, *82*, 655-666.

25. Zhang, L.; Shi, C.; Lu, Q.; Liu, Q.; Zeng, H., Probing Molecular Interactions of Asphaltenes in Heptol Using a Surface Forces Apparatus: Implications on Stability of Water-in-Oil Emulsions. *Langmuir* **2016**, *32*, 4886-4895.

26. Natarajan, A.; Xie, J.; Wang, S.; Liu, Q.; Masliyah, J.; Zeng, H.; Xu, Z., Understanding Molecular Interactions of Asphaltenes in Organic Solvents Using a Surface Force Apparatus. *J. Phys. Chem. C* **2011**, *115*, 16043-16051.

27. Wang, J.; van der Tuuk Opedal, N.; Lu, Q.; Xu, Z.; Zeng, H.; Sjöblom, J., Probing Molecular Interactions of an Asphaltene Model Compound in Organic Solvents Using a Surface Forces Apparatus (Sfa). *Energy Fuels* **2011**, *26*, 2591-2599.

28. Xiong, Y.; Li, Z.; Cao, T.; Xu, S.; Yuan, S.; Sjoblom, J.; Xu, Z., Synergistic Adsorption of Polyaromatic Compounds on Silica Surfaces Studied by Molecular Dynamics Simulation. *J. Phys. Chem. C* **2018**, *122*, 4290-4299.

29. Zhu, X.; Chen, D.; Wu, G., Insights into Asphaltene Aggregation in the Na-Montmorillonite Interlayer. *Chemosphere* **2016**, *160*, 62-70.

30. Marczewski, A. W.; Szymula, M., Adsorption of Asphaltenes from Toluene on Mineral Surface. *Colloids Surf., A* **2002**, *208*, 259-266.

31. Wang, S.; Liu, J.; Zhang, L.; Masliyah, J.; Xu, Z., Interaction Forces between Asphaltene Surfaces in Organic Solvents. *Langmuir* **2009**, *26*, 183-190.

32. Zhang, K.; Jia, N.; Zeng, F., Application of Predicted Bubble-Rising Velocities for Estimating the Minimum Miscibility Pressures of the Light Crude Oil–Co 2 Systems with the Rising Bubble Apparatus. *Fuel* **2018**, *220*, 412-419.

33. Zahabi, A.; Gray, M. R.; Dabros, T., Kinetics and Properties of Asphaltene Adsorption on Surfaces. *Energy Fuels* **2012**, *26*, 1009-1018.

34. Dudášová, D.; Silset, A.; Sjöblom, J., Quartz Crystal Microbalance Monitoring of Asphaltene Adsorption/Deposition. *J. Dispersion Sci. Technol.* **2008**, *29*, 139-146.

35. Rudrake, A.; Karan, K.; Horton, J. H., A Combined Qcm and Xps Investigation of Asphaltene Adsorption on Metal Surfaces. *J. Colloid Interface Sci.* **2009**, *332*, 22-31.

36. Alagha, L.; Wang, S.; Yan, L.; Xu, Z.; Masliyah, J., Probing Adsorption of Polyacrylamide-Based Polymers on Anisotropic Basal Planes of Kaolinite Using Quartz Crystal Microbalance. *Langmuir* **2013**, *29*, 3989-3998.

37. Kelesoglu, S.; Volden, S.; Kes, M.; Sjoblom, J., Adsorption of Naphthenic Acids onto Mineral Surfaces Studied by Quartz Crystal Microbalance with Dissipation Monitoring (Qcm-D). *Energy Fuels* **2012**, *26*, 5060-5068.

38. Ducker, W. A.; Senden, T. J.; Pashley, R. M., Direct Measurement of Colloidal Forces Using an Atomic Force Microscope. *Nature* **1991**, *353*, 239.

39. Butt, H.-J.; Cappella, B.; Kappl, M., Force Measurements with the Atomic Force Microscope: Technique, Interpretation and Applications. *Surf. Sci. Rep.* **2005**, *59*, 1-152.

40. Wang, J.; Li, J.; Xie, L.; Shi, C.; Liu, Q.; Zeng, H., Interactions between Elemental Selenium and Hydrophilic/Hydrophobic Surfaces: Direct Force Measurements Using Afm. *Chem. Eng. J.* **2016**, *303*, 646-654.

41. Yang, G.; Chen, T.; Zhao, J.; Yu, D.; Liu, F.; Wang, D.; Fan, M.; Chen, W.; Zhang, J.; Yang, H., Desorption Mechanism of Asphaltenes in the Presence of Electrolyte and the Extended Derjaguin–Landau–Verwey–Overbeek Theory. *Energy Fuels* **2015**, *29*, 4272-4280.

42. Sauerbrey, G., Verwendung Von Schwingquarzen Zur Wägung Dünner Schichten Und Zur Mikrowägung. *Z. Phys. A* **1959**, *155*, 206-222.

43. Tavakkoli, M.; Panuganti, S. R.; Vargas, F. M.; Taghikhani, V.; Pishvaie, M. R.; Chapman, W. G., Asphaltene Deposition in Different Depositing Environments: Part 1. Model Oil. *Energy Fuels* **2013**, *28*, 1617-1628.

44. Jin, Y.; Liu, W.; Liu, Q.; Yeung, A., Aggregation of Silica Particles in Non-Aqueous Media. *Fuel* **2011**, *90*, 2592-2597.

45. Fischer, H.; Stadler, H.; Erina, N., Quantitative Temperature-Depending Mapping of Mechanical Properties of Bitumen at the Nanoscale Using the Afm Operated with Peakforce Tappingtm Mode. *J. Microsc.* **2013**, *250*, 210-217.

46. Rebelo, L.; De Sousa, J.; Abreu, A.; Baroni, M.; Alencar, A.; Soares, S.; Mendes Filho, J.; Soares, J., Aging of Asphaltic Binders Investigated with Atomic Force Microscopy. *Fuel* **2014**, *117*, 15-25.

47. Natarajan, A.; Kuznicki, N.; Harbottle, D.; Masliyah, J.; Zeng, H.; Xu, Z., Understanding Mechanisms of Asphaltene Adsorption from Organic Solvent on Mica. *Langmuir* **2014**, *30*, 9370-9377.

48. Israelachvili, J. N., *Intermolecular and Surface Forces*; Academic press, **2015**.

49. Lewis, J. A., Colloidal Processing of Ceramics. *J. Am. Ceram. Soc.* **2000**, *83*, 2341-2359.

50. Butt, H.-J.; Kappl, M.; Mueller, H.; Raiteri, R.; Meyer, W.; Rühe, J., Steric Forces Measured with the Atomic Force Microscope at Various Temperatures. *Langmuir* **1999**, *15*, 2559-2565.

51. O'shea, S.; Welland, M.; Rayment, T., An Atomic Force Microscope Study of Grafted Polymers on Mica. *Langmuir* **1993**, *9*, 1826-1835.

52. Masliyah, J. H.; Bhattacharjee, S., *Electrokinetic and Colloid Transport Phenomena*; John Wiley & Sons, 2006.

53. De Gennes, P., Polymers at an Interface; a Simplified View. *Adv. Colloid Interface Sci.* **1987**, *27*, 189-209.

54. Alexander, S., Adsorption of Chain Molecules with a Polar Head a Scaling Description. *J. Phys.* **1977**, *38*, 983-987.

55. Tavakkoli, M.; Panuganti, S. R.; Taghikhani, V.; Pishvaie, M. R.; Chapman, W. G., Asphaltene Deposition in Different Depositing Environments: Part 2. Real Oil. *Energy Fuels* **2014**, *28*, 3594-3603.

56. Xie, K.; Karan, K., Kinetics and Thermodynamics of Asphaltene Adsorption on Metal Surfaces: A Preliminary Study. *Energy Fuels* **2005**, *19*, 1252-1260.

57. Abudu, A.; Goual, L., Adsorption of Crude Oil on Surfaces Using Quartz Crystal Microbalance with Dissipation (Qcm-D) under Flow Conditions. *Energy Fuels* **2009**, *23*, 1237-1248.

58. Sedghi, M.; Goual, L.; Welch, W.; Kubelka, J., Effect of Asphaltene Structure on Association and Aggregation Using Molecular Dynamics. *J. Phys. Chem. B* **2013**, *117*, 5765-5776.

59. Agrawala, M.; Yarranton, H. W., An Asphaltene Association Model Analogous to Linear Polymerization. *Ind. Eng. Chem. Res.* **2001**, *40*, 4664-4672.

60. Hoepfner, M. P.; Limsakoune, V.; Chuenmeechao, V.; Maqbool, T.; Fogler, H. S., A Fundamental Study of Asphaltene Deposition. *Energy Fuels* **2013**, *27*, 725-735.

61. Hoepfner, M. P.; Vilas Bôas Fávero, C. u.; Haji-Akbari, N.; Fogler, H. S., The Fractal Aggregation of Asphaltenes. *Langmuir* **2013**, *29*, 8799-8808.

62. Kurup, A. S.; Wang, J.; Subramani, H. J.; Buckley, J.; Creek, J. L.; Chapman, W. G., Revisiting Asphaltene Deposition Tool (Adept): Field Application. *Energy Fuels* **2012**, *26*, 5702-5710.

63. Liu, D.; Li, Z.; Fu, Y.; Zhang, Y.; Gao, P.; Dai, C.; Zheng, K., Investigation on Asphaltene Structures During Venezuela Heavy Oil Hydrocracking under Various Hydrogen Pressures. *Energy Fuels* **2013**, *27*, 3692-3698.

Chapter 5 Removing Fine Solids in Oil Media through Wettability Modification and Water-Assisted Agglomeration

5.1 Introduction

Removal of fine solids from liquid phase plays a dominant role in many chemical and environmental engineering processes with ever-increasing demands on improving the quality of product quality and/or alleviating environmental impact of waste residues. Relevant studies in aqueous system are well established in various fields such as wastewater treatment, mineral processing and paper recycling, while the understanding on the organic systems is very limited and the solid/liquid separation still remains challenging in these systems. For instance, difficulties in removing mineral solids from coal derived liquids has been a major obstacle to economic production of liquefied coal products.1 Similarly, in oil sands industry, fine mineral solids (diameter $\leqslant 44$ μm) can readily find their way into oil, imposing detrimental impacts on the quality of bitumen products and processing facilities.[2-3] Removing the fine solids suspended in oil media is complicated, and in some systems, e.g. non-aqueous extraction (NAE) of oil sands, the solid content in oil cannot be lowered to an acceptable level even after a series of elaborate filtration.[4] Therefore, research has been conducted in this work to develop a viable approach to destabilize the fine solids suspended in oil media in the context of solids removal in NAE process.

The concept of NAE was proposed as a potential substitute to the current commercial Clark hot water extraction (CHWE) process, which is used in oil sands production,[5] to alleviate severe environmental issues inherent to CHWE such as massive consumption of fresh water and fast

accumulation of slow-settling tailings. In NAE, organic solvent is used to dissolve and liberate bitumen from raw oil sands ore and can be ultimately recovered via a distillation process and recycled upstream.[6-7] Due to high bitumen recovery and good applicability for all kinds of oil sands, as well as the generation of dry stackable extraction tailings, NAE has gained increasing attention from the industry and academic fields.[8-10] However, no commercial NAE process has been established, and this has been attributed to some perennial bottlenecks, one of which arises from the migration of considerable amount fine solids to oil media. Previous studies have revealed that the adsorbed organic matter on the fine solids surfaces plays a dominant role in the formation of stable suspension of fine solids in oil media,[11-12] making it extremely difficult to remove the fine solids by conventional gravitational/centrifugal settling or filtration.

During the last decades, some attempts have been made to destabilize the fine solids in oil media. The most practical strategy is to trigger the formation of large aggregates of the fine solids. There are two optional approaches, i.e., homo-aggregation and hetero-aggregation. Studies on the homo-aggregation technique have been widely reported. Precipitation of asphaltenes (i.e., major fraction of bitumen) by aliphatic solvents (e.g., *n*-heptane)[13-15] can be used to generate the homo-aggregation of fine solids in organic media because the precipitated asphaltene acts as bonding bridges among the fine solids.[3, 16-17] Aliphatic solvents can also weaken the steric repulsion between fine solids by shrinking adsorbed asphaltene layer on solids surfaces, thereby enhancing the particle-particle colloidal attraction.[11, 18-20] However, such method requests a substantial consumption of aliphatic solvents in order to achieve a relatively low solid content, which would apparently increase the cost and difficulty in the subsequent operations.[16]

In a hetero-aggregation processes, the solid particles usually aggregate with added process aids. For example, after adding ionic liquids (e.g., [Bmmim][BF4]), the solid content in oil media

could be significantly lowered.[21-25] It has been reported that ionic liquids can preferentially wet the solids due to strong electrostatic attraction between the ionic liquids and the mineral surface, which effectively displaces the bitumen coating.[26-27] The resultant clean mineral solids undergo aggregation in ionic liquids and can be readily removed because the highly polar ionic liquids are completely immiscible with organic solvent. The drawbacks of ionic liquids are mainly associated with their high cost and uncertainty in toxicity to the oil products and the ecological environment. Since the 1980s, research work has been conducted to investigate the role of small amount of water in agglomerating the fine particles in oil media.[28-31] The hydrophilic and relatively clean solids were found to be physically trapped by the added water and the formation of solid-water agglomerates successfully improved the efficiency of subsequent solids/oil separations.[30] Nonetheless, this method failed to lower solid content to a satisfied level because water was not able to wet the hydrophobic bitumen-coated fine solids that account for the majority of mineral contaminants in the diluted bitumen. Recently, switchable-hydrophilicity solvents (e.g., tertiary amines) have been used to reduce the hydrophobicity of the bitumen-coated solids surfaces.[32-34] In the presence of CO_2, the protonated tertiary amine generated in water can effectively form ion pairs with bitumen components to enhance the bitumen liberation from mineral solids. However, such aqueous-nonaqueous hybrid extraction with essential high dosage of water inevitably gave rise to the formation of oil-water emulsions.

Inspired by the water agglomeration method, in this work, we have developed a novel two-step approach to lower the content of fine solids suspended in oil media, that is, to reduce the hydrophobicity of the bitumen-coated fine solids and subsequently remove the particles by introducing a small amount of water. A cost-effective and environmentally friendly material, poly(ethylene glycol)-block-poly(propylene glycol)-block-poly(ethylene glycol) (PEG-PPG-

PEG), was applied to modify the surface wettability of the bitumen-coated fine solids. The hydrophilic PEG segments can reduce the hydrophobicity of the fine solids[35] and increase their affinity for water,[36-38] while the lipophilic PPG segments increase the solubility of the block polymer in cyclohexane. The performance of the two-step agglomeration method in removing the fine silica particles in cyclohexane was quantitatively evaluated through sedimentation tests. The relevant physical interaction mechanisms were investigated using atomic force microscope (AFM) and quartz crystal microbalance with dissipation monitoring (QCM-D). Batch sedimentation tests were also conducted with addition of only water, PEG-PPG-PEG or PEG-PPG-PEG aqueous solution, which highlight the necessity and applicability of the two-step approach. This research work will shed instructive light on the development of efficient and economical approaches to removing intractable fine solids in oil media, ultimately improving the quality of petroleum and petrochemical products and simplifying the technological process to extract oil from the oil sands.

5.2. Materials and Methods

5.2.1. Materials

Athabasca bitumen was provided by Syncrude Canada Ltd. Cyclohexane (Certified ACS grade, > 99.0%), toluene (Certified ACS grade, > 99.5%) and octadecyltrichlorosilane (OTS, 95%) were purchased from Fisher Scientific, Canada. Silica microspheres (~ 5 μm in diameter), silica solid particles (~ 0.5-10 μm in diameter), PEG-PPG-PEG (*Mn* ~ 8400, PEG content ~ 80 wt%) and 11-Mercapto-1-undecanol (97%) were purchased from Sigma-Aldrich, Canada. Silicon wafer with 0.5 μm thermal oxide film was purchased from the NanoFab, University of Alberta. The AT-cut crystal (5 MHz) QCM-D sensor coated with 50 nm silica (QSX 303) was purchased from Biolin Scientific, Sweden. A bitumen solution (0.1 wt%) was prepared by dissolving bitumen in

cyclohexane under sonication for 10 min. The PEG-PPG-PEG aqueous solutions of various concentrations (e.g., 25 mg/mL, 55 mg/mL, etc.) were prepared by dissolving PEG-PPG-PEG in Milli-Q water with a resistance ≥18.2 MΩ·cm.

5.2.2. Preparation of sample fine particles and flat surfaces

The bitumen-coated silica particles were used to mimic indigenous mineral fine solids found in the NAE bitumen and were prepared according to a method reported elsewhere.[39] Briefly, 10 g silica particles were dispersed in 100 mL bitumen-in-cyclohexane solution and the mixture was sonicated for 5 min and agitated under magnetic stirring (1000 rpm) for 10 min to allow bitumen adsorption onto the silica particles. The resulting particles were rinsed with cyclohexane through centrifugation (4000 rpm) to remove non-adsorbing bitumen components or loose deposit from the solid particles. Afterwards, the particles were collected and dried in a fume hood for 48 h.

A flat bitumen surface was prepared using a dip-coating method: a pre-cleaned silicon wafer (~ 1 × 1 cm^2) was immersed in the bitumen-in-cyclohexane solution for 10 min, rinsed with cyclohexane to remove any weakly adsorbed bitumen components, and dried in vacuum to remove the residual solvent. A PEG-PPG-PEG/bitumen surface was prepared by further dip-coating the bitumen surface in cyclohexane containing 1000 ppm PEG-PPG-PEG for 1 min, followed by thoroughly rinsing with cyclohexane and drying in vacuum to remove the solvent. The wettability of these flat substrate surfaces was characterized by measuring the static water contact angle (WCA) in both air and cyclohexane using a contact angle tensiometer (Ramé-hart Instrument Company, USA) under ambient conditions. The volume of the water droplet was kept at ~ 0.4 μL throughout

this work. The surface topography of the flat substrate surfaces was probed by AFM imaging operated on MFP-3D-Bio AFM (Asylum Research, Santa Barbara, CA).

5.2.3 Interfacial tension (IFT) measurement

The IFT between PEG-PPG-PEG aqueous solution and cyclohexane was measured using a goniometer (Ramé-hart Instrument Company, USA). During a typical measurement, cyclohexane was first loaded in a syringe connected with a U-shaped needle. The needle was immersed into a quartz fluid cell filled with PEG-PPG-PEG aqueous solution and a cyclohexane drop with volume about ~ 5-8 μL was generated by the syringe. IFT was measured by analyzing the drop profile every two seconds using a camera.

5.2.4. QCM-D measurement

Adsorption process of PEG-PPG-PEG onto the bitumen-coated silica surface was investigated at nanoscale using QCM-D technique under ambient condition. The experimental setup and procedures for typical tests have been reported previously.[40-42] In this study, the QCM-D measurement started with flowing cyclohexane over the silica sensor mounted in the flow module to establish a stable baseline. Next, bitumen-in-cyclohexane solution was driven to flow through the flow module for 10 min, and subsequently the solution was switched to pure cyclohexane to sweep the weakly adsorbed bitumen off from the silica sensor. After an equilibrium state was reached, PEG-PPG-PEG-in-cyclohexane (1000 ppm) was fed into the flow module. The real-time responses of the silica sensor, i.e., shifts in frequency (Δf) and dissipation (ΔD), were monitored synchronously during the QCM-D measurement, and the recorded experiment data

were analyzed to unravel the adsorption behavior of PEG-PPG-PEG on the bitumen-coated silica sensor surface.

5.2.5. Sedimentation tests

The sedimentation tests followed a modified procedure reported previously.[43] Figure 5. 1A schematically shows the sedimentation process of bitumen-coated silica particles in cyclohexane. Briefly, a suspension of bitumen-coated silica particles (mass fraction ~ 1.0 wt%) in cyclohexane was prepared by vigorous agitation through sonication in an ultrasound bath for 5 min and magnetic stirring (1100 rpm) for an additional 10 min. Then, a specific amount of additive, i.e., water or PEG-PPG-PEG, was introduced to the suspension, and the entire system was stirred for another 1 min at constant stirring speed (1100 rpm). The additive content in the suspension was expressed on the basis of the amount of cyclohexane used. To analyze the role of additives in destabilizing the bitumen-coated silica particles, four types of batch tests were conducted with (1) addition of only water, (2) addition of only PEG-PPG-PEG, (3) two-step addition of PEG-PPG-PEG and water and (4) one-step addition of only PEG-PPG-PEG aqueous solution, respectively. Specifically, in batch tests (2) and (3), PEG-PPG-PEG was first dispersed in cyclohexane by sonication prior to each addition. Afterwards, the whole mixture was transferred to a 100 mL graduated glass cylinder and the variation in the mudline height (h) with time (t) was recorded during the settling process, as shown in Figure 5. 1B. The initial settling rate (ISR) at the beginning of the process was determined by calculating the initial slope of the settling curve (h vs. t). At sedimentation time t = 30 min, supernatants were collected from the cylinder for turbidity measurement by Micro-100 Turbidimeter (Fisher Scientific, Canada) and expressed in NTU (nephelometric turbidity unit). By evaporating all cyclohexane from the sample supernatant under

vacuum, the content of residual solids in the supernatant was obtained by calculating the ratio of the residue's dry weight over the sample's initial weight.

5.2.6. AFM force measurements and AFM imaging

All the AFM force measurements were performed on the MFP-3D-Bio AFM. The interactions of water droplet with bitumen surface and with PEG-PPG-PEG/bitumen surface were investigated using a drop/bubble probe AFM technique,[44-48] and the schematics of the experimental setup is illustrated in Figure 5. 1C. Details on preparing the water drop probe have been reported elsewhere.[49-50] Briefly, water droplets were injected into an AFM fluid cell filled with cyclohexane using a custom-made ultrasharp glass pipet. In a typical force measurement, a water drop was first picked up by an AFM cantilever to generate a water drop probe and the drop-anchored probe was then relocated above the flat sample substrate for force measurements. A customized rectangular silicon AFM cantilever ended with a circular gold patch (diameter ~ 65 μm, thickness ~ 30 μm) was used, and the gold patch was hydrophilized by 11-mercapto-1-undecanol to favorably anchor a water drop. The spring constant (k) of the cantilever was calibrated using Hutter's method before loading the water drop.[51] The glass substrate of the fluid cell was pre-hydrophobized by OTS to facilitate easy lifting of water drop. The nominal velocity of the force measurement was set as 1 μm/s to minimize the hydrodynamic effect in surface force measurements. The maximum force load was set to 2 nN, and the force data was collected and recorded by the AFM software system.

To measure the interaction forces between two solids surfaces, a colloidal probe AFM technique was applied (Figure 5. 1D). A modified procedure according to the literature was used for preparing the colloidal probe.[52-54] Briefly, a silica microsphere (diameter ~ 5 μm) was glued to the end of a triangular tipless silicon nitride AFM cantilever using an epoxy adhesive which was

cured for 48 h. Then, the colloidal probe was immersed in the bitumen-in-cyclohexane solution for 10 min to allow bitumen adsorption onto the silica microsphere, which was followed by thorough rinsing with cyclohexane and complete drying in a vacuum desiccator. The colloidal probe was manipulated to approach and retract from the flat substrate samples placed in the fluid cell filled with cyclohexane. The maximum force load was set to 5 nN, and the force data was collected and recorded by the AFM software system.

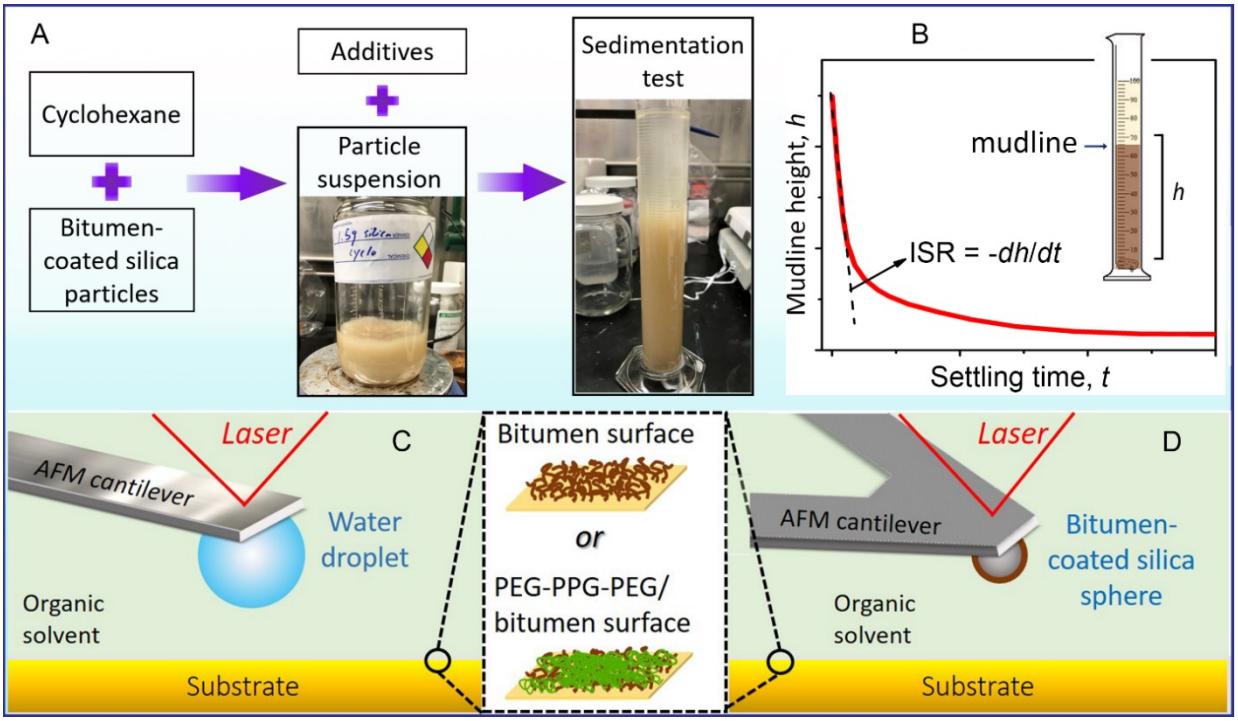

Figure 5. 1. Schematics of (A) the process of a typical sedimentation test, (B) initial settling rate (ISR) estimated from the settling results of mudline height (h) vs. settling time (t), and the experimental setup using (C) drop probe AFM and (D) colloidal probe AFM techniques, respectively.

5.3. Results and discussion

5.3.1. Sedimentation tests without additives

The bitumen-coated silica particles were slightly blackened compared to the bare silica particles due to the presence of irreversible adsorption of bitumen on the particles surface. Wettability measurements of the bitumen-coated silica substrate surface showed water contact angle (WCA) of ~ 91° ± 1°, which was consistent with that of the indigenous fine solids collected from the NAE bitumen.[4, 55] This result suggests that the adsorption of bitumen components could notably increase the surface hydrophobicity of silica surface (i.e., WCA of bare silica surface was 30° ± 1°).

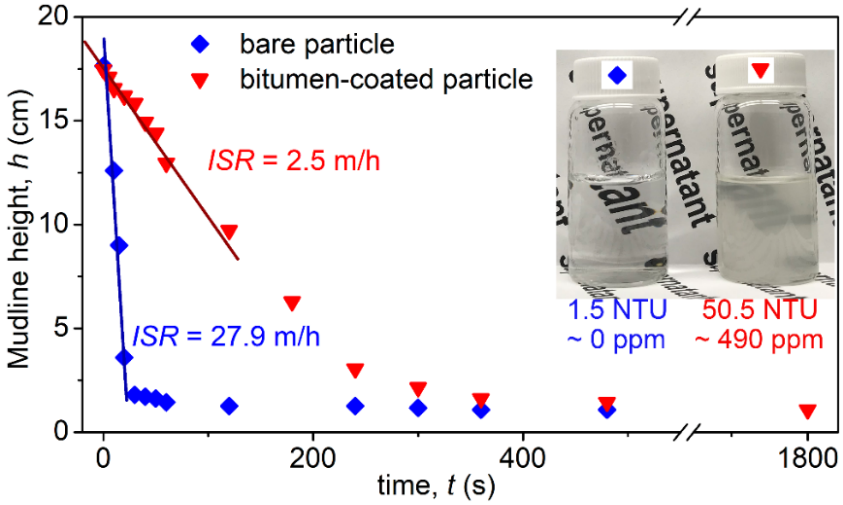

Figure 5. 2. The sedimentation results of the bare and bitumen-coated silica particles in cyclohexane without any additives. The inset displays the photographs of the sample supernatants collected at t = 30 min.

As shown in Figure 5. 2, when no additives were applied, the case of bitumen-coated silica particles exhibited an ISR value of ~ 2.5 m/h in cyclohexane, which was 11 times smaller than that of the bare silica case (~ 27.9 m/h). After 30 min settling, the supernatant turbidity for bare silica particles was measured to be ~ 1.5 NTU and the corresponding solid content in the supernatant

was almost negligible. In comparison, for the case of bitumen-coated particles the supernatant turbidity and solid content reached ~ 50.5 NTU and ~ 490 ppm, respectively, demonstrating that the adsorbed bitumen coating could contribute to the stable suspension of the fine particles owing to their hydrophobic nature and the steric inter-particle repulsion in cyclohexane.

5.3.2. Sedimentation tests with addition of water

Sedimentation tests with addition of only water were conducted to investigate the effect of water on destabilizing the bitumen-coated solid particles in cyclohexane. Figure 5. 3A shows the measured ISR as a function of water content in the suspension system. It is clear that the ISR value increased from ~ 2.5 m/h to ~ 5.3 m/h after a small amount of water (600 ppm) was introduced. With increasing the water content added, the ISR continued to increase and reached a plateau (~ 8.0 m/h) at the water content of ~ 2.5×10^4 ppm. This phenomenon indicate that the added water suspended as drops could be able to capture some of the solid particles whose surfaces were relatively less hydrophobic possibly due the interfacial-active nature of certain bitumen components,[55] leading to the formation of solid-water agglomerates that facilitates the particle sedimentation to some extent. FBRM measurements showed that the added water in cyclohexane under agitation (1000 rpm) displayed a drop size distribution ranging from ~ 10-35 μm in diameter at the water dosage of 6000 ppm. Figure 5. 3B shows the variation of supernatant turbidity and residual solid content with respect to the different water contents introduced. The supernatant turbidity firstly showed an evident drop from ~ 50.5 NTU to ~ 24.5 NTU when the water content rose from 0 to 6000 ppm, and then leveled off when the water content was increased further. The corresponding relationship between the residual solid content and the applied water content was found to follow the similar trend. Clearly, within the applied water contents, the lowest solid residue content remained as high as ~ 370 ppm, more than three quarters of that in the case of no

additives (~ 490 ppm). This result demonstrates that most of the hydrophobic bitumen-coated silica particles could not be destabilized and settle out from the supernatant by simply introducing water to the suspension system.

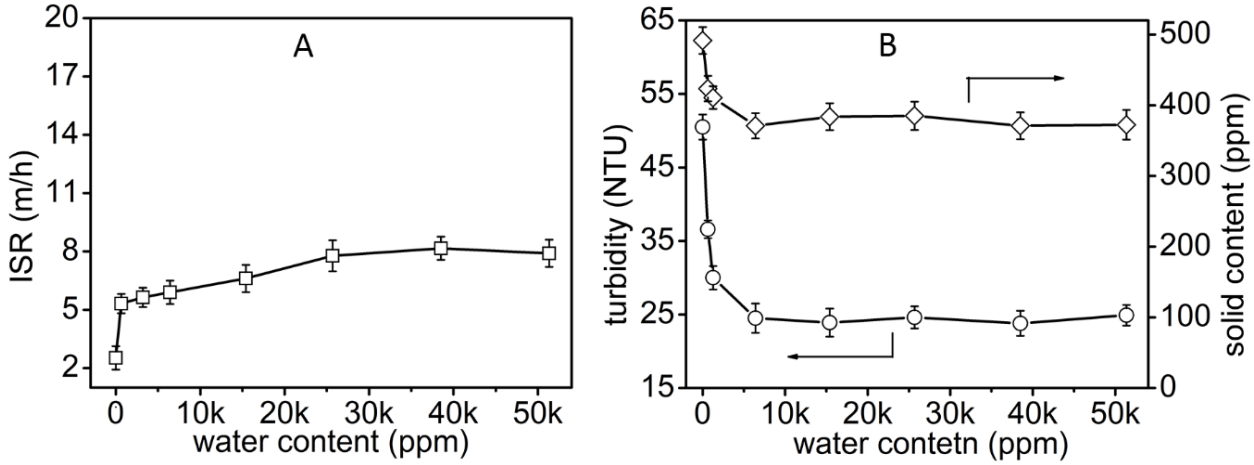

Figure 5. 3. Sedimentation tests of the bitumen-coated silica particles in cyclohexane with the addition of only water: (A) the measured ISR and (B) supernatant turbidity and residual solid content after 30 min settling as a function of water content in the silica-in-cyclohexane suspensions.

5.3.3. Sedimentation tests with two-step addition of PEG-PPG-PEG and water

Considering the limited performance of water agglomeration, it can be speculated that the hydrophobic nature of bitumen-coated silica particles has played a critical role in the stabilization of the particles. Hence, a two-step method has been proposed by applying PEG-PPG-PEG polymer as the surface modifier and subsequently introducing water to agglomerate the modified particles. As discussed above, the lowest solid content was achieved at 6000 ppm water content in the case of addition of only water. In the two-step method, the water content was therefore fixed at 6000 ppm to examine whether the sedimentation performance could be further improved by modifying the surface wettability of the particles, and the settling results are displayed in Figure 5. 4 (wine

symbols). It is noticed that an ISR as high as ~ 17 m/h was facilely achieved when only a trace amount of PEG-PPG-PEG (~ 70 ppm) was applied (Figure 5. 4A), which doubled the maximum ISR (~ 8 m/h) achieved by adding water only. The ISR value rose to ~ 18 m/h as the PEG-PPG-PEG content increased to 150 ppm. Meanwhile, as shown in Figure 5. 4B and 5. 4C, the residual solid content and supernatant turbidity were found to fall sharply to ~ 100 ppm and ~12 NTU, respectively, at the PEG-PPG-PEG content of 150 ppm. These results demonstrate that the two-step agglomeration method could synchronously enhance the settling process and reduce residual solid content. Figure 5. 4D shows the schematic physical model associated with the two-step method. Compared to the case without any additives, the solid particles modified by PEG-PPG-PEG should possess stronger affinity for water and could be more rapidly captured by the added water. However, the intriguing performance of the two-step method was just observed under low PEG-PPG-PEG dosage conditions. With the PEG-PPG-PEG content increasing from 150 ppm to 1000 ppm, the solid content gradually climbed up to ~ 200 ppm and the turbidity slightly increased to ~ 16 NTU. Correspondingly, the ISR underwent a remarkable decline with increasing the PEG-PPG-PEG dosage. The probable cause is the excessive amount of PEG-PPG-PEG migrating to the water/oil interface, which therefore might prevent the water droplets from capturing the dispersed particles and adversely affect the sedimentation performance. This proposed hypothesis will be investigated in the later section.

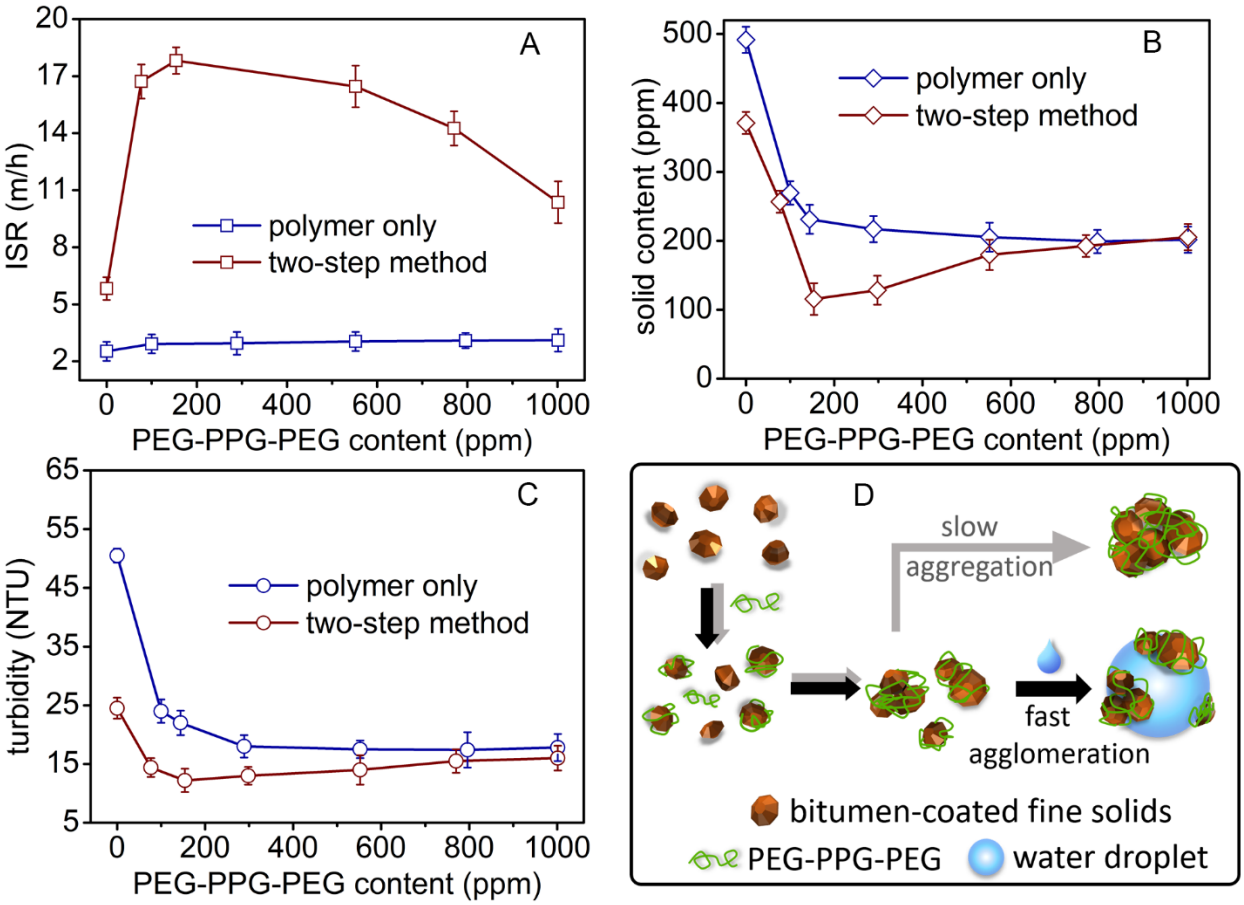

Figure 5. 4. Sedimentation tests of the bitumen-coated silica particles in cyclohexane with the two-step method (wine symbol) and the addition of only PEG-PPG-PEG (royal symbol): (A) ISR, (B) solid residue content of supernatant and (C) supernatant turbidity as a function of PEG-PPG-PEG content added in the particle suspensions. (D) Illustration for the interactions associated with the particle settling process using the two-step agglomeration method (black arrow) and with addition of only PEG-PPG-PEG (grey arrow).

To verify the synergistic effects of PEG-PG-PEG and water on destabilizing the bitumen-coated silica particles, batch tests with addition of PEG-PPG-PEG only were conducted and the results are also presented in Figure. 4A-C (royal symbols). Clearly, when the PEG-PPG-PEG content were increased from 0 to 1000 ppm, the ISR maintained at very low level and only increased from 2.5 m/h to 3.2 m/h, which implies that the addition of only PEG-PPG-PEG was

unable to enhance the settling rate (Figure 5. 4A). However, the beneficial role of PEG-PPG-PEG in lowering solid content at prolonged settling time (i.e., t = 30 min) was gradually realized by raising the PEG-PPG-PEG content. It is interesting to note that the residual solid content decreased sharply to ~ 230 ppm when the PEG-PPG-PEG content was increased to ~ 140 ppm, and then gradually reached a plateau of ~ 200 ppm when the PEG-PPG-PEG content exceeded 500 ppm (Figure 5. 4B). Exhibiting the similar trend, the supernatant turbidity firstly decreased to ~ 14 NTU at the PEG-PPG-PEG content of 550 ppm which then leveled off (Figure 5. 4C). The possible reason for these results is that the adsorbed PEG-PPG-PEG were able to bridge the neighboring particles into small aggregates, and the resultant aggregates could further grow into large ones to accelerate gravitational settling (Figure 5. 4D). The settling rate should be controlled by the growth-rate of the particle aggregates which however was much slower than the formation of solid-water agglomerates according to the ISR data. Therefore, even though the addition of PEG-PPG-PEG only could reduce the solid content, its performance in enhancing the sedimentation rate is not significant unless water was added subsequently. In addition, the excessive amount of PEG-PPG-PEG in the solid suspensions did not further lower the residual solid content, which might arise from the saturation of adsorbed PEG-PPG-PEG on the solid particles. The non-adsorbing PEG-PPG-PEG ended up precipitation down the bottom of the suspension system when the sedimentation test was completed.

5.3.3. QCM-D adsorption tests and surface force measurements

The physical mechanism underlying the sedimentation performance of the two-step method was explored using both QCM-D adsorption tests and surface force measurements using drop prob AFM at the nanoscale. Figure 5. 5 presents the variations in resonance frequency and energy dissipation responses versus time (t) for the adsorption test of PEG-PPG-PEG onto a QCM-

D silica sensor surface. For the sake of simplicity, three harmonics (n = 5, 7, 9) are shown in the results. After injection of cyclohexane as baseline (t = 0-2.5 min), the resonance of crystal sensor shows a strong negative frequency and positive dissipation shifts synchronously when the silica sensor surface was exposed to the bitumen-in-cyclohexane solution, exhibiting a rapid adsorption of bitumen onto the silica surface. Then it shows a continuous adsorption with no saturation plateau of frequency or dissipation shifts within 10 min, after which the surface was thoroughly rinsed by cyclohexane to remove any weakly bounded bitumen components. Only a slight increase in frequency and drop in dissipation were observed, responsible for a strong and irreversible adsorption of bitumen on the surface. The WCA of the resultant bitumen-adsorbed silica sensor was measured to be 92º ± 1º. Upon the introduction of PEG-PPG-PEG, an immediate drop in frequency and rise in dissipation responses were detected, which indicates that PEG-PPG-PEG adsorbed onto the bitumen surface in cyclohexane. After the initial changes, PEG-PPG-PEG continued adsorbing onto the surface with time at a much lower rate considering the milder variations in frequency and dissipation. At the end of QCM-D measurements, the sensor surface showed WCA of 39º ± 0.5º, demonstrating that PEG-PPG-PEG modified the wettability of the bitumen-coated silica surface. The adsorption of PEG-PPG-PEG on bitumen-coated silica surfaces in cyclohexane could be driven by the van der Waals interactions between the polymer chains and bitumen, as well as the hydrogen bonding interactions of the polar oxygen-containing segments of PEG and PPG with the polar groups (e.g., -COOH and -OH) in certain bitumen components.[56-57]

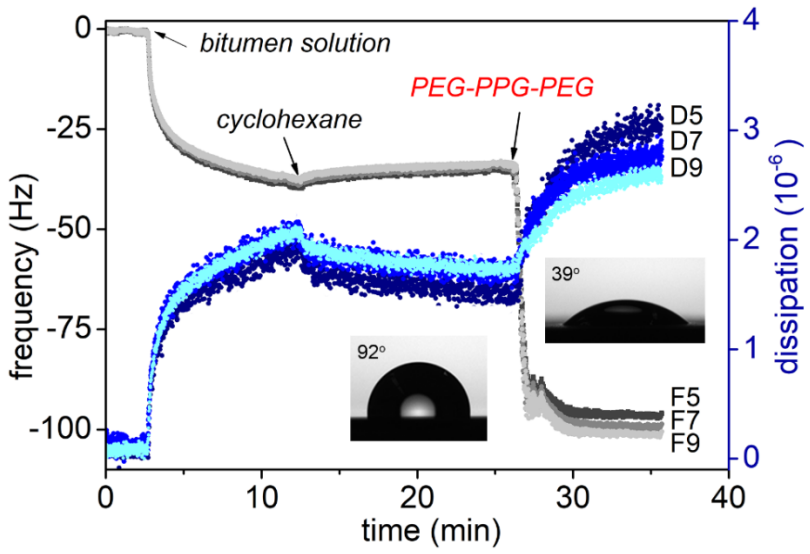

Figure 5. 5. QCM-D measurement of bitumen adsorption and PEG-PPG-PEG adsorption onto a silica sensor surface in sequence. The insets show the changes in water contact angle on the bitumen-adsorbed silica sensor before and after PEG-PPG-PEG adsorption process.

The adsorbed PEG-PPG-PEG can also profoundly modulate the inter-particle interactions, which have been quantitatively investigated using the colloidal probe AFM technique. Figure 5. 6A shows the typical force-separation curves measured between a flat bitumen-coated silica surface and a bitumen-coated silica probe in cyclohexane. As the colloidal probe approached the flat bitumen-coated silica surface, noticeable repulsion was detected which grew steeply when the separation distance was smaller than 14 nm. Such phenomenon was attributed to the dominant steric force arising from the swelling of interfacial bitumen coatings, contributing to the stabilization of bitumen-coated silica solids in cyclohexane.[12] During the retraction process, the force curve almost overlapped with the approach curve, except for a very weak adhesion at ~ 0.07 mN/m possibly due to slight interdigitation and bridging behaviors between two contact bitumen surfaces. Typical topographic image of the bitumen surface is displayed in the inset of Figure 5. 6A. Many small protrusion nanostructures were observed due to the self-assembly of bitumen

aggregates, and the root-mean-square (rms) roughness of the bitumen surface is about 0.37 nm. After being modified by PEG-PPG-PEG, the substrate surface showed polymer nanoaggregates with much larger size in comparison with the bitumen aggregates with rms slightly increasing to 0.51 nm (inset of Figure 5. 6B), which indicates that the adsorption of PEG-PPG-PEG did not significantly change the surface roughness. However, the corresponding interaction force measured on the PEG-PPG-PEG/bitumen surface had distinct features, as shown in Figure 5. 6B. Specifically, the force curve upon approach showed a "jump-in" behavior when the separation was close to ~ 7 nm, implying that a strong attraction pulled the two surfaces into contact. Moreover, a relatively strong adhesion (~ 0.7 mN/m) denoted by a distinct "jump-out" behavior was recorded during the retraction process. These behaviors indicate that the adsorbed PEG-PPG-PEG was still capable of physically bridging the bitumen-coated silica particles, supporting our hypothesis that small aggregates of silica particles could be formed due to the addition of PEG-PPG-PEG.

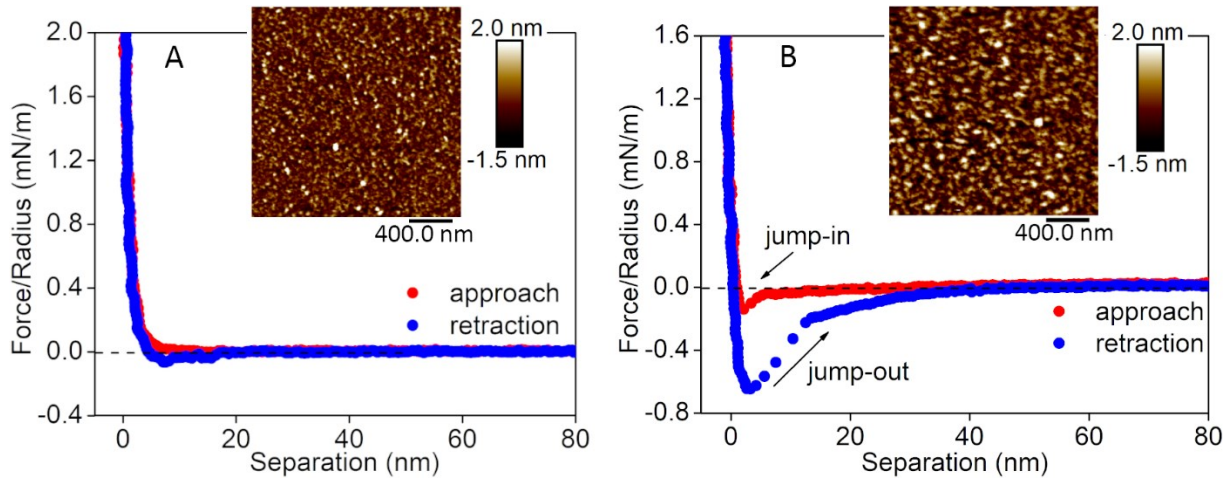

Figure 5. 6. Force-separation curves obtained on (A) a bitumen surface and (B) a PEG-PPG-PEG/bitumen surface in cyclohexane using the colloidal probe AFM technique. The insets show topographic images (2 × 2 μm) on the corresponding surface.

As discussed above, PEG-PPG-PEG exhibits strong tendency to adsorb onto the bitumen-coated silica particles and the adsorbed polymer profoundly affected the inter-particle interactions in cyclohexane. What's more, the PEG-PPG-PEG modified particles can be favorably wetted by the added water, as indicated by contact angle measurements on the flat substrate surfaces in cyclohexane. The WCA was about 123 º ± 0.5º for the bitumen surface and significantly decreased to about 42º ± 1 º after the adsorption of PEG-PPG-PEG (insets of Figure 5. 7). The associated interaction mechanism was investigated by surface force measurements using the drop probe AFM technique, as shown in Figure 5. 7. Here, the piezo-displacement refers to the relative movement of the AFM cantilever, and the point where the water droplet was in contact with the substrate surface is arbitrarily selected as the zero point. Figure 5. 7A shows the interaction forces between a water droplet and the bitumen surface in cyclohexane. The measured force during approach was first slightly repulsive due to the weak hydrodynamic repulsion. When the force reached about 0.3 nN, a small "jump-in" behavior was observed, which indicated that the water droplet came into contact with the bitumen surface. This phenomenon may have something to do with the fact that some interfacial-active components of bitumen were exposed to the oil media, rendering a weak affinity of the bitumen surface for water, which was also responsible for the moderate hydrophobicity (i.e., WCA ~ 90º) of the bitumen-coated silica surface. However, the water droplet did not detach from the upper cantilever after the contact and the strength of repulsion continued growing as the droplet-loaded cantilever kept approaching the surface until the maximum load force of ~ 2 nN was detected. During the retraction process, the water droplet sequentially detached from the substrate surface and a stepwise "jump-out" behavior was observed before the load force returned to zero, which was possibly due to stick-slip movement of the water droplet on chemically heterogeneous surface.[58-59] The detachment of water droplet also implies the relatively weak

affinity of the bitumen surface for water in comparison with the hydrophilized cantilever. In striking contrast, the force curve of the PEG-PPG-PEG/bitumen surface showed different characteristics, as shown in Figure 5. 7B. After overcoming the weak hydrodynamic force, the water droplet suddenly detached from the cantilever and coalesced with the bottom substrate. The attachment of water droplet was observed accompanied with the formation of a large drop on the surface. This result clearly demonstrated the strong affinity of the PEG-PPG-PEG/bitumen surface for water and elucidated the synergistic effects of PEG-PPG-PEG additive and water on the agglomeration of the bitumen-coated silica particles.

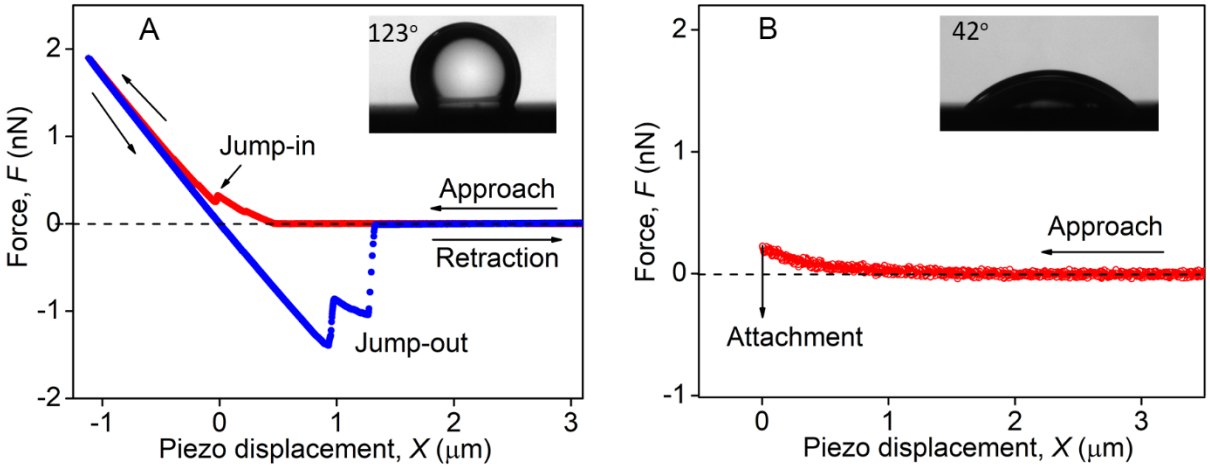

Figure 5. 7 Measured interaction force of (A) bitumen surface and (B) PEG-PPG-PEG/bitumen surface with a water droplet (radius = 35 μm) in cyclohexane. The arrows indicate the movement of the water droplet on the cantilever. The inserts display the water contact angle on bottom substrate surface measured in cyclohexane.

5.3.4. Settling tests by one-step addition of PEG-PPG-PEG and water

To further investigate the necessity of the two-step procedure in settling the bitumen-coated silica particles, sedimentation tests incorporating a one-step addition of a PEG-PPG-PEG aqueous

solution were conducted. Again, the water content was fixed at 6000 ppm. The PEG-PPG-PEG contents in the solid suspensions were adjusted by varying the content of PEG-PPG-PEG in aqueous solutions. Results of residual solid content obtained from the one-step method were compared with those in the two-step method test at three different PEG-PPG-PEG dosages, i.e., 150 ppm, 550 ppm and 1000 ppm, as presented in Figure 5. 8. The corresponding PEG-PPG-PEG concentration in initial aqueous solutions was 25 mg/mL, 90 mg/mL and 150 mg/mL, respectively. Clearly, the solid content was much higher in the one-step test than that in the two-step test under all PEG-PPG-PEG contents, indicating that the hydrophobic bitumen-coated particles could not be effectively destabilized by the addition of PEG-PPG-PEG aqueous drops and demonstrating the necessity of the two-step agglomeration method. More importantly, a noticeable upward trend in solid content was observed when the PEG-PPG-PEG content was continuously raised from 150 to 1000 ppm (Figure 5. 9A). At 1000 ppm PEG-PPG-PEG, the solid content reached ~ 455 ppm which was close to that in the case of no additives (~ 490 ppm). It is interesting to note that the contact angle of PEG-PPG-PEG aqueous drop on the bitumen surface in cyclohexane gradually increased from 148º, 155º to 163º when the applied PEG-PPG-PEG concentration in water was raised from 25 mg/mL, 90 mg/mL to 150 mg/mL, respectively (insets in Figure 5. 8). This result suggested that water drops containing highly concentrated PEG-PPG-PEG were relatively deficient in wetting the bitumen-coated silica particles.

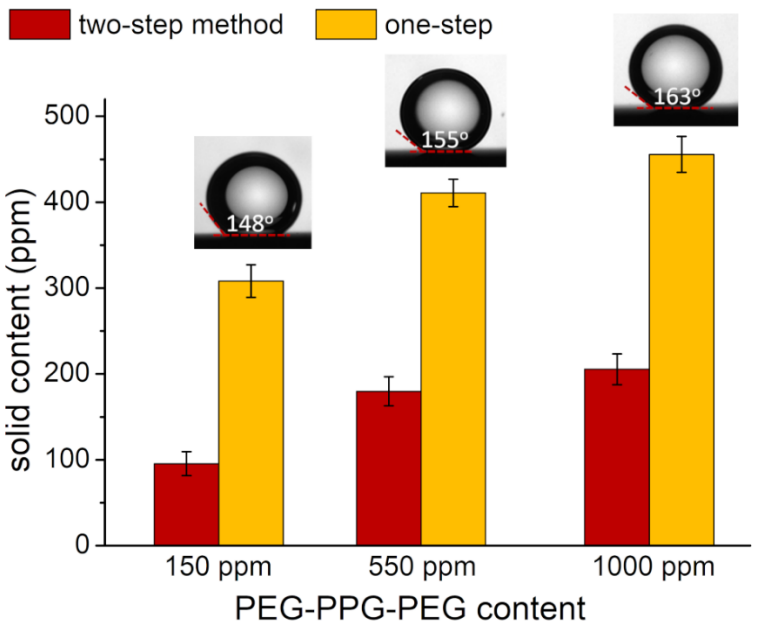

Figure 5. 8. Solid content of supernatant in the sedimentation tests with one-step addition method by adding PEG-PPG-PEG aqueous solution (orange column) and two-step addition method (wine column). The inset displays contact angle of PEG-PPG-PEG aqueous drop on the bitumen surface in cyclohexane.

Figure 5. 9 shows the IFT data with different applied PEG-PPG-PEG concentrations in aqueous solution. For the PEG-PPG-PEG concentration of 0 mg/ml, the IFT shows a rapid reduction during the initial time and turns to be constant with prolonged time. At the equilibrium state, the IFT between water and cyclohexane was measured to be ~50 mN/m, which is consistent with the value reported elsewhere. For the PEG-PPG-PEG concentrations of 25-150 mg/mL, variations of IFT show the same trend, that is, a continuous reduction in IFT was observed with time. It was noticed that the IFT decreases with the PEG-PPG-PEG concentration increasing, indicating that a growing number of PEG-PPG-PEG migrate to the water/oil interface under higher concentration conditions. This result indicates that a growing number of PEG-PPG-PEG occupied the water/oil interface under higher concentration condition, which would prevent the migration

and adsorption of the bitumen-coated particles onto the interface. Moreover, the PEG segments might preferentially reside in the water phase and stay highly hydrated, significantly inhibiting the formation of the hydrogen bonds between PEG-PPG-PEG and interfacial-active components of the bitumen layer adsorbed on the solid particles. In the case of the two-step method, it's reasonable to assume that the excess amount of PEG-PPG-PEG in cyclohexane would also migrate to the water/oil interface, and thereby the introduced water drops heavily occupied with PEG-PPG-PEG could not capture the solid particles further. As a result, the addition of PEG-PPG-PEG at high dosages to the suspension system negatively affected the sedimentation performance of the two-step agglomeration method.

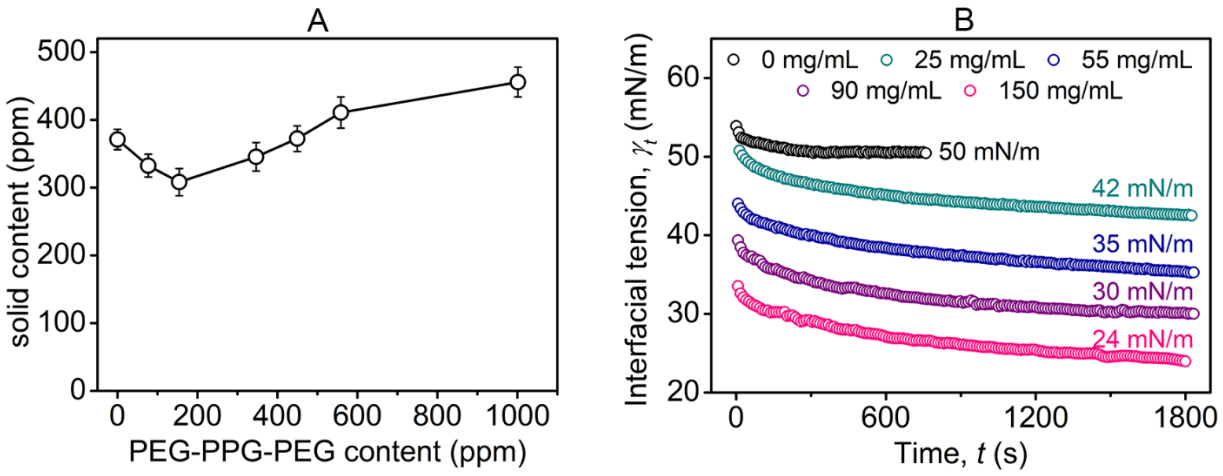

Figure 5. 9 (A) residual solid content after 30 min settling in the batch test with addition of PEG-PPG-PEG aqueous solution. (B) Variation of IFT between PEG-PPG-PEG aqueous solution and cyclohexane with different PEG-PPG-PEG concentrations in aqueous solutions.

5.4 Conclusion

Removing fine solids suspended in oil media is crucial for the achievement of high-quality oil products and the simplification of technological processes in many chemical and environmental

engineering practices. In this work, a two-step agglomeration process has been developed to enhance sedimentation of hydrophobic bitumen-coated silica particles in cyclohexane. In the first step a polymer modifier PEG-PPG-PEG was used to alter surface wettability of the bitumen-coated silica particles and modulate the inter-particle interactions, and small amount of water was then used as the second step to trigger the generation of solid-water agglomerates. The performance of this two-step agglomeration method was evaluated by sedimentation tests, which shows high initial settling rate (ISR, as high as ~ 17 m/h) and low content of residual solids (~ 100 ppm) in the supernatant synchronously at the low PEG-PPG-PEG dosages. Batch sedimentation tests with addition of only water, PEG-PPG-PEG or PEG-PPG-PEG aqueous solution were also conducted, whose performances were found much less desirable in comparison with the two-step approach. In summary, the addition of only PEG-PPG-PEG was also found to be able to significantly decrease solid content (~ 200 ppm) in the supernatant but showed extremely low ISR (~ 3 m/h) at all PEG-PPG-PEG dosages (0-1000 ppm). The addition of only water achieved a moderately high ISR (~ 8.0 m/h) but the resultant supernatant still contained high content of residual fine solids (~ 370 ppm). The batch test with addition of PEG-PPG-PEG aqueous solution showed that if large number of PEG-PPG-PEG migrated to the water/oil interface, the water drops would be relatively deficient in wetting the bitumen-coated silica particles, resulting in a large number of solid particles (as high as ~ 455 ppm) remaining suspended in the supernatant.

The underlying physical interaction mechanism of two-step method were analyzed using QCM-D adsorption test and AFM force measurement. It was found that the surface of bitumen-coated silica particles could be effectively modified by PEG-PPG-PEG due to a favorable adsorption of PEG-PPG-PEG to the bitumen-coated silica surface in cyclohexane. The modified particles were relatively hydrophilic and showed improved water wettability in cyclohexane. As a

result, they could be readily captured by the added water to form solid-water agglomerates that would then settle much faster in oil media. Our work provides implications for the development of practical and facile strategies to destabilize and remove the hydrophobic bitumen-coated fine solids in oil media.

Reference

1. Henry Jr, J.; Prudich, M.; Vaidyanathan, K., Novel Separation Processes for Solid/Liquid Separations in Coal Derived Liquids. *Sep. Purif. Methods* **1979**, *8*, 81-118.

2. Speight, J. G., *Fouling in Refineries*; Gulf Professional Publishing, 2015.

3. Kotlyar, L.; Sparks, B.; Woods, J.; Chung, K., Solids Associated with the Asphaltene Fraction of Oil Sands Bitumen. *Energy Fuels* **1999**, *13*, 346-350.

4. Nikakhtari, H.; Wolf, S.; Choi, P.; Liu, Q.; Gray, M. R., Migration of Fine Solids into Product Bitumen from Solvent Extraction of Alberta Oilsands. *Energy Fuels* **2014**, *28*, 2925-2932.

5. Sheppard, M. C., *Oil Sands Scientist: The Letters of Karl A. Clark, 1920-1949*; University of Alberta, 1989.

6. West, R. C., Non-Aqueous Process for the Recovery of Bitumen from Tar Sands. Google Patents: 1964.

7. Lin, F.; Stoyanov, S. R.; Xu, Y., Recent Advances in Nonaqueous Extraction of Bitumen from Mineable Oil Sands: A Review. *Org. Process Res. Dev.* **2017**, *21*, 492-510.

8. Ng, Y. M. S.; Knapper, B.; Kresta, J., Naphtha Based Fungible Bitumen Process. Google Patents: 2014.

9. Pal, K.; Nogueira Branco, L. d. P.; Heintz, A.; Choi, P.; Liu, Q.; Seidl, P. R.; Gray, M. R., Performance of Solvent Mixtures for Non-Aqueous Extraction of Alberta Oil Sands. *Energy Fuels* **2015**, *29*, 2261-2267.

10. Nikakhtari, H.; Vagi, L.; Choi, P.; Liu, Q.; Gray, M. R., Solvent Screening for Non-Aqueous Extraction of Alberta Oil Sands. *The Canadian Journal of Chemical Engineering* **2013**, *91*, 1153-1160.

11. Zhang, L.; Shi, C.; Lu, Q.; Liu, Q.; Zeng, H., Probing Molecular Interactions of Asphaltenes in Heptol Using a Surface Forces Apparatus: Implications on Stability of Water-in-Oil Emulsions. *Langmuir* **2016**, *32*, 4886-4895.

12. Liu, J.; Cui, X.; Huang, J.; Xie, L.; Tan, X.; Liu, Q.; Zeng, H., Understanding the Stabilization Mechanism of Bitumen-Coated Fine Solids in Organic Media from Non-Aqueous Extraction of Oil Sands. *Fuel* **2019**, *242*, 255-264.

13. Brons, G.; Yu, J. M., Solvent Deasphalting Effects on Whole Cold Lake Bitumen. *Energy Fuels* **1995**, *9*, 641-647.

14. Gray, M. R.; Tykwinski, R. R.; Stryker, J. M.; Tan, X., Supramolecular Assembly Model for Aggregation of Petroleum Asphaltenes. *Energy Fuels* **2011**, *25*, 3125-3134.

15. Maqbool, T.; Balgoa, A. T.; Fogler, H. S., Revisiting Asphaltene Precipitation from Crude Oils: A Case of Neglected Kinetic Effects. *Energy Fuels* **2009**, *23*, 3681-3686.

16. Farnand, J.; Meadus, F.; Sparks, B., Removal of Intractable Fine Solids from Bitumen Solutions Obtained by Solvent Extraction of Oil Sands. *Fuel processing technology* **1985**, *10*, 131-144.

17. Rao, F.; Liu, Q., Froth Treatment in Athabasca Oil Sands Bitumen Recovery Process: A Review. *Energy Fuels* **2013**, *27*, 7199-7207.

18. Natarajan, A.; Kuznicki, N.; Harbottle, D.; Masliyah, J.; Zeng, H.; Xu, Z., Understanding Mechanisms of Asphaltene Adsorption from Organic Solvent on Mica. *Langmuir* **2014**, *30*, 9370-9377.

19. Natarajan, A.; Xie, J.; Wang, S.; Liu, Q.; Masliyah, J.; Zeng, H.; Xu, Z., Understanding Molecular Interactions of Asphaltenes in Organic Solvents Using a Surface Force Apparatus. *J. Phys. Chem. C* **2011**, *115*, 16043-16051.

20. Israelachvili, J. N., *Intermolecular and Surface Forces*; Academic press, 2011.

21. Painter, P.; Williams, P.; Mannebach, E., Recovery of Bitumen from Oil or Tar Sands Using Ionic Liquids. *Energy Fuels* **2009**, *24*, 1094-1098.

22. Painter, P.; Williams, P.; Lupinsky, A., Recovery of Bitumen from Utah Tar Sands Using Ionic Liquids. *Energy Fuels* **2010**, *24*, 5081-5088.

23. Pulati, N.; Lupinsky, A.; Miller, B.; Painter, P., Extraction of Bitumen from Oil Sands Using Deep Eutectic Ionic Liquid Analogues. *Energy Fuels* **2015**, *29*, 4927-4935.

24. Li, X.; Sun, W.; Wu, G.; He, L.; Li, H.; Sui, H., Ionic Liquid Enhanced Solvent Extraction for Bitumen Recovery from Oil Sands. *Energy Fuels* **2011**, *25*, 5224-5231.

25. Tourvieille, J.-N.; Larachi, F.; Duchesne, C.; Chen, J., Nir Hyperspectral Investigation of Extraction Kinetics of Ionic-Liquid Assisted Bitumen Extraction. *Chem. Eng. J.***2017**, *308*, 1185-1199.

26. Hogshead, C. G.; Manias, E.; Williams, P.; Lupinsky, A.; Painter, P., Studies of Bitumen− Silica and Oil− Silica Interactions in Ionic Liquids. *Energy Fuels* **2010**, *25*, 293-299.

27. Li, X.; Wang, J.; He, L.; Sui, H.; Yin, W., Ionic Liquid-Assisted Solvent Extraction for Unconventional Oil Recovery: Computational Simulation and Experimental Tests. *Energy Fuels* **2016**, *30*, 7074-7081.

28. Sparks, B.; Meadus, F., A Study of Some Factors Affecting Solvent Losses in the Solvent Extraction—Spherical Agglomeration of Oil Sands. *Fuel Processing Technology* **1981**, *4*, 251-264.

29. Meadus, F.; Chevrier, P.; Sparks, B., Solvent Extraction of Athabasca Oil-Sand in a Rotating Mill Part 1. Dissolution of Bitumen. *Fuel Processing Technology* **1982**, *6*, 277-287.

30. Meadus, F.; Bassaw, B.; Sparks, B., Solvent Extraction of Athabasca Oil-Sand in a Rotating Mill Part 2. Solids—Liquid Separation and Bitumen Quality. *Fuel Processing Technology* **1982**, *6*, 289-300.

31. Sparks, B. D.; Meadus, F. W.; Hoefele, E. O., Solvent Extraction Spherical Agglomeration of Oil Sands. Google Patents: 1988.

32. Jessop, P. G.; Phan, L.; Carrier, A.; Robinson, S.; Dürr, C. J.; Harjani, J. R., A Solvent Having Switchable Hydrophilicity. *Green Chemistry* **2010**, *12*, 809-814.

33. Holland, A.; Wechsler, D.; Patel, A.; Molloy, B. M.; Boyd, A. R.; Jessop, P. G., Separation of Bitumen from Oil Sands Using a Switchable Hydrophilicity Solvent. *Can. J. Chem.* **2012**, *90*, 805-810.

34. Sui, H.; Xu, L.; Li, X.; He, L., Understanding the Roles of Switchable-Hydrophilicity Tertiary Amines in Recovering Heavy Hydrocarbons from Oil Sands. *Chem. Eng. J.***2016**, *290*, 312-318.

35. Ngnie, G.; Baitan, D.; Dedzo, G. K.; Detellier, C., Sedimentation of Fine Particles of Kaolinite and Polymer-Coated Kaolinite in Cyclohexane: Implications for Fines Removal from Extracted Bitumen in Non-Aqueous Processes. *Fuel* **2018**, *234*, 218-224.

36. Branca, C.; Magazu, S.; Maisano, G.; Migliardo, P.; Migliardo, F.; Romeo, G., Hydration Parameters of Aqueous Solutions of Poly (Ethylene Glycol) S by Viscosity Data. *Physica Scripta* **2002**, *66*, 175.

37. Mueller, M.; Fabretto, M.; Evans, D.; Hojati-Talemi, P.; Gruber, C.; Murphy, P., Vacuum Vapour Phase Polymerization of High Conductivity Pedot: Role of Peg-Ppg-Peg, the Origin of Water, and Choice of Oxidant. *Polymer* **2012**, *53*, 2146-2151.

38. Branca, C.; Magazu, S.; Maisano, G.; Migliardo, F.; Migliardo, P.; Romeo, G., Hydration Study of Peg/Water Mixtures by Quasi Elastic Light Scattering, Acoustic and Rheological Measurements. *J. Phys. Chem. B* **2002**, *106*, 10272-10276.

39. Jin, Y.; Liu, W.; Liu, Q.; Yeung, A., Aggregation of Silica Particles in Non-Aqueous Media. *Fuel* **2011**, *90*, 2592-2597.

40. Abudu, A.; Goual, L., Adsorption of Crude Oil on Surfaces Using Quartz Crystal Microbalance with Dissipation (Qcm-D) under Flow Conditions. *Energy Fuels* **2008**, *23*, 1237-1248.

41. Ekholm, P.; Blomberg, E.; Claesson, P.; Auflem, I. H.; Sjöblom, J.; Kornfeldt, A., A Quartz Crystal Microbalance Study of the Adsorption of Asphaltenes and Resins onto a Hydrophilic Surface. *J. Colloid Interface Sci.* **2002**, *247*, 342-350.

42. Dudášová, D.; Silset, A.; Sjöblom, J., Quartz Crystal Microbalance Monitoring of Asphaltene Adsorption/Deposition. *J. Dispersion Sci. Technol.* **2008**, *29*, 139-146.

43. Lu, Q.; Yan, B.; Xie, L.; Huang, J.; Liu, Y.; Zeng, H., A Two-Step Flocculation Process on Oil Sands Tailings Treatment Using Oppositely Charged Polymer Flocculants. *Sci. Total Environ.* **2016**, *565*, 369-375.

44. Shi, C.; Zhang, L.; Xie, L.; Lu, X.; Liu, Q.; Mantilla, C. A.; van den Berg, F. G.; Zeng, H., Interaction Mechanism of Oil-in-Water Emulsions with Asphaltenes Determined Using Droplet Probe Afm. *Langmuir* **2016**, *32*, 2302-2310.

45. Cui, X.; Shi, C.; Xie, L.; Liu, J.; Zeng, H., Probing Interactions between Air Bubble and Hydrophobic Polymer Surface: Impact of Solution Salinity and Interfacial Nanobubbles. *Langmuir* **2016**, *32*, 11236-11244.

46. Shi, C.; Yan, B.; Xie, L.; Zhang, L.; Wang, J.; Takahara, A.; Zeng, H., Long-Range Hydrophilic Attraction between Water and Polyelectrolyte Surfaces in Oil. *Angew. Chem., Int. Ed.* **2016**, *55*, 15017-15021.

47. Xie, L.; Wang, J.; Yuan, D.; Shi, C.; Cui, X.; Zhang, H.; Liu, Q.; Liu, Q.; Zeng, H., Interaction Mechanisms between Air Bubble and Molybdenite Surface: Impact of Solution Salinity and Polymer Adsorption. *Langmuir* **2017**, *33*, 2353-2361.

48. Cui, X.; Liu, J.; Xie, L.; Huang, J.; Liu, Q.; Israelachvili, J. N.; Zeng, H., Modulation of Hydrophobic Interaction by Mediating Surface Nanoscale Structure and Chemistry, Not Monotonically by Hydrophobicity. *Angew. Chem., Int. Ed.* **2018**, *57*, 11903-11908.

49. Shi, C.; Zhang, L.; Xie, L.; Lu, X.; Liu, Q.; He, J.; Mantilla, C. A.; Van den Berg, F. G.; Zeng, H., Surface Interaction of Water-in-Oil Emulsion Droplets with Interfacially Active Asphaltenes. *Langmuir* **2017**, *33*, 1265-1274.

50. Mao, X.; Gong, L.; Xie, L.; Qian, H.; Wang, X.; Zeng, H., Novel Fe3o4 Based Superhydrophilic Core-Shell Microspheres for Breaking Asphaltenes-Stabilized Water-in-Oil Emulsion. *Chem. Eng. J.***2019**, *358*, 869-877.

51. Hutter, J. L.; Bechhoefer, J., Calibration of Atomic-Force Microscope Tips. *Review of Scientific Instruments* **1993**, *64*, 1868-1873.

52. Wang, J.; Li, J.; Xie, L.; Shi, C.; Liu, Q.; Zeng, H., Interactions between Elemental Selenium and Hydrophilic/Hydrophobic Surfaces: Direct Force Measurements Using Afm. *Chem. Eng. J.***2016**, *303*, 646-654.

53. Ducker, W. A.; Senden, T. J.; Pashley, R. M., Direct Measurement of Colloidal Forces Using an Atomic Force Microscope. *nature* **1991**, *353*, 239.

54. Butt, H.-J.; Cappella, B.; Kappl, M., Force Measurements with the Atomic Force Microscope: Technique, Interpretation and Applications. *Surface science reports* **2005**, *59*, 1-152.

55. Liu, J.; Wang, J.; Huang, J.; Cui, X.; Tan, X.; Liu, Q.; Zeng, H., Heterogeneous Distribution of Adsorbed Bitumen on Fine Solids from Solvent-Based Extraction of Oil Sands Probed by Afm. *Energy Fuels* **2017**, *31*, 8833-8842.

56. Paul Maruska, H.; Rao, B. M., The Role of Polar Species in the Aggregation of Asphaltenes. *Fuel Sci. Technol. Int.***1987**, *5*, 119-168.

57. Philippova, O.; Kuchanov, S.; Topchieva, I.; Kabanov, V., Hydrogen Bonds in Dilute Solutions of Poly (Ethylene Glycol). *Macromolecules* **1985**, *18*, 1628-1633.

58. Varagnolo, S.; Ferraro, D.; Fantinel, P.; Pierno, M.; Mistura, G.; Amati, G.; Biferale, L.; Sbragaglia, M., Stick-Slip Sliding of Water Drops on Chemically Heterogeneous Surfaces. *Phys. Rev. Lett.***2013**, *111*, 066101.

59. Mirsaidov, U. M.; Zheng, H.; Bhattacharya, D.; Casana, Y.; Matsudaira, P., Direct Observation of Stick-Slip Movements of Water Nanodroplets Induced by an Electron Beam. *Proc. Natl. Acad. Sci.* **2012**, *109*, 7187-7190.

Chapter 6 Conclusions and Future Work

6.1 Major conclusions

In this project, surface properties, stabilization and destabilization mechanisms of bitumen-coated fine solids in organic media have been systematically studied mainly using nanomechanical techniques such as AFM and QCM-D with implications on understanding the behavior of the fine solids in organic media during the non-aqueous (NAE) extraction process and developing more effective and economic strategies of removing the fine solids from diluted bitumen.

Results of elemental analysis and surface wettability measurements showed a strong signature of organic coatings on the surface of fine solids collected from the NAE bitumen, suggesting the presence of adsorbed bitumen layer on the solids surfaces. By virtue of AFM force measurement and nanomechanical mapping, the distribution of such adsorbed bitumen on the surface could be well-defined and was found to be heterogenous instead of homogeneous. The regime with thick bitumen layer showed the stretching behavior upon force measurement and the relative low modulus value, which indicates that the regime is relatively viscous and soft. In contrast, the regime without or with thin bitumen layer experienced a steep and sudden jump-out during the force measurement and showed the relative high modulus value. In addition, AFM force mapping in water using a hydrophobized AFM tip gave rise to the distribution of hydrophobicity of the solid surface, which could also be used to tell the regime with or without adsorbed bitumen apart. Specifically, force curves obtained on the mineral regime (no bitumen coating) could be well fitted by the classical DLVO theory, while additional hydrophobic attraction should be considered to fit the force curves obtained on the bitumen domains. The hydrophobic attraction

between the hydrophobized tip and bitumen domains led to an obvious “jump in” behavior during approach and relatively long-range “stretching” during separation.

Interactions between fine solids in organic media were investigated by measuring interactions between a silica microsphere and a flat silica substrate using the colloidal probe AFM technique. The theoretical model, sum of VDW force and steric force, was applied to investigate the interaction mechanisms involving the fine solids. It was noticed that upon approach a steric repulsion was observed between the silica microsphere and the bitumen-coated silica substrate in cyclohexane, which was attributed to the swelling behavior of bitumen layer in good solvent. In the mixture of cyclohexane and heptane, the steric repulsion was gradually weakened when lower volume fraction of cyclohexane (φ_c) was applied, and finally turned to a weak attraction in the pure heptane arising from the collapse of the bitumen layer in poor solvent. Under the same solvent condition, both the range and the magnitude of the steric repulsion could be enhanced when the silica microsphere was also coated with bitumen. During retraction, the adhesion force required to separate two contact surfaces was found to increase with decreasing φ_c. The inter-particle interactions mediated by surrounding organic solvent could further significantly impact the stability of bitumen-coated silica particles in organic media.

Behaviors of bitumen adsorption to fine solids in organic media were monitored using QCM-D. A silica sensor was used to mimic the mineral solid surface. The results showed that the initial adsorption of bitumen was mainly controlled by the interactions between bitumen components and the silica surface, while bitumen adsorption at long time was synchronously affected by multiple factors such as deposition, diffusion, aggregation, precipitation and convection processes. Before the precipitation onset of asphaltenes (i.e., important fraction of bitumen), the self-associated primary asphaltene nanoaggregates mainly contributed to the

bitumen deposition which accounts for the main constituent of the bitumen layer adsorbed on the silica surface, and a slight increase in φ_c in organic media was found to enhance the bitumen deposition. After the precipitation onset, large aggregate particles of asphaltenes were formed which were immediately flushed away from the silica surface without deposition, resulting in the notable decrease in the amount of adsorption mass. In summary, the largest amount of adsorption mass was acquired when φ_c was close the precipitation onset of asphaltenes. Increase in the degree of bitumen adsorption could further slightly enhance the stability of bitumen-coated silica particles in organic media.

The performance of destabilizing fine solids in organic media with assistance of chemical additives was intuitively estimated by the sedimentation test. A two-step agglomeration process was developed to enhance sedimentation of bitumen-coated silica particles in cyclohexane. A polymer modifier PEG-PPG-PEG was first used to alter surface wettability of the bitumen-coated silica particles, and small amount of water was then used to trigger the generation of solid-water agglomerates. The performance of this two-step agglomeration method was evaluated by sedimentation tests, which shows high initial settling rate and low content of residual solids in the supernatant simultaneously. It was found that the surface of bitumen-coated silica particles could be effectively modified by PEG-PPG-PEG due to a favorable adsorption of PEG-PPG-PEG to the bitumen-coated silica surface in cyclohexane. The modified particles were less hydrophobic and showed improved affinity for water drops in cyclohexane. As a result, they could be readily captured by the added water to form solid-water agglomerates that would then settle much faster in oil media. Batch sedimentation tests with addition of only water, PEG-PPG-PEG or PEG-PPG-PEG aqueous solution were also conducted, whose performances were found much less desirable in comparison with the two-step approach.

6.2 Original contributions

This work has provided facile and useful methodologies for characterizing the heterogeneous bitumen coating on the surface of indigenous fine solids in NAE bitumen, which can be further employed to study heterogeneous surface properties of solid matters in other fields. The PeakForce QNM imaging and the AFM force mapping with hydrophobized AFM tip were first applied to probe the distributions of nano-mechanical properties and surface hydrophobicity of bitumen-coated fine solids, with important implications in better understanding the behaviors of solid particles during the NAE process.

A combined AFM and QCM-D investigation of stabilization mechanism of fine solids in organic media during the NAE process has been systematically conducted. The results revealed that the steric repulsion arising from the swelling of bitumen layer in good solvent played a dominant role in stabilizing the bitumen-coated fine solids. The introduction of small amount of poor solvent to the organic media could suppress bitumen swelling, which however could increase degree of adsorption of bitumen onto the solid surface. The surrounding organic solvent played a crucial role in mediating inter-particle interactions and adsorption behaviors of bitumen to solids surfaces synchronously, ultimately affecting the stability of fine solids during the NAE process.

For the first time, a novel two-step agglomeration method has been proposed to destabilize a suspension of bitumen-coated fine solids in oil media, that is, to reduce the hydrophobicity of the bitumen-coated fine solids and subsequently remove the particles by introducing process aids. In this work, polymer PEG-PPG-PEG was used as the wettability modifier and a small amount of water was used to agglomerate the modified fine solids. The results of sedimentation test revealed that this two-step method achieved a high settling rate and low residual solid content

synchronously. The underlying physical interaction mechanism of two-step method has been studied using the drop probe AFM, colloidal probe AFM and QCM-D techniques. Our work provides implications for the development of facile strategies to remove the hydrophobic bitumen-coated fine solids in oil media during the NAE process.

6.3 Suggestions for future work

(1) To better elucidate the stabilization mechanisms of fine solids, interactions between bitumen-coated fine solids in oil media can be more explored. It is recommended that interaction between bitumen components and different mineral surfaces, including kaolinite and montmorillonite can be investigated. The effects of various organic solvents, such as pentane, ethylbenzene and limonene, can be studied to fully understand the stabilization mechanisms of fine solids.

(2) For the sedimentation test, addition of bitumen to the suspension of fine solids is recommended, and the influence of the bitumen addition and the bitumen content can be explored. Moreover, different types of polymer modifiers and process aids (e.g., alkaline solution, ionic liquid) can be applied to enhance the performance of the two-step agglomeration method. Application of bio-inspired polymer can be an interesting topic in settling the fine solids. Parameters like wettability of polymer modifier, mechanical agitation and temperature can be studied.

(3) Interactions between water droplet and different solid surfaces in oil media can be studied to understand the affinity of fine solids to water. The impacts of organic solvent, water chemistry, surface morphology of solid surface can be further studied using the techniques like drop probe AFM.

(4) With improved understanding of the stabilization mechanisms, developed strategies to settle and remove the bitumen-coated silica particles can be employed to remove the fine solids in

practical NAE bitumen products in oil sands industry. The impacts like solvent/bitumen ratio (S/B), and operating parameters such as mechanical agitation and temperature should be further investigated and optimized.

Bibliography

1. Butler, R.; McNab, G.; Lo, H., Theoretical Studies on the Gravity Drainage of Heavy Oil During in-Situ Steam Heating. *Can. J. Chem. Eng.* **1981**, *59*, 455-460.

2. Berkowitz, N.; Speight, J. G., The Oil Sands of Alberta. *Fuel* 1975, *54*, 138-149.

3. Sheppard, M. C., *Oil Sands Scientist: The Letters of Karl A. Clark, 1920-1949*; University of Alberta, **1989**.

4. Lin, F.; Stoyanov, S. R.; Xu, Y., Recent Advances in Nonaqueous Extraction of Bitumen from Mineable Oil Sands: A Review. *Org. Process Res. Dev.* **2017**, *21*, 492-510.

5. Allen, E. W., Process Water Treatment in Canada's Oil Sands Industry: I. Target Pollutants and Treatment Objectives. *J. Environ. Eng. Sci* **2008**, *7*, 123-138.

6. Sparks, B.; Meadus, F., A Study of Some Factors Affecting Solvent Losses in the Solvent Extraction—Spherical Agglomeration of Oil Sands. *Fuel Process. Technol.* **1981**, *4*, 251-264.

7. Sparks, B. D.; Meadus, F. W.; Hoefele, E. O., Solvent Extraction Spherical Agglomeration of Oil Sands. Google Patents: 1988.

8. Meadus, F.; Chevrier, P.; Sparks, B., Solvent Extraction of Athabasca Oil-Sand in a Rotating Mill Part 1. Dissolution of Bitumen. *Fuel Process. Technol.* **1982**, *6*, 277-287.

9. Leung, H.; Phillips, C. R., Solvent Extraction of Mined Athabasca Oil Sands. *Ind. Eng. Chem. Fundam.* **1985**, *24*, 373-379.

10. Wu, J.; Dabros, T., Process for Solvent Extraction of Bitumen from Oil Sand. *Energy Fuels* **2012**, *26*, 1002-1008.

11. Hooshiar, A.; Uhlik, P.; Liu, Q.; Etsell, T. H.; Ivey, D. G., Clay Minerals in Nonaqueous Extraction of Bitumen from Alberta Oil Sands: Part 1. Nonaqueous Extraction Procedure. *Fuel Process. Technol.* **2012**, *94*, 80-85.

12. Nikakhtari, H.; Vagi, L.; Choi, P.; Liu, Q.; Gray, M. R., Solvent Screening for Non-Aqueous Extraction of Alberta Oil Sands. *Can. J. Chem. Eng.* **2013**, *91*, 1153-1160.

13. Nikakhtari, H.; Wolf, S.; Choi, P.; Liu, Q.; Gray, M. R., Migration of Fine Solids into Product Bitumen from Solvent Extraction of Alberta Oilsands. *Energy Fuels* **2014**, *28*, 2925-2932.

14. Kumar, K.; Dao, E.; Mohanty, K., AFM Study of Mineral Wettability with Reservoir Oils. *J. Colloid Interface Sci.***2005**, *289*, 206-217.

15. Ng, Y. M. S.; Knapper, B.; Kresta, J., Naphtha Based Fungible Bitumen Process. Google Patents: 2014.

16. Pal, K.; Nogueira Branco, L. d. P.; Heintz, A.; Choi, P.; Liu, Q.; Seidl, P. R.; Gray, M. R., Performance of Solvent Mixtures for Non-Aqueous Extraction of Alberta Oil Sands. *Energy Fuels* **2015**, *29*, 2261-2267.

17. Buckley, J.; Liu, Y., Some Mechanisms of Crude Oil/Brine/Solid Interactions. *J. Pet. Sci. Eng.* **1998**, *20*, 155-160.

18. Buckley, J.; Liu, Y.; Monsterleet, S., Mechanisms of Wetting Alteration by Crude Oils. *SPE journal* **1998**, *3*, 54-61.

19. Wang, S.; Liu, Q.; Tan, X.; Xu, C.; Gray, M. R., Study of Asphaltene Adsorption on Kaolinite by X-Ray Photoelectron Spectroscopy and Time-of-Flight Secondary Ion Mass Spectroscopy. *Energy Fuels* **2013**, *27*, 2465-2473.

20. Liu, J.; Wang, J.; Huang, J.; Cui, X.; Tan, X.; Liu, Q.; Zeng, H., Heterogeneous Distribution of Adsorbed Bitumen on Fine Solids from Solvent-Based Extraction of Oil Sands Probed by AFM. *Energy Fuels* **2017**. 31, 8833-8842.

21. Walther, A.; Müller, A. H., Janus Particles. *Soft Matter* **2008**, *4*, 663-668.

22. Marczewski, A. W.; Szymula, M., Adsorption of Asphaltenes from Toluene on Mineral Surface. *Colloids Surf., A* **2002**, *208*, 259-266.

23. Zahabi, A.; Gray, M. R.; Dabros, T., Kinetics and Properties of Asphaltene Adsorption on Surfaces. *Energy Fuels* **2012**, *26*, 1009-1018.

24. Xiong, Y.; Li, Z.; Cao, T.; Xu, S.; Yuan, S.; Sjoblom, J.; Xu, Z., Synergistic Adsorption of Polyaromatic Compounds on Silica Surfaces Studied by Molecular Dynamics Simulation. *J. Phys. Chem. C* **2018**, *122*, 4290-4299.

25. Xiong, Y.; Cao, T.; Chen, Q.; Li, Z.; Yang, Y.; Xu, S.; Yuan, S.; Sjöblom, J.; Xu, Z., Adsorption of a Polyaromatic Compound on Silica Surfaces from Organic Solvents Studied by Molecular Dynamics Simulation and Afm Imaging. *J. Phys. Chem. C* **2017**, *121*, 5020-5028.

26. Wu, G.; He, L.; Chen, D., Sorption and Distribution of Asphaltene, Resin, Aromatic and Saturate Fractions of Heavy Crude Oil on Quartz Surface: Molecular Dynamic Simulation. *Chemosphere* **2013**, *92*, 1465-1471.

27. Dudášová, D.; Silset, A.; Sjöblom, J., Quartz Crystal Microbalance Monitoring of Asphaltene Adsorption/Deposition. *J. Dispersion Sci. Technol.* **2008**, *29*, 139-146.

28. Ekholm, P.; Blomberg, E.; Claesson, P.; Auflem, I. H.; Sjöblom, J.; Kornfeldt, A., A Quartz Crystal Microbalance Study of the Adsorption of Asphaltenes and Resins onto a Hydrophilic Surface. *J. Colloid Interface Sci.***2002**, *247*, 342-350.

29. Rudrake, A.; Karan, K.; Horton, J. H., A Combined Qcm and Xps Investigation of Asphaltene Adsorption on Metal Surfaces. *J. Colloid Interface Sci.***2009**, *332*, 22-31

30. Tavakkoli, M.; Panuganti, S. R.; Vargas, F. M.; Taghikhani, V.; Pishvaie, M. R.; Chapman, W. G., Asphaltene Deposition in Different Depositing Environments: Part 1. Model Oil. *Energy Fuels* **2013**, *28*, 1617-1628.

31. Tavakkoli, M.; Panuganti, S. R.; Taghikhani, V.; Pishvaie, M. R.; Chapman, W. G., Asphaltene Deposition in Different Depositing Environments: Part 2. Real Oil. *Energy Fuels* **2014**, *28*, 3594-3603.

32. Zhang, L.; Shi, C.; Lu, Q.; Liu, Q.; Zeng, H., Probing Molecular Interactions of Asphaltenes in Heptol Using a Surface Forces Apparatus: Implications on Stability of Water-in-Oil Emulsions. *Langmuir* **2016**, *32*, 4886-4895.

33. Shi, C.; Zhang, L.; Xie, L.; Lu, X.; Liu, Q.; He, J.; Mantilla, C. A.; Van den Berg, F. G.; Zeng, H., Surface Interaction of Water-in-Oil Emulsion Droplets with Interfacially Active Asphaltenes. *Langmuir* **2017**, *33*, 1265-1274.

34. Liu, J.; Xu, Z.; Masliyah, J., Studies on Bitumen− Silica Interaction in Aqueous Solutions by Atomic Force Microscopy. *Langmuir* **2003**, *19*, 3911-3920.

35. Liu, J.; Xu, Z.; Masliyah, J., Interaction between Bitumen and Fines in Oil Sands Extraction System: Implication to Bitumen Recovery. *Can. J. Chem. Eng.* **2004**, *82*, 655-666.

36. Long, J.; Zhang, L.; Xu, Z.; Masliyah, J. H., Colloidal Interactions between Langmuir− Blodgett Bitumen Films and Fine Solid Particles. *Langmuir* **2006**, *22*, 8831-8839.

37. Liu, J.; Xu, Z.; Masliyah, J., Role of Fine Clays in Bitumen Extraction from Oil Sands. *AIChE journal* **2004**, *50*, 1917-1927.

38. Zhang, Y.; Ding, M.; Liu, J.; Jia, W.; Ren, S., Studies on Bitumen–Silica Interaction in Surfactants and Divalent Cations Solutions by Atomic Force Microscopy. *Colloids Surf., A* **2015**, *482*, 241-247.

39. Liu, J.; Xu, Z.; Masliyah, J., Colloidal Forces between Bitumen Surfaces in Aqueous Solutions Measured with Atomic Force Microscope. *Colloids Surf., A* **2005**, *260*, 217-228.

40. Liu, J.; Xu, Z.; Masliyah, J., Interaction Forces in Bitumen Extraction from Oil Sands. *J. Colloid Interface Sci.***2005**, *287*, 507-520.

41. Liu, J.; Zhang, L.; Xu, Z.; Masliyah, J., Colloidal Interactions between Asphaltene Surfaces in Aqueous Solutions. *Langmuir* **2006**, *22*, 1485-1492.

42. Long, J.; Xu, Z.; Masliyah, J. H., Single Molecule Force Spectroscopy of Asphaltene Aggregates. *Langmuir* **2007**, *23*, 6182-6190.

43. Long, J.; Xu, Z.; Masliyah, J. H., Role of Illite–Illite Interactions in Oil Sands Processing. *Colloids Surf., A* **2006**, *281*, 202-214.

44. Li, H.; Long, J.; Xu, Z.; Masliyah, J., Synergetic Role of Polymer Flocculant in Low-Temperature Bitumen Extraction and Tailings Treatment. *Energy Fuels* **2005**, *19*, 936-943.

45. Natarajan, A.; Xie, J.; Wang, S.; Liu, Q.; Masliyah, J.; Zeng, H.; Xu, Z., Understanding Molecular Interactions of Asphaltenes in Organic Solvents Using a Surface Force Apparatus. *J. Phys. Chem. C* **2011**, *115*, 16043-16051.

46. Natarajan, A.; Kuznicki, N.; Harbottle, D.; Masliyah, J.; Zeng, H.; Xu, Z., Understanding Mechanisms of Asphaltene Adsorption from Organic Solvent on Mica. *Langmuir* **2014**, *30*, 9370-9377.

47. Wang, J.; van der Tuuk Opedal, N.; Lu, Q.; Xu, Z.; Zeng, H.; Sjöblom, J., Probing Molecular Interactions of an Asphaltene Model Compound in Organic Solvents Using a Surface Forces Apparatus (Sfa). *Energy Fuels* **2011**, *26*, 2591-2599.

48. Wang, S.; Liu, J.; Zhang, L.; Xu, Z.; Masliyah, J., Colloidal Interactions between Asphaltene Surfaces in Toluene. *Energy Fuels* **2008**, *23*, 862-869.

49. Israelachvili, J. N., *Intermolecular and Surface Forces*; Academic press, **2011**.

50. Butt, H.-J.; Kappl, M.; Mueller, H.; Raiteri, R.; Meyer, W.; Rühe, J., Steric Forces Measured with the Atomic Force Microscope at Various Temperatures. *Langmuir* **1999**, *15*, 2559-2565.

51. Zhulina, E.; Borisov, O., Structure and Stabilizing Properties of Grafted Polymer Layers in a Polymer Medium. *J. Colloid Interface Sci.***1991**, *144*, 507-520.

52. Farnand, J.; Meadus, F.; Sparks, B., Removal of Intractable Fine Solids from Bitumen Solutions Obtained by Solvent Extraction of Oil Sands. *Fuel Process. Technol.* **1985**, *10*, 131-144.

53. Brons, G.; Yu, J. M., Solvent Deasphalting Effects on Whole Cold Lake Bitumen. *Energy Fuels* **1995**, *9*, 641-647.

54. Gray, M. R.; Tykwinski, R. R.; Stryker, J. M.; Tan, X., Supramolecular Assembly Model for Aggregation of Petroleum Asphaltenes. *Energy Fuels* **2011**, *25*, 3125-3134.

55. Maqbool, T.; Balgoa, A. T.; Fogler, H. S., Revisiting Asphaltene Precipitation from Crude Oils: A Case of Neglected Kinetic Effects. *Energy Fuels* **2009**, *23*, 3681-3686.

56. Rao, F.; Liu, Q., Froth Treatment in Athabasca Oil Sands Bitumen Recovery Process: A Review. *Energy Fuels* **2013**, *27*, 7199-7207.

57. Kotlyar, L.; Sparks, B.; Woods, J.; Chung, K., Solids Associated with the Asphaltene Fraction of Oil Sands Bitumen. *Energy Fuels* **1999**, *13*, 346-350.

58. Painter, P.; Williams, P.; Lupinsky, A., Recovery of Bitumen from Utah Tar Sands Using Ionic Liquids. *Energy Fuels* **2010**, *24*, 5081-5088.

59. Painter, P.; Williams, P.; Mannebach, E., Recovery of Bitumen from Oil or Tar Sands Using Ionic Liquids. *Energy Fuels* **2009**, *24*, 1094-1098.

60. Pulati, N.; Lupinsky, A.; Miller, B.; Painter, P., Extraction of Bitumen from Oil Sands Using Deep Eutectic Ionic Liquid Analogues. *Energy Fuels* **2015**, *29*, 4927-4935.

61. Li, X.; Sun, W.; Wu, G.; He, L.; Li, H.; Sui, H., Ionic Liquid Enhanced Solvent Extraction for Bitumen Recovery from Oil Sands. *Energy Fuels* **2011**, *25*, 5224-5231.

62. Tourvieille, J.-N.; Larachi, F.; Duchesne, C.; Chen, J., Nir Hyperspectral Investigation of Extraction Kinetics of Ionic-Liquid Assisted Bitumen Extraction. *Chem. Eng. J.***2017**, *308*, 1185-1199.

63. Hogshead, C. G.; Manias, E.; Williams, P.; Lupinsky, A.; Painter, P., Studies of Bitumen− Silica and Oil− Silica Interactions in Ionic Liquids. *Energy Fuels* **2010**, *25*, 293-299.

64. Li, X.; Wang, J.; He, L.; Sui, H.; Yin, W., Ionic Liquid-Assisted Solvent Extraction for Unconventional Oil Recovery: Computational Simulation and Experimental Tests. *Energy Fuels* **2016**, *30*, 7074-7081.

65. Meadus, F.; Bassaw, B.; Sparks, B., Solvent Extraction of Athabasca Oil-Sand in a Rotating Mill Part 2. Solids—Liquid Separation and Bitumen Quality. *Fuel Process. Technol.* **1982**, *6*, 289-300.

66. Nikakhtari, H.; Pal, K.; Wolf, S.; Choi, P.; Liu, Q.; Gray, M. R., Solvent Removal from Cyclohexane-Extracted Oil Sands Gangue. *Can. J. Chem. Eng.* **2016**, *94*, 408-414.

67. Jessop, P. G.; Phan, L.; Carrier, A.; Robinson, S.; Dürr, C. J.; Harjani, J. R., A Solvent Having Switchable Hydrophilicity. *Green Chemistry* **2010**, *12*, 809-814.

68. Holland, A.; Wechsler, D.; Patel, A.; Molloy, B. M.; Boyd, A. R.; Jessop, P. G., Separation of Bitumen from Oil Sands Using a Switchable Hydrophilicity Solvent. *Can. J. Chem.* **2012**, *90*, 805-810.

69. Sui, H.; Xu, L.; Li, X.; He, L., Understanding the Roles of Switchable-Hydrophilicity Tertiary Amines in Recovering Heavy Hydrocarbons from Oil Sands. *Chem. Eng. J.***2016**, *290*, 312-318.

70. Atta, A. M.; Fadda, A. A.; Abdel-Rahman, A. A.-H.; Ismail, H. S.; Fouad, R. R., Application of New Modified Poly (Ethylene Oxide)-Block-Poly (Propylene Oxide)-Block-Poly (Ethylene Oxide) Copolymers as Demulsifier for Petroleum Crude Oil Emulsion. *J. Dispersion Sci. Technol.* **2012**, *33*, 775-785.

71. Peña, A. A.; Hirasaki, G. J.; Miller, C. A., Chemically Induced Destabilization of Water-in-Crude Oil Emulsions. *Ind. Eng. Chem. Res.* **2005**, *44*, 1139-1149.

72. Hirasaki, G. J.; Miller, C. A.; Raney, O. G.; Poindexter, M. K.; Nguyen, D. T.; Hera, J., Separation of Produced Emulsions from Surfactant Enhanced Oil Recovery Processes. *Energy Fuels* **2010**, *25*, 555-561.

73. Pensini, E.; Harbottle, D.; Yang, F.; Tchoukov, P.; Li, Z.; Kailey, I.; Behles, J.; Masliyah, J.; Xu, Z., Demulsification Mechanism of Asphaltene-Stabilized Water-in-Oil Emulsions by a Polymeric Ethylene Oxide–Propylene Oxide Demulsifier. *Energy Fuels* **2014**, *28*, 6760-6771.

74. Xu, Y.; Wu, J.; Dabros, T.; Hamza, H.; Venter, J., Optimizing the Polyethylene Oxide and Polypropylene Oxide Contents in Diethylenetriamine-Based Surfactants for Destabilization of a Water-in-Oil Emulsion. *Energy Fuels* **2005**, *19*, 916-921.

75. Feng, X.; Xu, Z.; Masliyah, J., Biodegradable Polymer for Demulsification of Water-in-Bitumen Emulsions. *Energy Fuels* **2008**, *23*, 451-456.

76. Feng, X.; Wang, S.; Hou, J.; Wang, L.; Cepuch, C.; Masliyah, J.; Xu, Z., Effect of Hydroxyl Content and Molecular Weight of Biodegradable Ethylcellulose on Demulsification of Water-in-Diluted Bitumen Emulsions. *Ind. Eng. Chem. Res.* **2011**, *50*, 6347-6354.

77. Feng, X.; Mussone, P.; Gao, S.; Wang, S.; Wu, S.-Y.; Masliyah, J. H.; Xu, Z., Mechanistic Study on Demulsification of Water-in-Diluted Bitumen Emulsions by Ethylcellulose. *Langmuir* **2009**, *26*, 3050-3057.

78. Jin, Y.; Liu, W.; Liu, Q.; Yeung, A., Aggregation of Silica Particles in Non-Aqueous Media. *Fuel* **2011**, *90*, 2592-2597.

79. Butt, H.-J.; Cappella, B.; Kappl, M., Force Measurements with the Atomic Force Microscope: Technique, Interpretation and Applications. *Surface science reports* **2005**, *59*, 1-152.

80. Cui, X.; Shi, C.; Xie, L.; Liu, J.; Zeng, H., Probing Interactions between Air Bubble and Hydrophobic Polymer Surface: Impact of Solution Salinity and Interfacial Nanobubbles. *Langmuir* **2016**, *32*, 11236-11244.

81. Xie, L.; Wang, J.; Shi, C.; Huang, J.; Zhang, H.; Liu, Q.; Liu, Q.; Zeng, H., Probing Surface Interactions of Electrochemically Active Galena Mineral Surface Using Atomic Force Microscopy. *J. Phys. Chem. C* **2016**, *120*, 22433-22442.

82. Cui, X.; Shi, C.; Zhang, S.; Xie, L.; Liu, J.; Jiang, D.; Zeng, H., Probing the Effect of Salinity and Ph on Surface Interactions between Air Bubbles and Hydrophobic Solids: Implications for Colloidal Assembly at Air/Water Interfaces. *Chemistry–An Asian Journal* **2017**, *12*, 1568-1577.

83. Ducker, W. A.; Senden, T. J.; Pashley, R. M., Direct Measurement of Colloidal Forces Using an Atomic Force Microscope. *nature* **1991**, *353*, 239.

84. Butt, H.-J., Measuring Electrostatic, Van Der Waals, and Hydration Forces in Electrolyte Solutions with an Atomic Force Microscope. *Biophysical Journal* **1991**, *60*, 1438-1444.

85. Pedersen, H. G.; Bergström, L., Forces Measured between Zirconia Surfaces in Poly (Acrylic Acid) Solutions. *Journal of the American Ceramic Society* **1999**, *82*, 1137-1145.

86. Nalaskowski, J.; Drelich, J.; Hupka, J.; Miller, J. D., Preparation of Hydrophobic Microspheres from Low-Temperature Melting Polymeric Materials. *Journal of adhesion science and technology* **1999**, *13*, 1-17.

87. Carambassis, A.; Rutland, M. W., Interactions of Cellulose Surfaces: Effect of Electrolyte. *Langmuir* **1999**, *15*, 5584-5590.

88. Wang, J.; Li, J.; Xie, L.; Shi, C.; Liu, Q.; Zeng, H., Interactions between Elemental Selenium and Hydrophilic/Hydrophobic Surfaces: Direct Force Measurements Using Afm. *Chem. Eng. J.***2016**, *303*, 646-654.

89. Zeng, G.; Duan, Y.; Besenbacher, F.; Dong, M., Nanomechanics of Amyloid Materials Studied by Atomic Force Microscopy. In *Atomic Force Microscopy Investigations into Biology-from Cell to Protein*, InTech: 2012.

90. Sauerbrey, G., Verwendung Von Schwingquarzen Zur Wägung Dünner Schichten Und Zur Mikrowägung. *Zeitschrift für physik* **1959**, *155*, 206-222.

91. Czarnecki, J.; Radoev, B.; Schramm, L. L.; Slavchev, R., On the Nature of Athabasca Oil Sands. *Adv. Colloid Interface Sci*. **2005**, 114, 53-60.

92. Wang, S.; Zhang, L.; Yan, B.; Xu, H.; Liu, Q.; Zeng, H., Molecular and Surface Interactions between Polymer Flocculant Chitosan-G-Polyacrylamide and Kaolinite Particles: Impact of Salinity. *J. Phys. Chem. C* **2015**, 119, 7327-7339.

93. Allen, E. W., Process Water Treatment in Canada's Oil Sands Industry: Ii. A Review of Emerging Technologies. *J. Environ. Eng. Sci.* **2008**, 7, 499-524.

94. Hanson, D. O.; Sherk, F. T., Solvent Extraction of Tar Sand. Google Patents: 1979.

95. Funk, E. W.; May, W. G.; Pirkle Jr, J. C., Solvent Extraction Process for Tar Sands. Google Patents: 1982.

96. Wang, T.; Zhang, C.; Zhao, R.; Zhu, C.; Yang, C.; Liu, C., Solvent Extraction of Bitumen from Oil Sands. *Energy Fuels* **2014**, 28, 2297-2304.

97. Bensebaa, F.; Kotlyar, L. S.; Sparks, B. D.; Chung, K. H., Organic Coated Solids in Athabasca Bitumen: Characterization and Process Implications. *Can. J. Chem. Eng*. **2000**, 78, 610-616.

98. Osacky, M.; Geramian, M.; Ivey, D. G.; Liu, Q.; Etsell, T. H., Mineralogical and Chemical Composition of Petrologic End Members of Alberta Oil Sands. *Fuel* **2013**, 113, 148-157.

99. Wang, S.; Chung, K.; Masliyah, J. H.; Gray, M. R., Toluene-Insoluble Fraction from Thermal Cracking of Athabasca Gas Oil: Formation of a Liquid-in-Oil Emulsion That Wets Hydrophobic Dispersed Solids. *Fuel* **1998**, 77, 1647-1653.

100. Chaisoontornyotin, W.; Haji-Akbari, N.; Fogler, H. S.; Hoepfner, M. P., Combined Asphaltene Aggregation and Deposition Investigation. *Energy Fuels* **2016**, 30, 1979-1986.

101. Pernyeszi, T.; Patzko, A.; Berkesi, O.; Dékány, I., Asphaltene Adsorption on Clays and Crude Oil Reservoir Rocks. *Colloids Surf., A* **1998**, 137, 373-384.

102. Liu, X.; Yan, W.; Stenby, E. H.; Thormann, E., Release of Crude Oil from Silica and Calcium Carbonate Surfaces: On the Alternation of Surface and Molecular Forces by High-and Low-Salinity Aqueous Salt Solutions. *Energy Fuels* **2016**, 30, 3986-3993.

103. Tu, Y.; Kingston, D.; Kung, J.; Kotlyar, L. S.; Sparks, B. D.; Chung, K. H., Adsorption of Pentane Insoluble Organic Matter from Oilsands Bitumen onto Clay Surfaces. *Pet. Sci. Technol.* **2006**, 24, 327-338.

104. Sparks, B.; Kotlyar, L.; O'Carroll, J.; Chung, K., Athabasca Oil Sands: Effect of Organic Coated Solids on Bitumen Recovery and Quality. *J. Pet. Sci. Eng.* **2003**, 39, 417-430.

105. Durand, C.; Beccat, P., Use of Xps for Reservoir Sandstone Wettability Evaluation. Application to Kaolinite and Illite. *J. Pet. Sci. Eng.* **1998**, 20, 259-265.

106. Abdallah, W. A.; Taylor, S. D., Study of Asphaltenes Adsorption on Metallic Surface Using Xps and Tof-Sims. *J. Phys. Chem. C* **2008**, 112, 18963-18972.

107. Guo, S.; Akhremitchev, B. B., Packing Density and Structural Heterogeneity of Insulin Amyloid Fibrils Measured by AFM Nanoindentation. *Biomacromolecules* **2006**, 7, 1630-1636.

108. Quist, A.; Doudevski, I.; Lin, H.; Azimova, R.; Ng, D.; Frangione, B.; Kagan, B.; Ghiso, J.; Lal, R., Amyloid Ion Channels: A Common Structural Link for Protein-Misfolding Disease. *Proc. Natl. Acad. Sci.* **2005**, 102, 10427-10432.

109. Pauli, A.; Grimes, R.; Beemer, A.; Turner, T.; Branthaver, J., Morphology of Asphalts, Asphalt Fractions and Model Wax-Doped Asphalts Studied by Atomic Force Microscopy. *Int. J. Pavement Eng.* **2011**, 12, 291-309.

110. Schön, P.; Bagdi, K.; Molnár, K.; Markus, P.; Pukánszky, B.; Vancso, G. J., Quantitative Mapping of Elastic Moduli at the Nanoscale in Phase Separated Polyurethanes by AFM. *Eur. Polym. J.* **2011**, 47, 692-698.

111. Jogikalmath, G.; Stuart, J.; Pungor, A.; Hlady, V., Adhesion Mapping of Chemically Modified and Poly (Ethylene Oxide)-Grafted Glass Surfaces. *Colloids Surf., A* **1999**, 154, 53-64.

112. Huang, Y.-W.; Gupta, V. K., A Spr and AFM Study of the Effect of Surface Heterogeneity on Adsorption of Proteins. *J. Chem. Phys*. **2004**, 121, 2264-2271.

113. Dufrêne, Y. F.; Martínez-Martín, D.; Medalsy, I.; Alsteens, D.; Müller, D. J., Multiparametric Imaging of Biological Systems by Force-Distance Curve-Based AFM. *Nat. Methods* **2013**, 10, 847-854.

114. Hinterdorfer, P.; Dufrêne, Y. F., Detection and Localization of Single Molecular Recognition Events Using Atomic Force Microscopy. *Nat. Methods* **2006**, 3, 347-355.

115. Dupres, V.; Menozzi, F. D.; Locht, C.; Clare, B. H.; Abbott, N. L.; Cuenot, S.; Bompard, C.; Raze, D.; Dufrêne, Y. F., Nanoscale Mapping and Functional Analysis of Individual Adhesins on Living Bacteria. *Nat. Methods* **2005**, 2, 515-520.

116. Lohse, D.; Zhang, X., Surface Nanobubbles and Nanodroplets. *Rev. Mod. Phys.* **2015**, 87, 981.

117. Neirinck, B.; Van Deursen, J.; Van der Biest, O.; Vleugels, J., Wettability Assessment of Submicrometer Alumina Powder Using a Modified Washburn Method. *J. Am. Ceram. Soc.* **2010**, 93, 2515-2518.

118. Sababi, M.; Kettle, J.; Rautkoski, H.; Claesson, P. M.; Thormann, E., Structural and Nanomechanical Properties of Paperboard Coatings Studied by Peak Force Tapping Atomic Force Microscopy. *ACS Appl. Mater. Interfaces* **2012**, 4, 5534-5541.

119. Xiao, X.; Qian, L., Investigation of Humidity-Dependent Capillary Force. *Langmuir* **2000**, 16, 8153-8158.

120. Maugis, D., Contact, Adhesion and Rupture of Elastic Solids; *Springer Science & Business Media*, **2013**; Vol. 130.

121. Hutter, J. L.; Bechhoefer, J., Calibration of Atomic-Force Microscope Tips. *Rev. Sci. Instrum.* **1993**, 64, 1868-1873.

122. Green, N. H.; Allen, S.; Davies, M. C.; Roberts, C. J.; Tendler, S. J.; Williams, P. M., Force Sensing and Mapping by Atomic Force Microscopy. TrAC, *Trends Anal. Chem.* **2002**, 21, 65-74.

123. Sung, M. M.; Kluth, G. J.; Maboudian, R., Formation of Alkylsiloxane Self-Assembled Monolayers on Si_3N_4. *J. Vac. Sci. Technol. A* **1999**, 17, 540-544.

124. Headrick, J. E.; Berrie, C. L., Alternative Method for Fabricating Chemically Functionalized AFM Tips: Silane Modification of Hf-Treated Si_3N_4 Probes. *Langmuir* **2004**, 20, 4124-4131.

125. Drelich, J.; Long, J.; Yeung, A., Determining Surface Potential of the Bitumen-Water Interface at Nanoscale Resolution Using Atomic Force Microscopy. *Can. J. Chem. Eng*. **2007**, 85, 625-634.

126. Israelachvili, J.; Pashley, R., Measurement of the Hydrophobic Interaction between Two Hydrophobic Surfaces in Aqueous Electrolyte Solutions. *J. Colloid Interface Sci.* **1984**, 98, 500-514.

127. Donaldson Jr, S. H.; Røyne, A.; Kristiansen, K.; Rapp, M. V.; Das, S.; Gebbie, M. A.; Lee, D. W.; Stock, P.; Valtiner, M.; Israelachvili, J., Developing a General Interaction Potential for Hydrophobic and Hydrophilic Interactions. *Langmuir* **2014**, 31, 2051-2064.

128. Ren, S.; Dang-Vu, T.; Zhao, H.; Long, J.; Xu, Z.; Masliyah, J., Effect of Weathering on Surface Characteristics of Solids and Bitumen from Oil Sands. *Energy Fuels* **2008**, 23, 334-341.

129. Liu, G.; Wu, S.; van de Ven, M.; Molenaar, A.; Besamusca, J., Characterization of Organic Surfactant on Montmorillonite Nanoclay to Be Used in Bitumen. *J. Mater. Civ. Eng*. **2010**, 22, 794-799.

130. Horgnies, M.; Darque-Ceretti, E.; Fezai, H.; Felder, E., Influence of the Interfacial Composition on the Adhesion between Aggregates and Bitumen: Investigations by Edx, Xps and Peel Tests. *Int. J. Adhes. Adhes.* **2011**, 31, 238-247.

131. Zhao, S.; Kotlyar, L.; Woods, J.; Sparks, B.; Hardacre, K.; Chung, K., Molecular Transformation of Athabasca Bitumen End-Cuts During Coking and Hydrocracking. *Fuel* **2001**, 80, 1155-1163.

132. Long, J.; Zhang, L.; Xu, Z.; Masliyah, J. H., Colloidal Interactions between Langmuir-Blodgett Bitumen Films and Fine Solid Particles. *Langmuir* **2006**, 22, 8831-8839.

133. Yarranton, H. W., Asphaltene Self-Association. *J. Dispersion Sci. Technol*. **2005**, 26, 5-8.

134. Sedghi, M.; Goual, L.; Welch, W.; Kubelka, J., Effect of Asphaltene Structure on Association and Aggregation Using Molecular Dynamics. *J. Phys. Chem. B* **2013**, 117, 5765-5776.

135. Zahabi, A.; Gray, M. R.; Dabros, T., Heterogeneity of Asphaltene Deposits on Gold Surfaces in Organic Phase Using Atomic Force Microscopy. *Energy Fuels* **2012**, 26, 2891-2898.

136. Chen, B.; Evans, J. R., Elastic Moduli of Clay Platelets. *Scripta Mater*. **2006**, 54, 1581-1585.

137. Lorenzoni, M.; Evangelio, L.; Verhaeghe, S.; Nicolet, C. l.; Navarro, C.; Pérez-Murano, F., Assessing the Local Nanomechanical Properties of Self-Assembled Block Copolymer Thin Films by Peak Force Tapping. *Langmuir* **2015**, 31, 11630-11638.

138. Vargha-Butler, E.; Potoczny, Z.; Zubovits, T.; Budziak, C.; Neumann, A., Surface Tension of Bitumen from Contact Angle Measurements on Films of Bitumen. *Energy Fuels* **1988**, 2, 653-656.

139. Ducker, W. A.; Xu, Z.; Israelachvili, J. N., Measurements of Hydrophobic and Dlvo Forces in Bubble-Surface Interactions in Aqueous Solutions. *Langmuir* **1994**, 10, 3279-3289.

140. Hartley, P. G.; Larson, I.; Scales, P. J., Electrokinetic and Direct Force Measurements between Silica and Mica Surfaces in Dilute Electrolyte Solutions. *Langmuir* **1997**, 13, 2207-2214.

141. Zeng, H.; Shi, C.; Huang, J.; Li, L.; Liu, G.; Zhong, H., Recent Experimental Advances on Hydrophobic Interactions at Solid/Water and Fluid/Water Interfaces. *Biointerphases* **2016**, 11, 018903.

142. Jessop, P. G.; Phan, L. N.; Carrier, A. J.; Resendes, R.; Wechsler, D., Switchable Hydrophilicity Solvents and Methods of Use Thereof. Google Patents: 2013.

143. Liu, Q.; Dong, M.; Asghari, K.; Tu, Y., Wettability Alteration by Magnesium Ion Binding in Heavy Oil/Brine/Chemical/Sand Systems—Analysis of Electrostatic Forces. *J. Pet. Sci. Eng.* **2007**, *59*, 147-156.

144. Tian, C.; Lu, Q.; Liu, Y.; Zeng, H.; Zhao, Y.; Zhang, J.; Gupta, R., Understanding of Physicochemical Properties and Formation Mechanisms of Fine Particular Matter Generated from Canadian Coal Combustion. *Fuel* **2016**, *165*, 224-234.

145. Shi, C.; Zhang, L.; Xie, L.; Lu, X.; Liu, Q.; Mantilla, C. A.; van den Berg, F. G.; Zeng, H., Interaction Mechanism of Oil-in-Water Emulsions with Asphaltenes Determined Using Droplet Probe Afm. *Langmuir* **2016**, *32*, 2302-2310.

146. Jian, C.; Poopari, M. R.; Liu, Q.; Zerpa, N.; Zeng, H.; Tang, T., Reduction of Water/Oil Interfacial Tension by Model Asphaltenes: The Governing Role of Surface Concentration. *J. Phys. Chem. B* **2016**, *120*, 5646-5654.

147. Zhu, X.; Chen, D.; Wu, G., Insights into Asphaltene Aggregation in the Na-Montmorillonite Interlayer. *Chemosphere* **2016**, *160*, 62-70.

148. Wang, S.; Liu, J.; Zhang, L.; Masliyah, J.; Xu, Z., Interaction Forces between Asphaltene Surfaces in Organic Solvents. *Langmuir* **2009**, *26*, 183-190.

149. Zhang, K.; Jia, N.; Zeng, F., Application of Predicted Bubble-Rising Velocities for Estimating the Minimum Miscibility Pressures of the Light Crude Oil–Co 2 Systems with the Rising Bubble Apparatus. *Fuel* **2018**, *220*, 412-419.

150. Alagha, L.; Wang, S.; Yan, L.; Xu, Z.; Masliyah, J., Probing Adsorption of Polyacrylamide-Based Polymers on Anisotropic Basal Planes of Kaolinite Using Quartz Crystal Microbalance. *Langmuir* **2013**, *29*, 3989-3998.

151. Kelesoglu, S.; Volden, S.; Kes, M.; Sjoblom, J., Adsorption of Naphthenic Acids onto Mineral Surfaces Studied by Quartz Crystal Microbalance with Dissipation Monitoring (Qcm-D). *Energy Fuels* **2012**, *26*, 5060-5068.

152. Yang, G.; Chen, T.; Zhao, J.; Yu, D.; Liu, F.; Wang, D.; Fan, M.; Chen, W.; Zhang, J.; Yang, H., Desorption Mechanism of Asphaltenes in the Presence of Electrolyte and the Extended Derjaguin–Landau–Verwey–Overbeek Theory. *Energy Fuels* **2015**, *29*, 4272-4280.

153. Fischer, H.; Stadler, H.; Erina, N., Quantitative Temperature-Depending Mapping of Mechanical Properties of Bitumen at the Nanoscale Using the Afm Operated with Peakforce Tappingtm Mode. *J. Microsc.* **2013**, *250*, 210-217.

154. Rebelo, L.; De Sousa, J.; Abreu, A.; Baroni, M.; Alencar, A.; Soares, S.; Mendes Filho, J.; Soares, J., Aging of Asphaltic Binders Investigated with Atomic Force Microscopy. *Fuel* **2014**, *117*, 15-25.

155. Lewis, J. A., Colloidal Processing of Ceramics. *J. Am. Ceram. Soc.* **2000**, *83*, 2341-2359.

156. O'shea, S.; Welland, M.; Rayment, T., An Atomic Force Microscope Study of Grafted Polymers on Mica. *Langmuir* **1993**, *9*, 1826-1835.

157. Alexander, S., Adsorption of Chain Molecules with a Polar Head a Scaling Description. *J. Phys.* **1977**, *38*, 983-987.

158. Xie, K.; Karan, K., Kinetics and Thermodynamics of Asphaltene Adsorption on Metal Surfaces: A Preliminary Study. *Energy Fuels* **2005**, *19*, 1252-1260.

159. Abudu, A.; Goual, L., Adsorption of Crude Oil on Surfaces Using Quartz Crystal Microbalance with Dissipation (QCM-D) under Flow Conditions. *Energy Fuels* **2009**, *23*, 1237-1248.

160. Agrawala, M.; Yarranton, H. W., An Asphaltene Association Model Analogous to Linear Polymerization. *Ind. Eng. Chem. Res.* **2001**, *40*, 4664-4672.

161. Hoepfner, M. P.; Limsakoune, V.; Chuenmeechao, V.; Maqbool, T.; Fogler, H. S., A Fundamental Study of Asphaltene Deposition. *Energy Fuels* **2013**, *27*, 725-735.

162. Hoepfner, M. P.; Vilas Bôas Fávero, C. u.; Haji-Akbari, N.; Fogler, H. S., The Fractal Aggregation of Asphaltenes. *Langmuir* **2013**, *29*, 8799-8808.

163. Kurup, A. S.; Wang, J.; Subramani, H. J.; Buckley, J.; Creek, J. L.; Chapman, W. G., Revisiting Asphaltene Deposition Tool (Adept): Field Application. *Energy Fuels* **2012**, *26*, 5702-5710.

164. Liu, D.; Li, Z.; Fu, Y.; Zhang, Y.; Gao, P.; Dai, C.; Zheng, K., Investigation on Asphaltene Structures During Venezuela Heavy Oil Hydrocracking under Various Hydrogen Pressures. *Energy Fuels* **2013**, *27*, 3692-3698.

165. West, R. C., Non-Aqueous Process for the Recovery of Bitumen from Tar Sands. Google Patents: 1964.

166. Liu, J.; Cui, X.; Huang, J.; Xie, L.; Tan, X.; Liu, Q.; Zeng, H., Understanding the Stabilization Mechanism of Bitumen-Coated Fine Solids in Organic Media from Non-Aqueous Extraction of Oil Sands. *Fuel* **2019**, 242, 255-264.

167. Ngnie, G.; Baitan, D.; Dedzo, G. K.; Detellier, C., Sedimentation of Fine Particles of Kaolinite and Polymer-Coated Kaolinite in Cyclohexane: Implications for Fines Removal from Extracted Bitumen in Non-Aqueous Processes. *Fuel* **2018**, 234, 218-224.

168. Branca, C.; Magazu, S.; Maisano, G.; Migliardo, P.; Migliardo, F.; Romeo, G., Hydration Parameters of Aqueous Solutions of Poly (Ethylene Glycol) S by Viscosity Data. *Physica Scripta* **2002**, 66, 175.

169. Mueller, M.; Fabretto, M.; Evans, D.; Hojati-Talemi, P.; Gruber, C.; Murphy, P., Vacuum Vapour Phase Polymerization of High Conductivity Pedot: Role of PEG-PPG-PEG, the Origin of Water, and Choice of Oxidant. *Polymer* **2012**, 53, 2146-2151.

170. Branca, C.; Magazu, S.; Maisano, G.; Migliardo, F.; Migliardo, P.; Romeo, G., Hydration Study of PEG/Water Mixtures by Quasi Elastic Light Scattering, Acoustic and Rheological Measurements. *J. Phys. Chem. B* **2002**, 106, 10272-10276.

171. Lu, Q.; Yan, B.; Xie, L.; Huang, J.; Liu, Y.; Zeng, H., A Two-Step Flocculation Process on Oil Sands Tailings Treatment Using Oppositely Charged Polymer Flocculants. *Sci. Total Environ.* **2016**, 565, 369-375.

172. Shi, C.; Yan, B.; Xie, L.; Zhang, L.; Wang, J.; Takahara, A.; Zeng, H., Long-Range Hydrophilic Attraction between Water and Polyelectrolyte Surfaces in Oil. *Angew. Chem., Int. Ed.* **2016**, 55, 15017-15021.

173. Xie, L.; Wang, J.; Yuan, D.; Shi, C.; Cui, X.; Zhang, H.; Liu, Q.; Liu, Q.; Zeng, H., Interaction Mechanisms between Air Bubble and Molybdenite Surface: Impact of Solution Salinity and Polymer Adsorption. *Langmuir* **2017**, 33, 2353-2361.

174. Cui, X.; Liu, J.; Xie, L.; Huang, J.; Liu, Q.; Israelachvili, J. N.; Zeng, H., Modulation of Hydrophobic Interaction by Mediating Surface Nanoscale Structure and Chemistry, Not Monotonically by Hydrophobicity. *Angew. Chem., Int. Ed.* **2018**, 57, 11903-11908.

175. Mao, X.; Gong, L.; Xie, L.; Qian, H.; Wang, X.; Zeng, H., Novel Fe_3O_4 Based Superhydrophilic Core-Shell Microspheres for Breaking Asphaltenes-Stabilized Water-in-Oil Emulsion. *Chem. Eng. J.* **2019**, 358, 869-877.

176. Paul Maruska, H.; Rao, B. M., The Role of Polar Species in the Aggregation of Asphaltenes. *Fuel Sci. Technol. Int.***1987**, 5, 119-168.

177. Philippova, O.; Kuchanov, S.; Topchieva, I.; Kabanov, V., Hydrogen Bonds in Dilute Solutions of Poly (Ethylene Glycol). *Macromolecules* **1985**, 18, 1628-1633.

178. Varagnolo, S.; Ferraro, D.; Fantinel, P.; Pierno, M.; Mistura, G.; Amati, G.; Biferale, L.; Sbragaglia, M., Stick-Slip Sliding of Water Drops on Chemically Heterogeneous Surfaces. *Phys. Rev. Lett.* **2013**, 111, 066101.

179. Mirsaidov, U. M.; Zheng, H.; Bhattacharya, D.; Casana, Y.; Matsudaira, P., Direct Observation of Stick-Slip Movements of Water Nanodroplets Induced by an Electron Beam. *Proc. Natl. Acad. Sci.* **2012**, 109, 7187-7190.